

Fredrik Baltzersen Hultin

High-Capacity PEM Fuel Cells and Electrolysers in Hybrid Energy System for Offshore Power Generation

Master's thesis in Mechanical Engineering

Supervisor: Lars O. Nord (main supervisor) and Marcin Pilarczyk (co-supervisor)

June 2020

Fredrik Baltzersen Hultin

High-Capacity PEM Fuel Cells and Electrolysers in Hybrid Energy System for Offshore Power Generation

Master's thesis in Mechanical Engineering
Supervisor: Lars O. Nord (main supervisor) and Marcin Pilarczyk (co-
supervisor)
June 2020

Norwegian University of Science and Technology
Faculty of Engineering
Department of Energy and Process Engineering



Kunnskap for en bedre verden

Abstract

In order to reduce the greenhouse gas emissions from the petroleum sector, there is a quest for providing renewable power offshore. Within this context, an Innovative Hybrid Energy System for Stable Power and Heat Supply in Offshore Oil & Gas Installation (HES-OFF) has been proposed. The system combines the power supply from already installed gas turbines at the offshore installations, with renewable power from offshore wind. A vital part of the HES-OFF concept is a system of polymer electrolyte membrane (PEM) fuel cells and electrolysers used to handle the intermittent wind power.

In this work, a model is developed of the PEM fuel cell and electrolyser system in the HES-OFF concept. The fuel cell and electrolyser stacks are modelled down to single cell level, as components of the big-size PEM system. Balance of plant components are covered by simpler means, which includes modelling of a storage tank for compressed gaseous hydrogen. In the reference case, it is assumed a system with total fuel cell and electrolyser capacity of 2 MW, and the model is tuned to represent state-of-the-art fuel cell and electrolyser stacks. The developed model considers both steady state and dynamic phenomena, and simulations to showcase the features and capabilities of the model are performed. In addition to development of the model, possible weights and footprints of the modelled system are discussed.

The main challenge in the development of the model was to obtain data for the given fuel cell and electrolyser stacks in order to tune the model parameters, and finally validate the results. Consequently, it was attempted to develop a model relying on the least amount of empirical parameters which require data for tuning. The outcome of the work will contribute to research activities which are already performing in the framework of the HES-OFF research project. Moreover, the work was performed with a broad scope in order to provide a basis for future modelling activities of PEM systems.

Sammendrag

For å redusere klimagassutslippene fra petroleumssektoren, er det en etterspørsel etter å tilgjengeliggjøre fornybar kraft offshore. I denne konteksten, har et Hybrid energisystem for stabil forsyning av kraft og varme til offshore olje- og gassinstallasjoner (HES-OFF) blitt foreslått. Systemet kombinerer kraften fra allerede installerte gassturbiner, med fornybar kraft fra havvind. En viktig del av HES-OFF-konseptet er et system av PEM (Polymer Elektrolytt Membran) brenselceller og elektrolysører for å håndtere den ustabile kraften fra havvindmøllene.

I dette arbeidet har det blitt utviklet en modell av brenselcellene og elektrolysørene som inngår i HES-OFF-konseptet. Cellestablene har blitt modellert ned til enkeltcellenivå, som komponenter i det storskala PEM-systemet. De resterende støtte-komponentene i brenselcelle- og elektrolytørsystemet er betraktet i enklere former. Dette inkluderer modellering av en lagringstank for komprimert hydrogengass. Det er antatt at både brenselcellesystemet og elektrolytørsystemet i HES-OFF-konseptet har samlede kapasiteter på 2 MW. Modellparameterne er stilt inn for å modellere markedets beste produkter. Modellen betrakter både stabile og dynamiske fenomener, og diverse simuleringer har blitt gjennomført med modellen for å vise modellens funksjoner og egenskaper. I tillegg til utviklingen av modellen, har det blitt drøftet sannsynlige estimater på vekt og dimensjoner til HES-OFF-systemet.

Hovedutfordringen ved utviklingen av modellen, var å få tilgang til nødvendige opplysninger om brenselcellene og elektrolysørene for kunne stille inn modell-parameterne riktig og videre validere resultatene. Derfor ble det forsøkt å utvikle en modell som avhenger minst mulig av empiriske parametere som videre krever data for å stilles inn riktig. Resultatet av arbeidet vil bidra til forskningsaktiviteter som allerede er påbegynt i forskningsprosjektet HES-OFF. I tillegg ble arbeidet utført med et bredt omfang, for å gi et grunnlag for fremtidig modellering av PEM systemer.

Acknowledgements

Through the work of this thesis, I have received help and support from several persons, and I would like to express my sincere gratitude to these persons.

First of all, I would like to thank my main supervisor, Associate Professor Lars Nord Olof Nord, for encouragement, assistance and inclusion in various activities. Also, I would like to thank him for proposing the topic of this Master's thesis. From the beginning of this 5-year Master's programme in Mechanical Engineering, I have wanted to have hydrogen technology as part of the curriculum. Not before in the very last year, this was made possible through the work on this thesis.

I would like to give a special thanks to my co-supervisor, and closest collaborator through this project, Postdoctoral Fellow Marcin Pilarczyk. Marcin has been an immense resource through the work and always been very patient and supportive. Without him, this work would not have been possible. I also admire him for his encouragement and boldness for entering into new research field, which have been very inspiring when entering the world of fuel cells and electrolyzers.

I would also like to thank the remaining members of the HES-OFF team. Thanks to the NTNU representatives for sharing their knowledge and including me in the research project. Thanks to the industry partners of the project, Lunding Energy Norway and Prototech, for their expertise, fruitful discussions and for inviting me to their offices. Special thanks to Dmitry Bokach at Prototech for sharing his fuel cell expertise and providing feedback on parts of my work.

Furthermore, I would like to thank Team Hydrogen NTNU for inviting me to their annual workshop. This was an inspirational event, and I believe this organization is important for the common quest for developing the hydrogen technology.

Last, but not least, a big thanks to my friends and family for the support and encouragement through the last five years.

Table of Contents

Abstract	i
Sammendrag	iii
Acknowledgements	v
Table of Contents	ix
List of Tables	xi
List of Figures	xiv
Abbreviations	xv
1 Introduction	1
1.1 Background	1
1.2 Work	3
1.2.1 Purpose and Main Goal	3
1.2.2 Limitation of Scope	3
1.2.3 Objectives	4
1.2.4 Research Approach	5
1.2.5 Contribution	5
1.3 Organisation of Thesis	6
2 Introduction to Hydrogen Energy Storage	7
2.1 Fuel Cells	7
2.1.1 General Principles of Fuel Cells	7
2.1.2 Polymer Electrolyte Membrane Fuel Cells (PEMFC)	7
2.1.3 Ideal Energy Output of Fuel Cells	10
2.1.4 Voltage and Losses at Steady State	11
2.1.5 Graphical Presentation	15
2.1.6 Fuel Cell Dynamics	16
2.1.7 Fuel Cell Efficiency	21

2.1.8	Waste Heat	23
2.2	Water Electrolysers	24
2.2.1	Introduction paragraph	24
2.2.2	PEM Water Electrolysers	25
2.2.3	Steady State Voltage	25
2.2.4	Electrolyser Dynamics	28
2.2.5	Electrolyser efficiency	29
2.2.6	Waste heat	30
2.3	Hydrogen Stored as Compressed Gas	30
2.3.1	Practical Aspects	30
2.3.2	Equation of State for Gaseous Hydrogen	30
2.4	Balance of Plant Components	33
2.4.1	Air Compression Unit	34
2.4.2	Hydrogen Compression Unit	35
2.4.3	Ejectors	37
2.4.4	Heat Exchangers	39
2.4.5	Humidifiers	39
2.4.6	Turbines	40
2.4.7	Hydrogen Purification System	41
2.4.8	Power Electronics	41
2.4.9	Other BoP Components	43
2.5	Degradation	43
2.5.1	Degradation in Fuel Cells	43
2.5.2	Degradation in Electrolysers	46
2.6	Weight and Footprint of Commercial Systems	49
2.6.1	Fuel Cell Stacks	49
2.6.2	Fuel Cell Systems	52
2.6.3	Electrolyser Stacks	53
2.6.4	Containerised Electrolyser Systems	53
2.7	Developed Matlab Simulink® implementations	54
2.7.1	Nehrir and Wang Simulink Model (NW Model)	54
2.7.2	Simulink® Simscape™ Library Fuel Cell Stack Block	57
3	Modelling of the HES-OFF system	61
3.1	Assumed System	61
3.1.1	System layout	61
3.1.2	Fuel Cell Stacks	63
3.1.3	Electrolyser Stacks	65
3.1.4	Balance of Plant Components	66
3.2	Developed Model	66
3.2.1	Input load	66
3.2.2	Modelling Approach	66
3.2.3	Further Simplifications	68
3.2.4	Tuning of Constant Input Parameters	69
3.2.5	Simulink Implementation	69

3.3	Evaluation of the Fuel Cell Model by Benchmarking with the Simscape Library Fuel Cell Stack Block	72
4	Results and Discussion	75
4.1	Demonstration of Fuel Cell Stack Submodel	75
4.1.1	Steady State Diagrams	75
4.1.2	Dynamic Behaviour	79
4.2	Demonstration of Electrolyser Stack Submodel	81
4.2.1	Steady State Diagrams	81
4.3	Demonstration of Fuel Cell and Electrolyser Modules	85
4.3.1	Total Power and Demonstration of Modular Loading Opportunities	85
4.3.2	Total Fuel Cell and Electrolyser Waste Heat	85
4.4	Demonstration of BoP Components	88
4.4.1	Air compressor	88
4.4.2	Purifier	88
4.4.3	Hydrogen Compressor and Storage Tank	89
4.5	Sensitivity Analysis	91
4.6	Benchmarking of the Fuel Cell Model	94
4.7	Consideration of Weight and Footprint	96
4.8	Discussion of Work	97
4.8.1	Strengths and Weaknesses of the Developed Model	97
4.8.2	Implications	97
4.8.3	Reliability and Validity of the Work	98
5	Conclusion and Further Work	99
5.1	Conclusion	99
5.2	Fulfillment of Objectives	102
5.3	Further Work	103
	Bibliography	103
A	Matlab Code for Steady State Diagrams	113
B	Screenshots from the Simulink® Implementation	119
B.1	Fuel Cells	121
C	Benchmarking with the Simscape FC Block	125
D	Sensitivity Analysis	127
D.1	Fuel Cell Stack Model	127
D.2	Electrolyser Stack Model	134

List of Tables

2.1	Reported degradation rates on different fuel cell projects	46
2.2	Degradation rates for electrolysers	48
2.3	Data for fuel cell stacks	50
2.4	Data for fuel cell systems	52
2.5	Data for fuel cell systems where information about the installed stacks is also provided	53
2.6	Data for commercial containerised electrolyser systems	54
2.7	Input parameters used in the NW model	58
3.1	Input parameters general for all fuel cell and electrolyser systems	69
3.2	Input parameters tuned for the PowerCell S3 stack, attempted to fit the experimental data in figure 3.2.	70
3.3	Input parameters tuned for the Proton OnSite M-series stack, attempted to fit the experimental data in figure 3.4.	71
3.4	Parameters tuned for typical BoP components	71
3.5	Input parameters in the developed model in the benchmarking with the Simscape FC block	72

List of Figures

1.1	Simplified schematic of the HES-OFF system	2
1.2	Model classification chart	4
2.1	Simplified sketch of a PEM fuel cell	8
2.2	Electrode structure for fuel cells	9
2.3	Simplified sketch of a 3 cell fuel cell stack	10
2.4	Relative humidity versus the hydration parameter	14
2.5	Typical polarization curve for a fuel cell	16
2.6	Charge double layer	19
2.7	Charge double layer described by equivalent electrical circuits	21
2.8	Graphical representation of energy conversion in fuel cells	24
2.9	Simplified sketch of a PEM electrolyser cell	26
2.10	Simplified sketch the MEA used in electrolysers	26
2.11	Typical polarization curve for an electrolyser	28
2.12	Compressibility chart for gaseous hydrogen	32
2.13	Ideal gas law versus van der Waals equation	32
2.14	Material and energy flows in and out of fuel cell stacks	33
2.15	Material and energy flows in and out of electrolyser stacks	34
2.16	Simplified sketch of an electrochemical compressor	37
2.17	Principles of ejectors	38
2.18	Hydrogen supply system with ejector	38
2.19	Time delay due to the purification system	41
2.20	Principles of buck and boost converters	42
2.21	Electrolyser degradation at low versus high current density	47
2.22	Power/weight ratios for fuel cell stacks	51
2.23	Power/volume ratios for fuel cell stacks	51
2.24	Fuel Cell Stack Block accessed in the Simscape™ library	59
3.1	Suggested and modelled HES-OFF hydrogen energy storage system	62
3.2	Polarization curve for PowerCell S3	63
3.3	Fuel cell stack organisation in the modelled system	64
3.4	Polarization curve of Proton OnSite M-series stack	65
3.5	Electrolyser stack organisation in the modelled system	66

3.6	Approach for modelling of charge double layer effect	67
3.7	Polarization and power curve obtained from the Simscape FC block	73
4.1	Modelled fuel cell polarization curve for PowerCell S3	76
4.2	Modelled fuel cell voltage efficiency plotted towards current	76
4.3	Modelled fuel cell power of PowerCell S3	78
4.4	Modelled performance parameter [MJ/kg] and voltage efficiency plotted towards stack power	79
4.5	Response of modelled fuel cell stack voltage to a step increase in current	80
4.6	Response of modelled fuel cell stack voltage to a step decrease in current	81
4.7	Modelled electrolyser polarization curve of Proton OnSite M-series 250 kW	82
4.8	Modelled voltage efficiency of Proton OnSite M-series 250 kW electrolyser stack	83
4.9	Modelled power of Proton OnSite M-series 250 kW electrolyser stack	84
4.10	Modelled performance parameter and voltage efficiency of Proton OnSite M-series 250 kW electrolyser stack	84
4.11	Total fuel cell power when all stacks are loaded simultaneously	86
4.12	Total fuel cell power with non-simultaneous loading of modules	86
4.13	Total electrolyser power when all stacks are loaded simultaneously	87
4.14	Total electrolyser power with non-simultaneous loading of modules	87
4.15	Waste heat when the system is ramped sequentially up to the maximum fuel cell and electrolyser capacity. Simultaneous loading of stacks is applied in this simulation	88
4.16	Demonstration of air compressor power	89
4.17	Demonstration of purifier time lag	90
4.18	Demonstration of hydrogen compressor power for increasing tank pressure	90
4.19	Fuel cell polarization curves demonstrating the sensitivity the limiting current density, i_L , and the charge transfer coefficient α	92
4.20	Sensitivity analysis for the fuel cell parameters τ_e , λ_e and C	93
4.21	Polarization and power curve obtained from the developed model and the Simscape FC block, both tuned to the 6 kW stack available as a preset in the Simscape FC block	94
4.22	Comparison of the voltage response of the developed model and the Simscape FC block when both are tuned to the 6 kW stack available as a preset in the Simscape FC block	95

Nomenclature

Symbols

a	Chemical activity (eq. 2.7, 2.8, 2.10, 2.54, 2.79- 2.81)	-
a	Empirical constant (eq. 2.39)	-
a	Coefficient in van der Waals equation (eq. 2.69)	$0.025m^6 Pa/mol^2$
A	Area	m^2
b	Empirical constant (eq. 2.39)	-
b	Coefficient in van der Waals (eq. 2.69)	$2.66 \cdot 10^{-5}m^3/mol$
c_p	Specific heat capacity	$J/(kg \cdot K)$
C	Capacitance of charge double layer	F
E	Voltage	V
d	Distance between capacitance layers	m
D	Binary diffusivity	m^2/s
F	Faraday's constant	C/mol
G	Gibbs energy	J
\hat{g}	Molar gibbs energy	J/mol
H	Enthalpy	J
i	Current density	A/cm^2
i_0	Exchange current density	A/cm^2
i_L	Limiting current density	A/cm^2
I	Current	A
I_L	Limiting current	A
l_m	Membrane thickness	cm
m	Mass	kg
M_m	Molar mass	g/mol
n	Electron transfer number	-
N	Amount of substance	mol
p	Partial pressure	bar, atm
P	Pressure	bar, atm
P	Power (eq. 2.22, 2.45, 2.46, 2.50, 2.51, 2.60, 2.61, 2.62, 2.64, 2.65)	W
S	Entropy	J/K
r	Area specific resistance	$\Omega \cdot cm^2$
R	Universal gas constant	$J/(mol \cdot K)$
R	Resistance (eq. 2.35, 2.37, 2.40, 2.86, 3.1, 4.1)	Ω
RH	Relative humidity	%
T	Temperature	K
T_C	Temperature inputted in $^{\circ}C$ value	$^{\circ}C$
v_i	Stoichiometric coefficient of species i	-
V	Volume	m^3

V	Voltage/voltage loss	V
Q	Heat	J
Z	Compressibility factor	-
x	Mole fraction	-

Greek symbols

α	Charge transfer coefficient	-
ϵ	Electrical permittivity	F/m
η	Efficiency	-
κ	Heat capacity ratio	-
λ_e	Empirical constant	Ω
λ_m	Membrane hydration parameter	-
τ	Time constant	s

Subscripts and superscripts

A,a	Anode
Act	Activation
C,c	Cathode
Comp	Compressor
Conc	Concentration
CV	Control Volume
d	Drop, used to denote the voltage drop associated with mass transfer delay
e	Used to denote parameters associated with gas flows
ELY	Electrolyser
Exp	Expander
FC	Fuel Cell
Ideal	Ideal
In	Inlet
Nernst	Nernst
OCV	Open Circuit Voltage
Ohmic	Ohmic
Out	Outlet
Rev	Reversible
Sat	Saturation
0	Parameter evaluated at standard conditions
Newton's notation for time derivative	Flow of the given parameter

Acronyms

BoP	Balance of Plant
D	Dimension
DC	Direct Current
ELY	Electrolyser
FC	Fuel Cell
GDL	Gas Diffusion Layer
GHG	Greenhouse Gas
HES-OFF	Innovative Hybrid Energy System for Stable Power and Heat Supply in Offshore Oil & Gas Installation
HHV	Higher Heating Value
HOR	Hydrogen Oxidation Reaction
LHV	Lower Heating Value
MEA	Membrane Electrode Assembly
ORR	Oxygen Reduction Reaction
PEM	Polymer Electrolyte Membrane
PTFE	Persulfonated polytetrafluoroethylene
SO	Solide Oxide

Introduction

1.1 Background

The presented work has been conducted within the framework of the ongoing research project at the Norwegian University of Science and Technology (NTNU) entitled Innovative Hybrid Energy System for Stable Power and Heat Supply in Offshore Oil & Gas Installation (HES-OFF). The project is done in collaboration with Lundin Energy Norway AS and Prototech AS, and the aim is to move a step forward in the quest for environmental-friendly and cost-effective solutions to supply energy offshore (NTNU, 2020).

Norwegian offshore oil and gas installations are today mainly powered by gas turbines, which contribute significant greenhouse gas (GHG) emissions from the petroleum sector. Indeed, this sector was in 2018 accounting for approximately 27% of the total GHG emissions in Norway, where around 67% of these emissions could further be traced back to the gas turbines (Norwegian Environment Agency, 2020). According to the Norwegian Climate Change Act, the goal of Norway is to reduce the total GHG emissions with 40% within 2030 compared to the reference year 1990, and 80-95% within 2050 (Climate Change Act, 2018). Reducing the emissions from the power supply to offshore installations can therefore be of crucial significance for Norway in order to reach these goals.

The HES-OFF concept is a hybrid energy system designed to reduce the emissions from offshore installations and is presented in the simplified schematic in figure 1.1. In addition to the original gas turbines used in the installations, wind turbines are installed to complement the power supply. To handle the intermittent wind power and provide a stable supply of renewable power, an energy storage system is also required. Energy storage in gaseous hydrogen has been selected for this purpose.

Hydrogen is described in Burheim (2017) as the most flexible energy storage medium. The book explains that energy storage systems using hydrogen can be designed with power capacities ranging from less than a kW to several MWs. Moreover, hydrogen possesses an extremely high specific energy (energy stored per unit mass of medium). On the

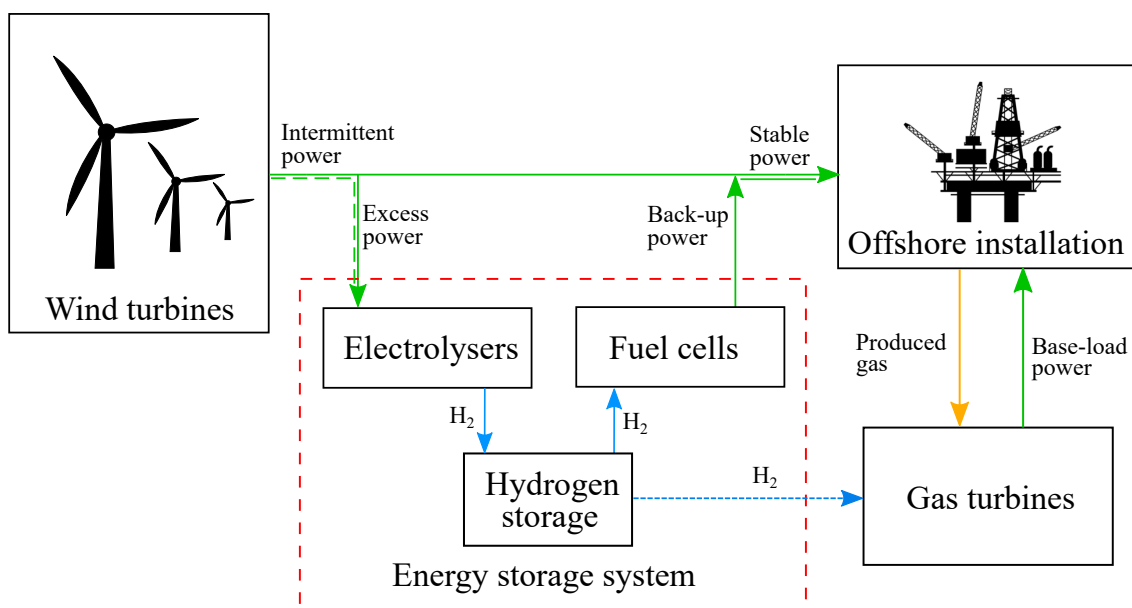


Figure 1.1: Simplified schematic of the HES-OFF system

contrary, the volumetric energy (energy stored per unit volume) at ambient temperature and pressure is relatively low. However, by means of different processing, the volumetric energy density of stored hydrogen can be increased to competitive values. These properties make hydrogen energy storage suitable for the HES-OFF concept, which requires a high capacity, while weight and footprint are crucial parameters.

In a hydrogen energy storage system, three main functions must be integrated; generation of hydrogen by use of energy, generation of energy by use of hydrogen and intermediate storage of the hydrogen. In the HES-OFF system, this is obtained by use of polymer electrolyte membrane (PEM) water electrolyzers and fuel cells, as well as storage tanks for gaseous hydrogen. In addition to these three main types of components, a set of Balance of Plant (BoP) components is needed in order to operate the system. The HES-OFF concept also includes the idea of co-feeding the gas turbines with a certain amount of the hydrogen produced by the electrolyzers. This can further reduce the carbon-footprint from the offshore installation.

Water electrolyzers are devices which can produce hydrogen (H_2) and oxygen (O_2) from water (H_2O), by use of direct current (DC) electricity. The electric energy is therefore stored as bond energy in the product molecules. This is obtained in a single step, without any moving parts (Coutanceau et al., 2018). The opposite of electrolyzers are fuel cells, which generate DC electricity by converting hydrogen and oxygen to water (Barbir, 2013). In the HES-OFF system, water electrolyzers are employed to generate hydrogen when there is excess wind power available. On the contrary, fuel cells are used to generate power from hydrogen and oxygen when the wind turbines are not producing the demanded power to the offshore installation. In the mediate, hydrogen is stored as compressed gas in tanks, while the oxygen is released to and supplied from the ambient air. Both electrol-

ysers and fuel cells can be categorised into three main categories: alkaline, solid oxide (SO) and polymer electrolyte membrane (PEM). Due to a combination of technology maturity, capacity and dimensions, PEM fuel cells and electrolyzers have been found as the most suitable for the HES-OFF system. Therefore, in the remaining parts of this thesis, the terms *fuel cells* and *electrolysers* are interpreted as PEM fuel cells and electrolyzers. Accordingly does *hydrogen energy storage system* refer to a system of PEM fuel cells and electrolyzers coupled with a hydrogen storage method.

1.2 Work

1.2.1 Purpose and Main Goal

The work on this Master's thesis is a continuation of a specialisation project conducted by the undersigned student. In this project, the main focus was on steady state modelling of fuel cell stacks. The purpose of this Master's project is to further pave the way in mathematical modelling of big-size fuel cell and electrolyser systems. The work should result in the main goal, which is a comprehensive model of the fuel cell and electrolyser system in the HES-OFF concept. However, through the mentioned specialisation project, it was identified that modelling of fuel cells and electrolyzers is a complex cross of multidisciplinary modelling fields. Further, models can be developed in very detailed manners according to the purpose they aim to fulfill. The developed model in this work is therefore not intended to be a complete model for a certain purpose. Instead, the model should represent a basis for further modelling activities and the thesis should showcase the obstacles one will encounter during modelling of big-size PEM fuel cell and electrolyser systems.

To develop the model, it must first be suggested a simplified design of the real system. Further, the developed model should be implemented in the Matlab Simulink® programming environment, because it is intended that further developments of the model can be used for real-time simulations through an OPAL-RT platform. In addition to the mathematical modelling, it should be performed a brief weight and footprint analysis of the modelled system.

1.2.2 Limitation of Scope

During the early stages of the work, it was identified that PEM fuel cells and electrolyzers can be modelled in a variety of approaches. Consequently, the following limitations of the scope had to be applied for the modelling activity.

The main focus of the modelling activity is on the PEM fuel cell and electrolyser stacks in the HES-OFF concept. The remaining Balance of Plant components and hydrogen storage are considered by means of simpler equations. In the open literature, it can be found several different approaches for modelling of fuel cell and electrolyser systems. Gao et al. (2012) claim that the models generally can be characterised by means of five

sub-categories; spatial dimensions, temporal behavior, the types of equations applied, modelled area and modelled phenomena. This is depicted in figure 1.2 and it is marked in red and green which characteristics are considered in this work.

According to figure 1.2, this work will consider the fuel cells and electrolyzers on stack level and down to single cell level (this will be explained in chapter 2). Both steady state and dynamic behaviours will be evaluated. For steady state, electrochemical phenomena will be modelled by means of 0D-parameters, for which it was identified in the specialization project that analytical and semi-empirical equations typically are available. For dynamic states, both the electrochemical, fluidic and thermal domain will be analysed by means of zero, one and pseudo two dimensions, where the usage of pseudo two dimensions imply approximation of 2D phenomena by use of 1D equations. It is expected that also empirical equations must be applied to obtain the dynamic modelling.

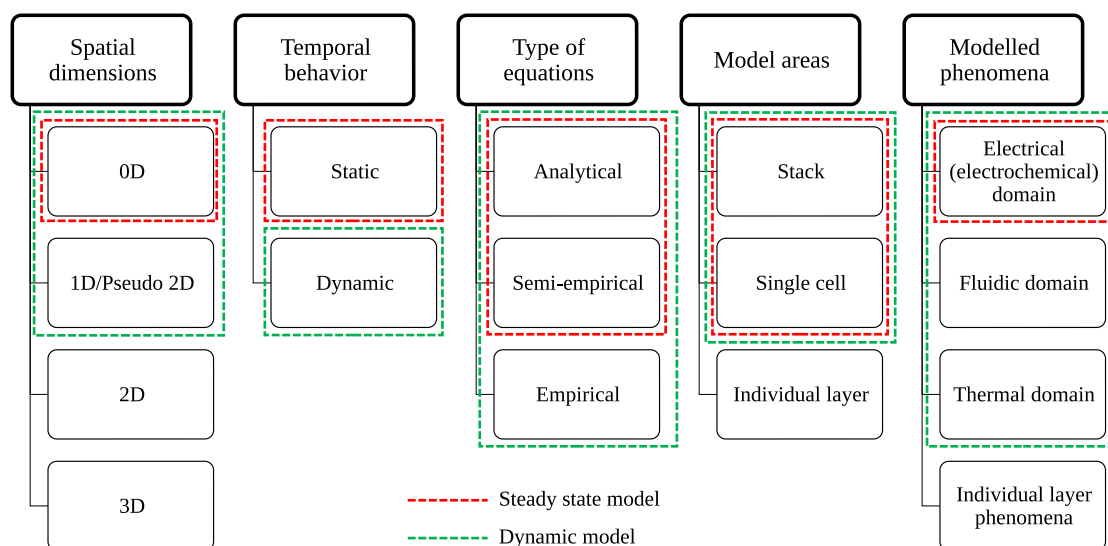


Figure 1.2: Model classification chart. Drawn on the basis of the classification in Gao et al. (2012).

1.2.3 Objectives

To achieve the thesis goals, the following objectives for the work have been identified:

1. Perform a comprehensive literature review on gaseous hydrogen energy storage systems comprising PEM fuel cells and electrolyzers
2. Search for relevant developed models implemented in the Matlab Simulink® environment and investigate the opportunity for adapting the models according to the needs in this modelling activity
3. Suggest a simplified design of the HES-OFF hydrogen energy storage system

4. Create a model of the suggested HES-OFF hydrogen energy storage system and implement it in the Matlab Simulink[®] environment
5. Apply the model to perform simulations showcasing the features and capabilities of the model
6. Perform a brief weight and footprint analysis of the suggested system

1.2.4 Research Approach

To approach the research field, the following activities have been conducted:

- Literature reviews to get insight in the industry
- Close collaboration with co-supervisor Postdoctoral Fellow Marcin Pilarczyk from the beginning of the specialization project and to the deadline of the Master's thesis. Additionally, there have been frequent meetings with supervisor Associate Professor Lars O. Nord
- Participation in HES-OFF meetings, including:
 - Internal meetings with the representatives from NTNU
 - Meeting at the office of Lundin, where both NTNU and Prototech was represented. Here, this Master's work was shortly presented
 - Meeting at the office of Prototech, where Prototech supervised the work as an expert on PEM fuel cells
- Participation in group meetings in the research group of supervisor Associate Professor Lars O. Nord
- Participation in the Team Hydrogen NTNU annual workshop, where the work was presented in a poster session

1.2.5 Contribution

Through the individual work with this thesis, and through discussions with the HES-OFF team, it has been identified that it is difficult to model fuel cells and electrolyzers as system components by adapting developed models from other research. The research field is characterised by extensive use of semi-empirical and empirical approaches, and several of these may be more detailed than what is needed. By use of these correlations, it is consequently required abundant access to experimental data for tuning of parameters. Unfortunately, through the meetings with the industry partners of the HES-OFF system, it has also been discussed that the manufacturers within the field are generally very cautious with providing information about their products. Therefore, it is desirable to employ correlations requiring the least amount of unconventional empirical parameters. Thus far, it has not been found any books or previous research suggesting sufficient models of fuel

cell and electrolyser systems which can easily be adapted to an arbitrary system.

This work attempts to contribute to the research field by paving the way in modelling of fuel cell and electrolyser stacks as system components by means easy adaptable correlations. This is obtained by gathering the most conventional correlations from previous research and combining these to a model representing the hydrogen energy storage system in the HES-OFF concept. The ambition is further that this will be fruitful information to the participants in the HES-OFF project and contribute in their quest for providing renewable power offshore.

1.3 Organisation of Thesis

The thesis is organised in five chapters, including this introduction. The second chapter presents the results of the literature review performed on hydrogen energy storage systems. This describes important principles of such systems and attempts to suggest how the system components can be modelled. Further, Chapter 3 presents the developed model of the HES-OFF energy storage system system. It is here presented a suggested design of the system and the methods for modelling this. The results of this work is largely the developed model. Therefore, this model is showcased by means of different simulation outputs in chapter 4 which are discussed consecutively in the text. In addition, some other results of the work are presented and discussed. In chapter 5, conclusions of the work are presented before the thesis is ended with a set of suggestions for further work within the modelling of the HES-OFF system.

Introduction to Hydrogen Energy Storage

2.1 Fuel Cells

2.1.1 General Principles of Fuel Cells

The basic principles of a fuel cell is described in the first chapter of O'Hayre et al. (2016). A fuel cell is a device that consumes a certain fuel and produces electricity. Several fuels can be used to produce electricity in such devices, among these is gaseous hydrogen, $H_2(g)$. The electricity is produced in a hydrogen fuel cell by letting hydrogen react with oxygen and form into water. This can be described by the following reaction:



There are several different techniques to make the fundamental reactions and mechanisms to occur in a fuel cell. The different techniques used, also set the framework for the classification of the fuel cells. In the HES-OFF project, fuel cells classified as polymer electrolyte membrane (PEM) fuel cells are integrated. The remaining parts of this report will therefore focus on PEM fuel cells.

2.1.2 Polymer Electrolyte Membrane Fuel Cells (PEMFC)

In PEM fuel cells, reaction 2.1 is divided into two separate half reactions. These are termed the hydrogen oxidation reaction (HOR) and the oxygen reduction reaction (ORR), and can respectively be expressed as follows:



As equation (2.2) shows, the HOR produces electrons (e^-) and protons (H^+). These same electrons and protons are further consumed in the ORR (2.3). By spatially separating these two half reactions, there must therefore be a flow of electrons and protons between the locations where the half reactions occur. Furthermore, if the electrons and protons are

forced to travel in two distinct routes (conductors), there will be a net flow of protons and a net flow of electrons. This is achieved in PEM fuel cells by forcing the protons through an electrolyte membrane only capable of carrying charged atoms, while the electrons are forced through a wire. This net flow of electrons through the wire is what is seen as the electrical current, I , produced by the fuel cell. Within the fuel cell subject, this current is often normalized by the cell active area, A_{cell} , which is the surface area of the electrode/electrolyte interface where the fuel cell reactions take place (O’Hayre et al., 2016). This yields the current density:

$$i = \frac{I}{A_{cell}} \quad (2.4)$$

Based on the descriptions in the first chapter of O’Hayre et al. (2016), figure 2.1 shows the principles of a simplified PEM fuel cell. The HOR (2.2) and ORR (2.3) occur at the surface of two different electrodes named the anode and cathode. The electrodes are spatially separated by a polymer electrolyte membrane and coupled together with a wire.

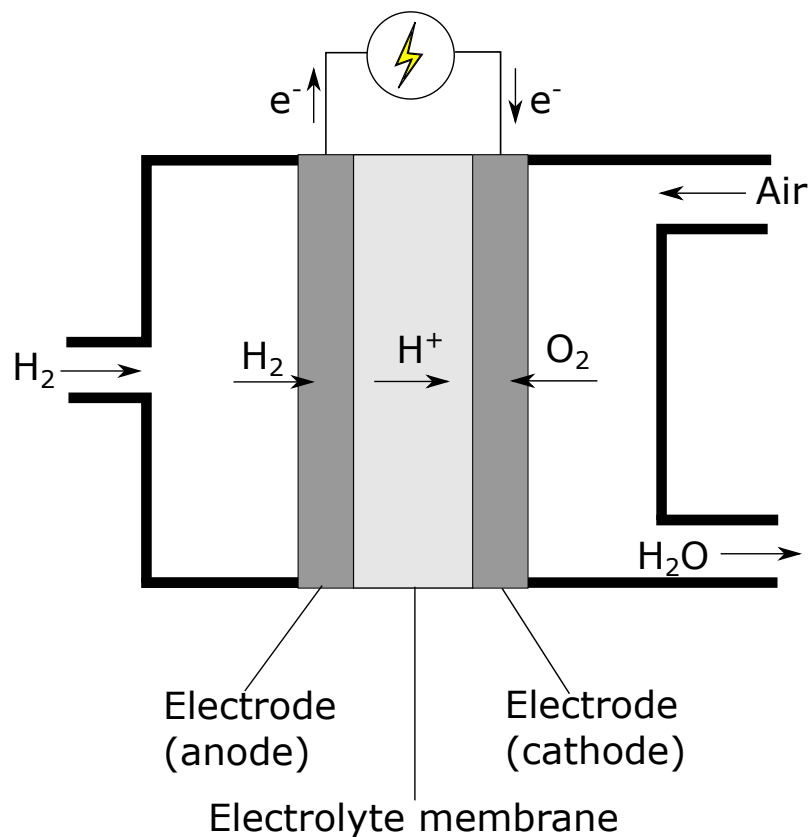


Figure 2.1: Simplified sketch of a PEM fuel cell

The electrodes are further built up by two layers, named the catalyst layer and the gas diffusion layer (GDL) (see figure 2.2). The HOR (2.2) and ORR (2.3) are actually taking place on the surfaces of the catalyst layers. In PEM fuel cells these are made of noble materials, commonly platinum. The gas diffusion layers are supporting structures with the purpose of reinforcing the structure and allow easy gas access to the catalysts. They also improve the electrical conductivity. The electrolyte membrane between the electrodes is usually made of Nafion, which is the more popular name of Persulfonated polytetrafluoroethylene (PTFE). This is a thin film, which possesses an extremely high proton conductivity. The total sandwich structure consisting of the membrane electrolyte film, catalyst layers and gas diffusion layers is often referred to as the membrane electrode assembly (MEA).

To obtain the desired outputs from a fuel cell system, single cells are commonly connected in series of several cells, referred to as fuel cell stacks. This is depicted in figure 2.3 (redrawn from a figure in Larminie and Dicks (2003)). In such systems, several MEAs are interconnected by so-called bipolar plates. These plates serve as electron conductors between the MEAs. They are therefore often made of a material with good electric conductivity, such as graphite or a metal (Larminie and Dicks, 2003). In addition, they have patterns on the surfaces, termed flow channels, guiding the gas flows to the electrode surfaces. Note that in the stacks, the electrons do not flow from the anode to the cathode electrode in the same MEA, but rather to the cathode in the MEA on the opposite side of the adjacent bipolar plate.

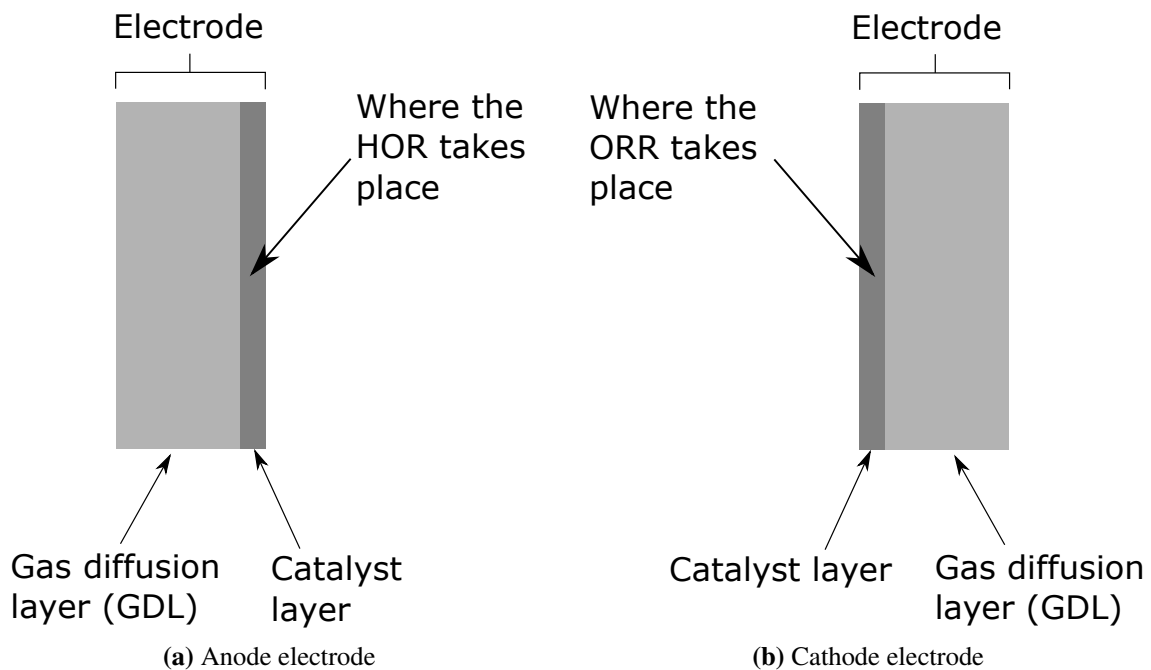


Figure 2.2: Electrode structure. HOR and ORR refer to the hydrogen oxidation reaction and the oxygen reduction reaction, respectively

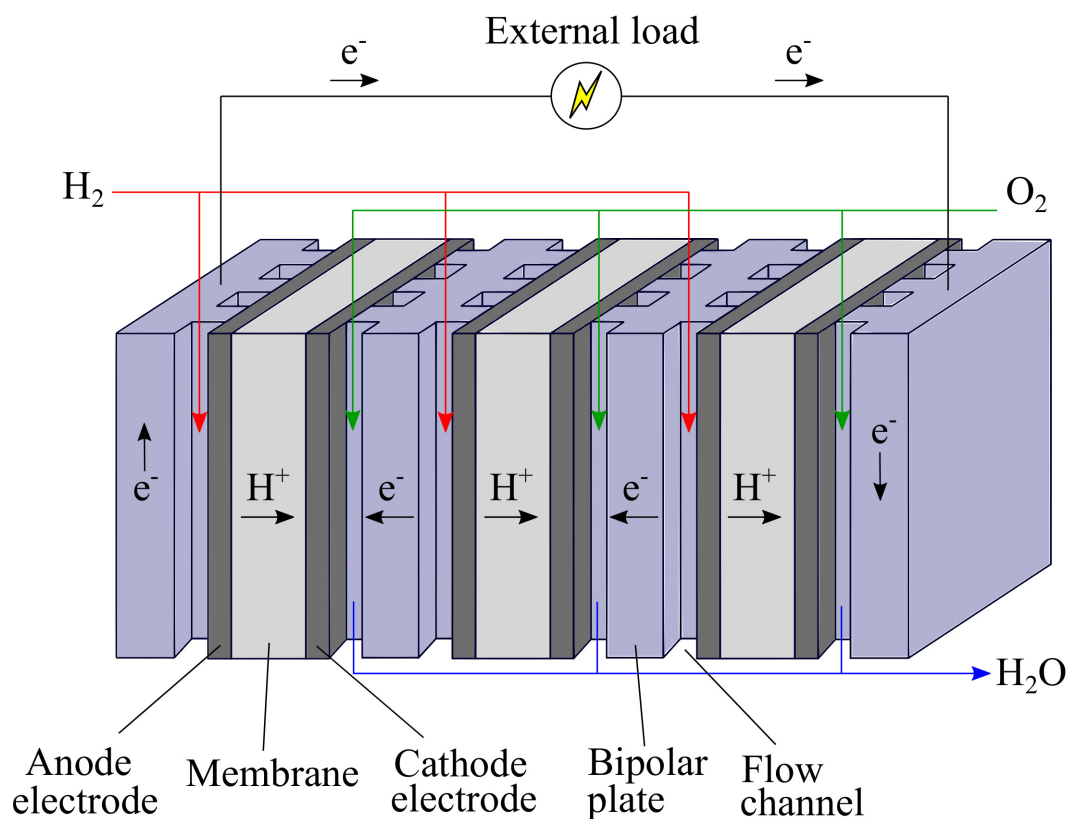


Figure 2.3: Simplified sketch of a 3 cell fuel cell stack

2.1.3 Ideal Energy Output of Fuel Cells

By analysing the thermodynamics of a fuel cell, the maximum energy that a fuel cell can deliver as electricity can be determined. The following section will outline the thermodynamics of a fuel cell, and is based on the second chapter of O'Hayre et al. (2016).

The energy that will be released when the overall chemical reaction (2.1) occurs in a fuel cell, is the enthalpy difference between the products and the reactants, ΔH . The second law of thermodynamics further states that some of this energy, even under reversible operation, must be released as heat due to an entropy change between the products and the reactants. This heat release, referred to as the reversible heat release, will have a magnitude of:

$$Q_{rev} = T\Delta S \quad (2.5)$$

where T is the system boundary temperature and ΔS is the entropy change between the products and reactants. The remaining energy which can be converted into electrical energy, is therefore:

$$\underbrace{\Delta G}_{\text{max electrical energy}} = \underbrace{\Delta H}_{\text{energy released}} - \underbrace{T\Delta S}_{\text{heat released}} \quad (2.6)$$

where ΔG is often referred to as the Gibbs free energy. For standard conditions and on a per mole basis, the Gibbs free energy, denoted $\Delta\hat{g}^0$, can be calculated by equation (2.6) using tabulated values. The standard conditions are taken as a temperature of 298.15K and a pressure of 1 bar. However, for different conditions, the Gibbs free energy will change due to changes of the chemical activities of the products and reactants in the fuel cell. For a general chemical reaction, the Gibbs free energy is given by:

$$\Delta\hat{g} = \Delta\hat{g}^0 + RT \ln\left(\frac{\prod a_{products}^{v_i}}{\prod a_{reactants}^{v_i}}\right) \quad (2.7)$$

where $a_{reactants}$ and $a_{products}$ are the activities of the products and reactants at the surface of the catalyts layers. v_i is the corresponding stoichiometric coefficient of each species. For a PEM fuel cell, the Gibbs free energy is therefore given by:

$$\Delta\hat{g} = \Delta\hat{g}^0 + RT \ln\left(\frac{a_{H_2O}}{a_{H_2} a_{O_2}^{1/2}}\right) \quad (2.8)$$

where a_{H_2O} , a_{H_2} and a_{O_2} are the chemical activities of H_2O , H_2 and O_2 where the respective half reactions take place. This is the maximum electrical energy that a fuel cell can produce when 1 mole of H_2 is consumed.

2.1.4 Voltage and Losses at Steady State

O'Hayre et al. (2016) give the following correlation between the Gibbs free energy and the ideal voltage of a fuel cell:

$$\Delta\hat{g} = -nFE \quad (2.9)$$

where n is the number of electrons transferred in the reaction, F is Faraday's constant and E is the ideal voltage of the fuel cell. Combining equation (2.8) and (2.9) therefore yields:

$$E = E^0 + \frac{RT}{nF} \ln\left(\frac{a_{H_2} a_{O_2}^{1/2}}{a_{H_2O}}\right) \quad (2.10)$$

Equation (2.10) is known as the Nernst's equation for a PEM fuel cell, and gives the ideal voltage that a fuel cell can deliver at the given conditions. E is often referred to as the Nernst voltage (E_{Nernst}), and is the voltage in the fuel cell if there are no losses present. This voltage will also be obtained when the fuel cell is connected in an open circuit, and is therefore frequently also termed the open circuit voltage, E_{OCV} . However, the activities comprised in equation 2.10 can often be difficult to determine, as these are the activities of the substances at the catalyst layers. Because the substances have to diffuse through the electrodes to reach the catalyst layers, these activities are not the same as the activities of the inlet and outlet streams of the fuel cell stack. Therefore, equation 2.10 often occurs

in different modified configurations (Larminie and Dicks, 2003; Nehrir and Wang, 2009). The following approach is presented in the book by Spiegel (2008):

$$E_{Nernst} = -\frac{\Delta\hat{g}_0}{nF} - \frac{RT}{nF} \ln \left(\frac{P_{sat,H_2O}}{p_{H_2} \cdot p_{O_2}^{1/2}} \right) \quad (2.11)$$

P_{sat,H_2O} is the saturation pressure of water at the operating temperature, and p_{H_2} and p_{O_2} are the partial pressures of hydrogen and oxygen at the catalyst layers. These parameters are further approximated by the following correlations:

$$\log_{10} P_{sat,H_2O} = -2.1794 + 0.02953 \cdot T_C - 9.1837 \cdot 10^{-5} \cdot T_C^2 + 1.4454 \cdot 10^{-7} \cdot T_C^3 \quad (2.12)$$

$$p_{H_2} = 0.5 \left(\frac{P_{H_2}}{\exp\left(\frac{1.653i}{T^{1.334}}\right)} - P_{sat,H_2O} \right) \quad (2.13)$$

$$p_{O_2} = \frac{P_{air}}{\exp\left(\frac{4.192i}{T^{1.334}}\right)} - P_{sat,H_2O} \quad (2.14)$$

T_C is here the temperature given in Celsius ($^{\circ}C$), while P_{H_2} and P_{air} are the absolute pressures of hydrogen and air at the stack inlet, given in atmospheres (atm).

Further, for non-idealized real conditions, there will especially be three significant losses present in a fuel cell. These three losses are described in chapter 3, 4 and 5 of O'Hayre et al. (2016), and are entitled the activation losses (V_{act}), ohmic losses (V_{ohmic}) and concentration losses (V_{conc}). The real output voltage of an operating fuel cell is therefore:

$$V_{FC} = E_{Nernst} - V_{act} - V_{ohmic} - V_{conc} \quad (2.15)$$

Activation losses

As the name explains, the activation losses are related to the activation of chemical reactions, and a description can be found in O'Hayre et al. (2016) chapter 3. In a fuel cell, the cell potentials at the anode and the cathode must be reduced in order for the overall reaction (2.1) to occur. This reaction is an equilibrium reaction, which means it can be separated into a forward and a reverse reaction. Because of the reduction in cell potentials at the anode and cathode, the activation energies of these reactions will be changed. This is affecting the net electric current density, which can be described by the Butler-Volmer equation:

$$i = i_0 \left(e^{\frac{\alpha n F V_{act}}{RT}} - e^{\frac{-(1-\alpha) n F V_{act}}{RT}} \right) \quad (2.16)$$

Here, α is a dimensionless charge transfer coefficient (often assumed to be 0.5 in the literature), F is Faraday's constant, R is the universal gas constant and T is the cell temperature. i_0 is the exchange current density, which is the current density obtained at equilibrium. V_{act} is the mentioned potential/voltage drop, which occurs as a loss for the overall fuel cell voltage. The first term of (2.16) represents the forward reaction rate,

while the second term represents the reverse reaction rate. In a system with high voltage losses, the last term of equation (2.16) can be neglected, and the equation reduces to:

$$i = i_0 e^{\frac{\alpha n F V_{act}}{RT}} \quad (2.17)$$

By solving this for V_{act} , we obtain an expression for the activation losses of the fuel cell:

$$V_{act} = \frac{RT}{\alpha n F} \ln\left(\frac{i}{i_0}\right) \quad (2.18)$$

Larminie and Dicks (2003) further state that the activation losses depend on the speed of the chemical reactions, and equation 2.18 may therefore occur in different configurations to fit a specific fuel cell.

It must be emphasised that equation 2.18 is only valid for $i > i_0$, otherwise the activation losses will occur as voltage gains and not losses. It can also be observed that these losses will tend to be constant for high current densities, i.e. the variations in activation losses will only be of importance for low current densities. This will be treated further in chapter 2.1.5, which is about interpretation of fuel cell voltage curves.

Ohmic losses

The principle of ohmic losses is outlined in O'Hayre et al. (2016) chapter 4, and summarised in the following. As already mentioned in chapter 2.1.1, one of the general principles of hydrogen fuel cells is that the electrons (e^-) and protons (H^+) are transported between two spatially separated locations in two different ways. However, in all real conductors there will be an intrinsic resistance to charge flow. In the transportation of the electrons and protons, the particles will therefore be affected by this resistance. This will occur as a voltage loss over the length of the conductors. The total voltage losses accounted for by the transportation of both electrons and protons are often referred to as the ohmic losses, and are given by:

$$V_{ohmic} = i r_{ohmic} \quad (2.19)$$

where $r_{ohmic} [Ohm \cdot cm^2]$ is called the area specific ohmic resistance and is constant for a given fuel cell. r_{ohmic} is often independent of the current density. The ohmic losses have therefore a linear relationship with the current density, which will be further discussed in chapter 2.1.5.

The ohmic resistance is however very dependent on the water content in the fuel cell, as water is very central in the mechanism of proton transportation in the Nafion membrane. The water content is commonly quantified by the relative humidity, often referred to as the RH value. This is defined as:

$$RH = \frac{p_w}{p_{sat}} \quad (2.20)$$

where p_w is the partial pressure of water vapor in the system, and p_{sat} is the saturation pressure of water at the system temperature. The resistance to charge flow is also strongly interrelated to the proton travelling distance (membrane thickness, l_m) and cell temperature. A quite frequently used empirical correlation which expresses these dependencies is also presented in O'Hayre et al. (2016):

$$r_{ohmic} = \frac{l_m}{(0.005139 \cdot \lambda_m + 0.00326) \cdot e^{1267(\frac{1}{303} - \frac{1}{T})}} \quad (2.21)$$

where λ_m is a parameter representing the water content in the membrane. Note that l_m must here have the unit [cm] to obtain r_{ohmic} in [$\Omega \cdot cm^2$]. λ_m can further be approximated by:

$$\lambda_m = \begin{cases} 0.043 + 17.18RH - 39.85RH^2 + 36.0RH^3, & \text{for } 0 < RH \leq 1. \\ 14 + 4(RH - 1), & \text{for } 1 < RH \leq 3 \end{cases} \quad (2.22)$$

The value of λ_m is plotted for relative humidity between 0 and 100% in figure 2.4. The figure shows that 100% relative humidity corresponds to λ_m around 13-14. At lower RH-values, the hydration parameter will decrease significantly, and therefore increase the ohmic resistance (equation 2.21) severely.

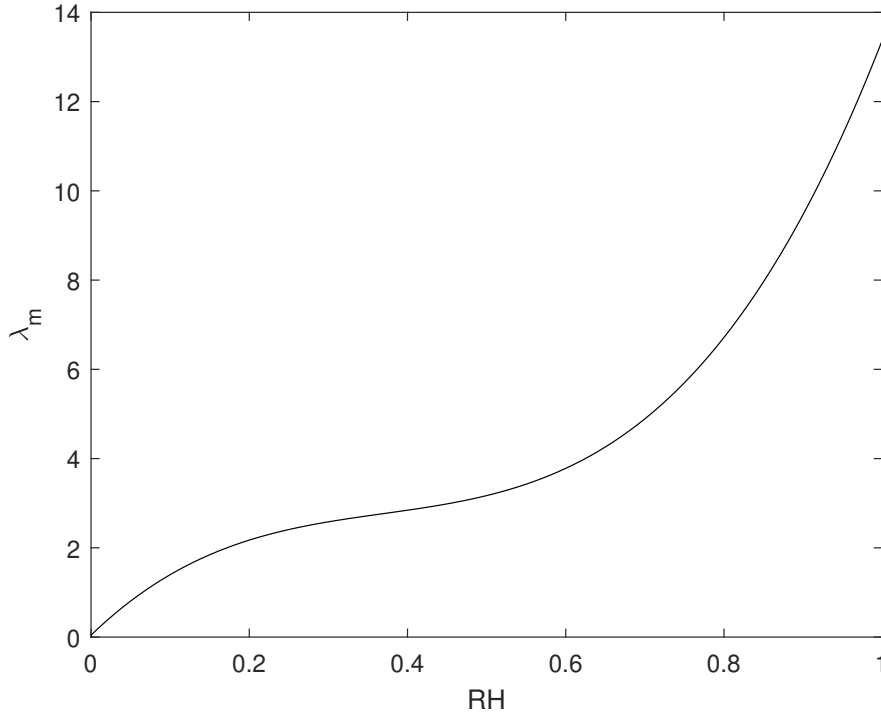


Figure 2.4: Relative humidity versus the hydration parameter λ_m . Redrawn from O'Hayre et al. (2016).

Concentration/mass transport losses

It can be shown that changes in concentrations of the chemical species at the surface of the catalyst layers will affect both the reversible fuel cell voltage (E_{Nernst}) and the activation losses (V_{act}). The joint losses which are caused due to these concentration changes are referred to as the concentration losses, V_{conc} . As the concentrations at the electrodes in a fuel cell are related to mass transport mechanisms, these losses are also commonly named mass transport losses. A description of the losses can be found in O'Hayre et al. (2016) chapter 5, and is outlined below.

To determine the concentration losses, it is crucial to understand the parameter named the limiting current density, i_L . This is defined as the current density that will make the reactants concentrations tend toward zero and is therefore the maximum current density which can appear in a fuel cell. Theoretically, there would be two ways of calculating the limiting current density, as there are two different reactant concentrations that can tend to zero. However, since O_2 diffuses more slowly than H_2 , the limiting current density will be determined based on the O_2 present in the fuel cell.

If both the changes in reversible fuel cell voltage and activation losses are accounted for, the theoretical total concentration losses can be calculated by:

$$V_{conc} = \frac{RT}{nF} \left(1 + \frac{1}{\alpha}\right) \ln\left(\frac{i_L}{i_L - i}\right) \quad (2.23)$$

However, it is stated in O'Hayre et al. (2016) that the real concentration losses are often larger than the theoretical losses calculated by equation 2.23. Adjustments to the equation may therefore be done to obtain the correct concentration losses, e.g. by reducing the value of α from the conventional value of 0.5. Eventually could other semi-empirical equations be used.

It can be observed from equation (2.23) that the concentration losses become increasingly significant for larger current densities. In fact, the concentration losses tend towards infinity when i tend towards the maximum obtainable current density, i_L . This effect will be subject to further discussion in chapter 2.1.5.

2.1.5 Graphical Presentation

The total cell voltage of a typical fuel cell is plotted against the current density in figure 2.5. This voltage is the Nernst voltage, minus the three significant losses outlined in section 2.1.4, in accordance to equation 2.15. Such plots are commonly entitled polarization curves, and are useful as they allow to compare performances of different stacks. Additionally, the different losses described in chapter 2.1.4 are plotted in the same figure. It can be observed how the different losses vary differently with the current density, i . While the activation losses only vary significantly for small current densities, do the concentration losses vary mostly for large current densities. However, the ohmic losses have

a linear relationship to the current density. The three distinct regions (activation-, ohmic- and concentration region) are therefore named after which type of losses contribute most to the variation of total voltage in the region.

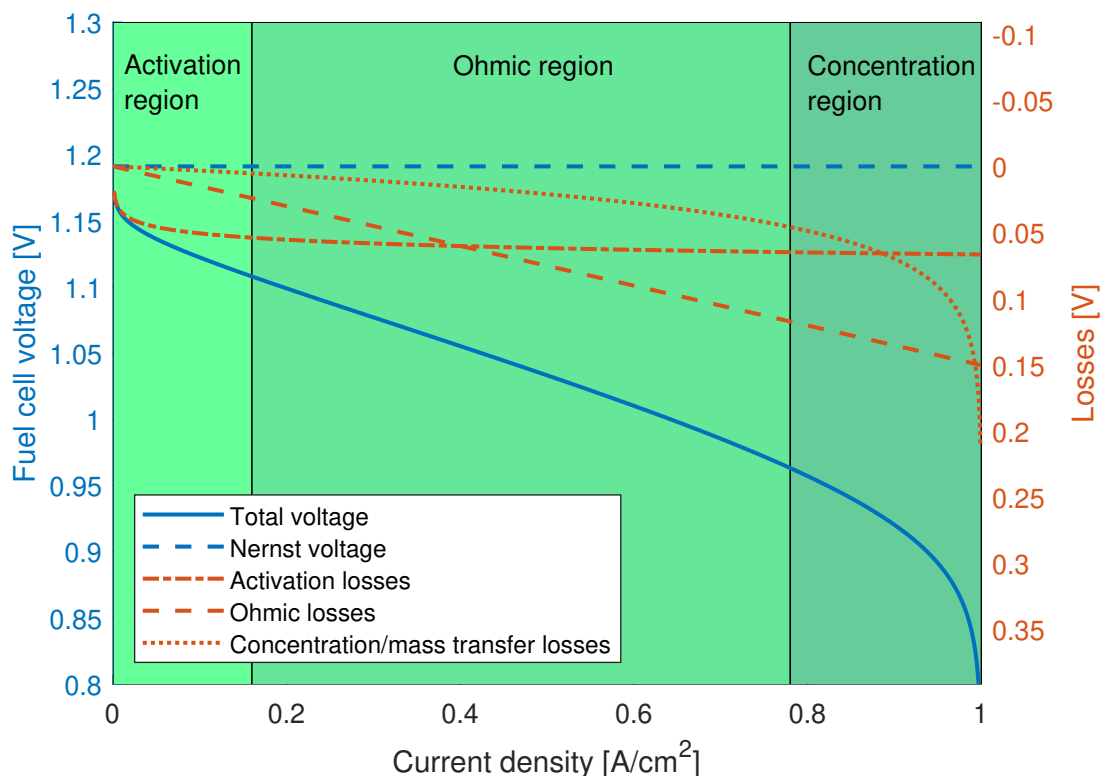


Figure 2.5: Example of a polarization curve including losses for a fuel cell

2.1.6 Fuel Cell Dynamics

For certain applications, fuel cells have to be operated under dynamic conditions. The equations outlined thus far in the thesis presuppose that the fuel cells are operated under steady states. For stationary power production where the load is relatively stable, this may be a valid assumption. On the contrary, for example in automotive applications where the load have to be continuously adjusted according to the driving pattern, the fuel cells are operated under dynamic states. Regarding the HES-OFF system, it is likely that the fuel cells frequently have to be operated under dynamic states, because the load have to be adjusted according to both the power demand from the offshore installation and the intermittent wind power. When a fuel cell is exposed to dynamic conditions, the voltage might deviate from what should be expected from the steady state polarization curves. O'Hayre et al. (2016) explains that this is due to several subtle reasons, such as the slowness of temperature changes or mass transport. The following section will outline a few dynamic behaviours for fuel cells which are described in the literature.

Mass Transport Delay

Fuel cells have to be fed with the right amount of hydrogen and air in order to maintain the desired pressures of the gases. When fuel cells are exposed to abrupt changes, there will due to the inertia of the gas flows take a certain time before the gas pressures are reestablished. This delay in mass transport will therefore affect the fuel cell performance. A description of this phenomenon can be found in Nehrir and Wang (2009) chapter 3, and is summarised below.

On a per mole basis, mass balance of a given substance for a given control volume can be written as:

$$\frac{dN_{CV}}{dt} = \sum_i \dot{N}_i - \sum_e \dot{N}_e + \dot{N}_{generated} - \dot{N}_{consumed} \quad (2.24)$$

where N_{CV} is the total amount of moles of the substance within the control volume, \dot{N}_i and \dot{N}_e are the mole flow rates of the substance in and out of the control volume, and $\dot{N}_{generated}$ and $\dot{N}_{consumed}$ are the amounts of the substance which are generated and consumed in chemical reactions within the control volume. If the ideal gas law and Faraday's law is applied, the mass balances of hydrogen and oxygen can be written for the anode and cathode volumes, V_a and V_c , as follows:

$$\frac{V_a}{RT} \frac{dp_{H_2}}{dt} = \dot{N}_{H_2,in} - \dot{N}_{H_2,out} - \frac{I}{2F} \quad (2.25)$$

$$\frac{V_c}{RT} \frac{dp_{O_2}}{dt} = \dot{N}_{O_2,in} - \dot{N}_{O_2,out} - \frac{I}{4F} \quad (2.26)$$

where p_{H_2} and p_{O_2} are the partial pressures of the hydrogen and oxygen respectively. From this, it follows that under steady state, the net flow of reactant species will be similar to the consumed amount, such that:

$$\dot{N}_{H_2,net} = \dot{N}_{H_2,in} - \dot{N}_{H_2,out} = \frac{I}{2F} \quad (2.27)$$

$$\dot{N}_{O_2,net} = \dot{N}_{O_2,in} - \dot{N}_{O_2,out} = \frac{I}{4F} \quad (2.28)$$

However, under transient state where the current is changed rapidly, there will be a delay between the net supply rate and consumption rate of species. Nehrir and Wang (2009) propose that this phenomenon can be modelled as first order time delay, such that:

$$\tau_a \frac{d\dot{N}_{H_2,net}}{dt} = \frac{I}{2F} - \dot{N}_{H_2,net} \quad (2.29)$$

$$\tau_c \frac{d\dot{N}_{O_2,net}}{dt} = \frac{I}{4F} - \dot{N}_{O_2,net} \quad (2.30)$$

τ_a and τ_c are referred to as the time constants for the gas flows into the anode and the cathode. These determine the time it will take for the flow rates to adjust to the changes. For

systems reacting slow to changes, the time constants will be large, while for fast systems the time constants will be small.

Unfortunately, the time constants above can be difficult to procure. It may therefore be more convenient to consider the joint effect of these time delays on the output voltage. Nehrir and Wang (2009) suggest an empirical approach to this. The book models the effect as a time dependant voltage drop per cell which is given by the following equation:

$$V_d = \lambda_e (I - I \otimes e^{-t/\tau_e}) \quad (2.31)$$

where λ_e [Ω] is an empirical constant and τ_e is the overall time constant of the gas flows. λ_e and τ_e must therefore be found empirically by fitting the modelled voltage curves with experimental data. The last term of equation 2.31 is the convolution of the current and a first order time lag representing the delay. Therefore, by virtue of the definition of first order time delays, τ_e is approximately 25% of the overall response time of the gas flows. Equation 2.31 can be easier to understand when it is converted into the Laplace domain:

$$V_d = \lambda_e I \left(1 - \frac{1}{\tau_e s + 1} \right) \quad (2.32)$$

In the Laplace domain, $s \rightarrow \infty$ corresponds to $t \rightarrow 0$ in the time domain, and oppositely for $s \rightarrow 0$. It can therefore be interpreted from equation 2.32, that the voltage drop will be of magnitude $\lambda_e I$ immediately after current changes are applied and diminish towards zero as time tends to infinity. Because the voltage drop, V_d , does not depend on the current, it is added as a subtraction to the open circuit voltage, such that the open circuit voltage is:

$$E_{OCV} = E_{Nernst} - V_d = E_{Nernst} - \lambda_e I \left(1 - \frac{1}{\tau_e s + 1} \right) \quad (2.33)$$

Charge Double Layer Effect

The charge double layer effect plays an important role in the dynamic behaviour of fuel cells. The phenomenon of electrical double layers is known to occur whenever two different materials are in contact. Larminie and Dicks (2003) state that this is a very complex phenomenon which several books have been written to explain. It is also difficult to find good approaches in the open literature for how charge double layers affect fuel cells. A suggested approach by Larminie and Dicks (2003) is reviewed in the following paragraphs.

As described in section 2.1.1, electrons in a fuel cell will flow from the anode through an external load, and collect at the surface of the cathode electrode. The protons will flow through the electrolyte membrane towards the cathode electrode. At the interface between the cathode electrode and the membrane, there will therefore be two charged layers meeting with opposite polarity as showed in figure 2.6. Such layers can store energy and behave much like electrical capacitors. The capacitance of such a capacitor is given by:

$$C = \epsilon \frac{A}{d} \quad (2.34)$$

where ϵ is the electrical permittivity, A is the surface area of the layer and d is the distance between the layers. As the separation between the layers is typically in the order of nanometers, and the surface area of the layers is much bigger, the capacitance is normally very large. Commonly, the magnitude of the capacitance can be up to few Farads, which is considered to be a quite high capacitance value.

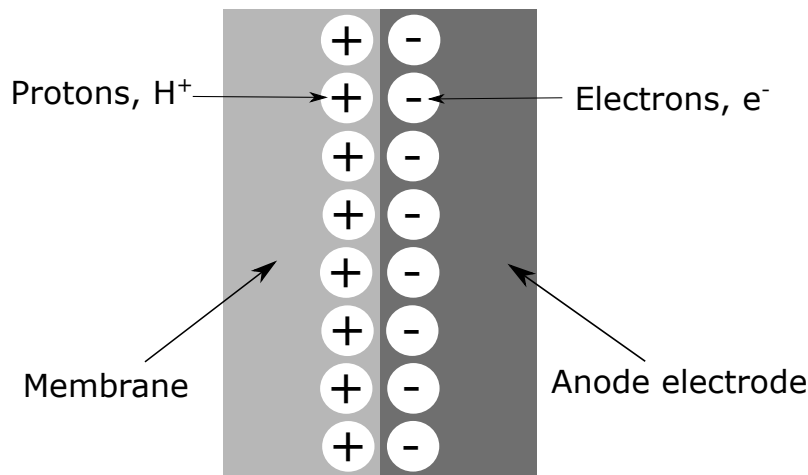


Figure 2.6: The charge double layer at the interface between the membrane and cathode electrode

Most literature describing the phenomenon, suggest that the double layer charge effect can be modelled by use of equivalent electrical circuits, with the charge double layer represented by an electrical capacitor. However, the presented models vary slightly. Larminie and Dicks (2003) propose that the double layer effect will affect the activation losses in the fuel cell. As it is described in section 2.1.4, the activation losses are voltage changes at the electrodes which must exist in order to drive the fuel cell reaction. The build-up of charges at the double layer will generate an electrical voltage, and therefore change the voltage at the electrodes. Indeed, Larminie and Dicks (2003) claim that the double layer is the actual source of the activation losses, and that double layers are therefore necessary in order for the fuel cell reaction to occur. It is suggested an equivalent electrical circuit representing this effect, which is redrawn in figure 2.7a. In this model, R_{ohmic} is the ohmic resistance [Ω], while R_{act} is the equivalent resistance associated with activation losses, such that:

$$R_{act} = \frac{V_{act}}{I} \quad (2.35)$$

The current drawn by the capacitor and the voltage over the parallel circuit in figure 2.7a are given by the following equations:

$$I = C \frac{dV}{dt} \quad (2.36)$$

$$V_C = \left(I - C \frac{dV_C}{dt} \right) R_{act} \quad (2.37)$$

The overall dynamic voltage is therefore given by:

$$V_{out} = E_{OCV} - V_C - V_{ohmic} \quad (2.38)$$

Note that the concentration losses are not included in this electrical circuit. This is probably because it is stated in the same book that concentration losses can be neglected in many cases.

Another book that suggests a modelling approach for the charge double layer effect, is Nehrir and Wang (2009). It is here claimed that the double layers also will affect the concentration losses in the fuel cells. The argument for this is that the potential in the double layers will affect the reaction rates, which will further affect the concentrations of the species in the fuel cells. The expression for the activation losses are also modified in the model. The activation losses are split into a sum of $V_{act,1}$ and $V_{act,2}$, where $V_{act,1}$ is only dependent on temperature and $V_{act,2}$ dependent on both temperature and current. It is assumed that only $V_{act,2}$ will be affected by the double layers. The equivalent electrical circuit for this approach is shown in figure 2.7b. The activation losses are here given semi-empirically by:

$$V_{act} = \underbrace{\eta_0 + (T - 298) \cdot a}_{V_{act,1}} + \underbrace{T \cdot b \ln I}_{V_{act,2}} \quad (2.39)$$

In this equation, η_0 , a and b are empirical constants which must be tuned to match each specific fuel cell polarization curve. The voltage over the parallel circuit in figure 2.7b is given by the following equation:

$$V_C = \left(I - C \frac{dV_C}{dt} \right) (R_{act,2} + R_{conc}) \quad (2.40)$$

where R_{conc} and $R_{act,2}$ again are the resistances associated with the concentration losses and the second activation losses ($V_{act,2}$). The overall dynamic voltage of the fuel cell can therefore be calculated by:

$$V_{out} = E - V_{act,1} - V_C - V_{ohmic} \quad (2.41)$$

It can be understood from equation 2.40 and 2.41 that the capacitor will have a delay effect on the fuel cell voltage when the fuel cell is exposed to current variations. If the current, I , is increased, the subtracting term V_C in 2.41 will also increase and decrease the overall voltage. However, the derivative of the voltage in equation 2.40 will always be of different sign than the current and therefore counteract and reduce the effect of current changes. The same damping effect will occur when the current is decreased.

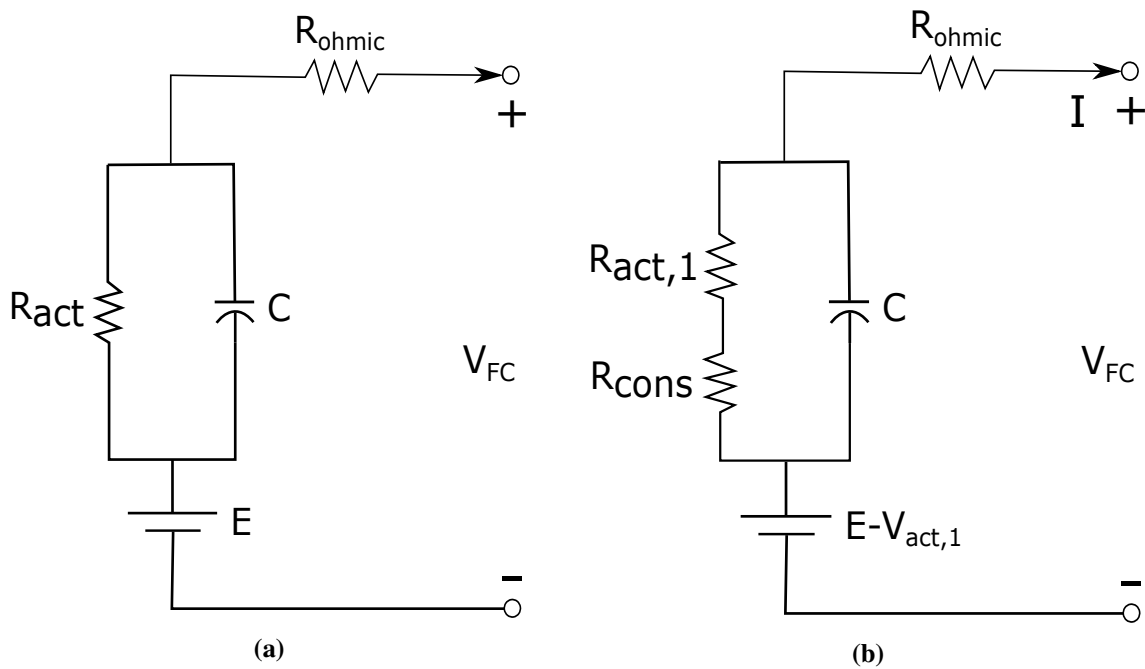


Figure 2.7: Equivalent electrical circuits describing the charge double layer effect, presented by (a) Larminie and Dicks (2003) and (b) Nehrir and Wang (2009)

Temperature Changes

Several of the equations listed so far in this text have shown that fuel cell performance depends on the temperature. As it will be further outlined in section 2.1.8, fuel cells will under operation produce waste heat which varies with the loading. Further, the materials in fuel cells and eventual cooling equipment will in reality also have a certain thermal inertia, such that the temperature in fuel cells will in operation in dynamic environments most probably not remain constant. Some works have attempted to make a thermal sub-model accounting for these variations (Nehrir and Wang, 2009; del Real et al., 2007). Typically, this is obtained by applying a heat balance for the entire fuel cell stack, which calculates the temperature. However, depending on how the modelling is performed, this generally requires considerably more information about the stacks (e.g. materials, cooling medium, component dimensions etc.). A thermal model accounting for temperature changes is therefore considered beyond the scope for this work, and all temperatures are assumed to be constant.

2.1.7 Fuel Cell Efficiency

O'Hayre et al. (2016) suggest several ways of how to define the efficiency of a fuel cell. However, an easy definition of the efficiency of a fuel cell is the ratio between the usable energy produced and the total energy released when the fuel is consumed. Barbir (2013) present in chapter 3 a derivation of such an efficiency. The total fuel cell efficiency is divided into two different efficiencies, such that:

$$\eta_{FC} = \eta_{FC,V} \cdot \eta_{FC,F} \quad (2.42)$$

where $\eta_{FC,V}$ and $\eta_{FC,F}$ are referred to as the voltage and current efficiency, respectively.

Voltage Efficiency

The voltage efficiency is defined as the ratio between the usable electric energy produced by the fuel cell and the total energy released in the fuel cell. The electric power output from a fuel cell is given by:

$$P_{FC} = IV_{FC} \quad (2.43)$$

Further, the molar consumption of hydrogen in a fuel cell is determined by Faraday's law of electrolysis:

$$N = \frac{I}{nF} \quad (2.44)$$

Because the molar quantity of energy released in a fuel cell is the reaction enthalpy, Δh [J/mol], the total energy release rate in a fuel cell is given by:

$$P_{total,FC} = \Delta \hat{h} \frac{I}{nF} \quad (2.45)$$

This yields the voltage efficiency of a fuel cell:

$$\eta_{FC,V} = \frac{P_{FC}}{P_{total,FC}} = \frac{IV_{FC}}{\Delta \hat{h} \frac{I}{nF}} = \frac{V_{FC}}{\Delta \hat{h}/nF} \quad (2.46)$$

However, which values of the reaction enthalpy should be used, is a subject of discussion. If the product water is in a liquid state, the reaction enthalpy will have a higher value than if the water is in vapor state. These two reaction enthalpies can be referred to as the higher and lower heating value (HHV and LHV). Accordingly, two different efficiencies are defined based on each of the reaction enthalpies.

$$\eta_{FC,V,HHV} = \frac{V_{FC}}{HHV/nF} \quad (2.47)$$

$$\eta_{FC,V,LHV} = \frac{V_{FC}}{LHV/nF} \quad (2.48)$$

Current Efficiency

In real fuel cells, some gaseous hydrogen and oxygen will diffuse through the Nafion membrane and not take part in the fuel cell reaction. This cross-permeation of gases will contribute to a decrease in the total fuel cell efficiency. In addition, there will be some internal currents in a fuel cell contributing to losses. The joint effect of these two losses is represented by the current efficiency, also known as the Faradaic efficiency. Barbir (2013) suggests the following definition of the current efficiency:

$$\eta_{FC,F} = \frac{i}{i + i_{loss}} \quad (2.49)$$

where i_{loss} is the current loss associated with the cross-permeation of gases and internal currents (Faradaic losses). This number has shown to be quite difficult to procure for individual fuel cell stack. However, it is further stated in Barbir (2013) that these losses are typically very low (order of few mA/cm^2) and are therefore only significant for very low current densities. During modelling of stacks, one should therefore be aware of the Faradaic losses, however one could in many applications neglect the contribution.

2.1.8 Waste Heat

In the previous sections, it has been presented how the reaction enthalpy of the fuel cell reaction (2.1) is transformed to electric power. This process is graphically illustrated in figure 2.8. Due to the reversible heat and different voltage losses, the waste heat release from a fuel cell is:

$$\dot{Q}_{wasteheat} = P_{total,FC} - P_{FC} \quad (2.50)$$

where $P_{total,FC}$ has previously been defined as the total energy release from the fuel cell, and P_{FC} is the electric power output. By use of this, it is derived in Larminie and Dicks (2003) a simple equation for calculating the waste heat as a function of the voltage efficiency:

$$\dot{Q}_{wasteheat} = P_{FC} \left(\frac{1}{\eta_{FC,V}} - 1 \right) \quad (2.51)$$

It was mentioned in section 2.1.7, that the voltage efficiency depends on the state of the product water, because this affects the reaction enthalpy change. Equation 2.51 therefore shows that the waste heat will also change according to the final state of the outlet water from the fuel cell. It must further be emphasized that equation 2.51 is the waste heat produced in the fuel cell reaction. As mentioned in section 2.1.6, there will be a certain thermal inertia in fuel cell stacks, and the instantaneous heat release from a fuel cell stack may therefore be different than the waste heat produced.

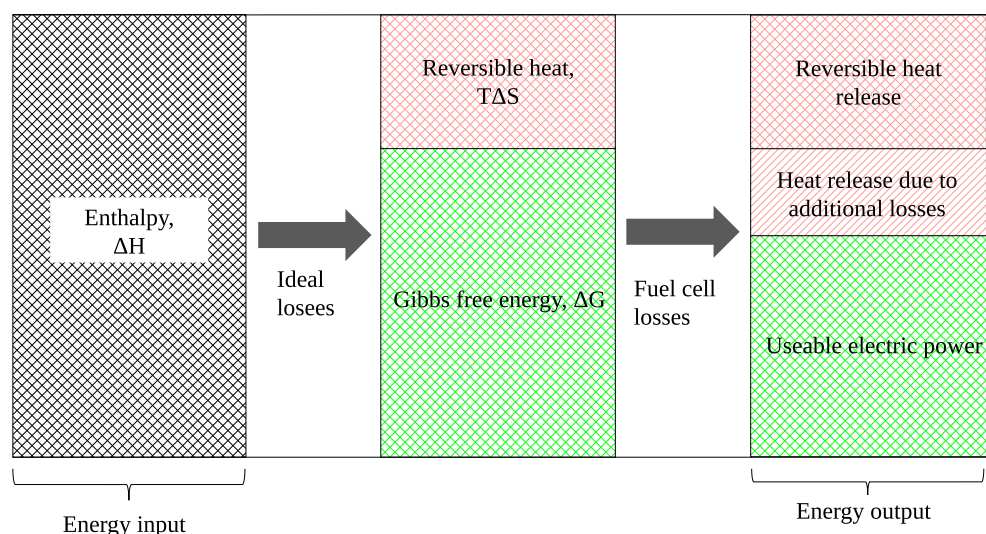


Figure 2.8: Graphical representation of energy conversion in fuel cells

2.2 Water Electrolysers

2.2.1 Introduction paragraph

A water electrolyser is a device that can produce hydrogen from water, by the use of electric energy. In an energy storage system where hydrogen is the energy carrier, the hydrogen could be produced in a variety of methods depending on the form of energy supplied by the energy source. For instance, if the energy source provides high temperature thermal energy, the hydrogen could be generated by thermolysis. Moreover, to store the energy from sunlight, hydrogen could potentially be produced by photoelectrolysis (Dincer and Acar, 2014). In the HES-OFF system, where the energy input is assumed to be solely electric energy, electrolysis is therefore chosen as the method of producing hydrogen.

Simplified, a water electrolyser can be considered as a reversed hydrogen fuel cell. Instead of producing energy by consuming hydrogen, the electrolyser produces hydrogen from water by consuming energy. The overall chemical reaction of a water electrolyser can therefore be written as:



Coutanceau et al. (2018) give a brief description of water electrolysers. Water electrolysers consist of the same fundamental components as the hydrogen fuel cells, namely two electrodes coupled together with an electrical conductor and separated by an electrolyte. Similar to fuel cells, electrolysers are classified according to which electrolyte is applied.

The three most common types are alkaline, polymer electrolyte membrane (PEM) and solid oxide (SO) electrolysers. Buttler and Spliethoff conducted in 2018 a study to investigate the current status of these three technologies. The alkaline electrolyser technology was found to be the most mature technology, reflected by the fact that these electrolysers have been commercially available for more than a century. Alkaline electrolysers exhibit the lowest specific investment and maintenance costs, and can offer the largest production capacities ranging up to several MWs per stack. Yet, the PEM electrolyser technology is under increasing development and several commercial stacks are now in the MW scale. PEM electrolysers commonly possess a more compact design and higher flexibility than alkaline electrolysers. However, this technology is generally more expensive than the alkaline technology, much due to the need of noble catalysts in PEM electrolysers. SO electrolysers are still not commercially realized, but are expected to feature higher efficiencies than the other technologies. In the framework of the HES-OFF project, weight and footprint of the electrolysers are of crucial importance, which is one of the reasons why PEM electrolysers are expected to be the best alternative for this application. The remaining parts of this thesis will therefore focus on PEM electrolysers.

2.2.2 PEM Water Electrolysers

Not surprisingly, the essential physical design of PEM electrolysers are very similar to PEM fuel cells. Indeed, Görgün (2006) claims that PEM electrolysers can be converted to fuel cells with only small alterations. Based on a drawing found in Grigoriev et al. (2006), figure 2.9 shows the principle of an electrolyser cell. The sandwich structure constituted by the electrodes and the membrane is again commonly known as the membrane electrode assembly (MEA) and is illustrated in figure 2.10. Carmo et al. reported in their study of current electrolyser technology in 2013, that similar membrane materials as for PEM fuel cells (commonly Nafion) is normally applied in PEM electrolysers. However, different materials are often used in the electrolyser electrodes. While platinum is the most used material for the cathode catalyst layer, iridium is frequently used in the anode catalyst layer, as this is found to have the best catalytic properties for the anode half-reaction. The remaining part of the electrode, which is commonly named the gas diffusion layer when speaking about fuel cells, are for electrolysers often referred to as current collectors. The majority of these components are either built of carbon or titanium. Similar to fuel cells, electrolysers can be scaled up by assembling several cells in electrolyser stacks.

2.2.3 Steady State Voltage

There are also similarities between PEM electrolysers and fuel cells when it comes to calculation of steady state voltage. Unfortunately, there are generally less books describing modelling of electrolysers. Yet the open literature agrees that the three main losses in electrolysers are the same as for fuel cells, namely the activation, ohmic and concentration losses (García-Valverde et al., 2012; Görgün, 2006; Awasthi et al., 2011; Lebbal and Lecœuche, 2009; Buttler and Spliethoff, 2018). Opposite from fuel cells, electrolysers

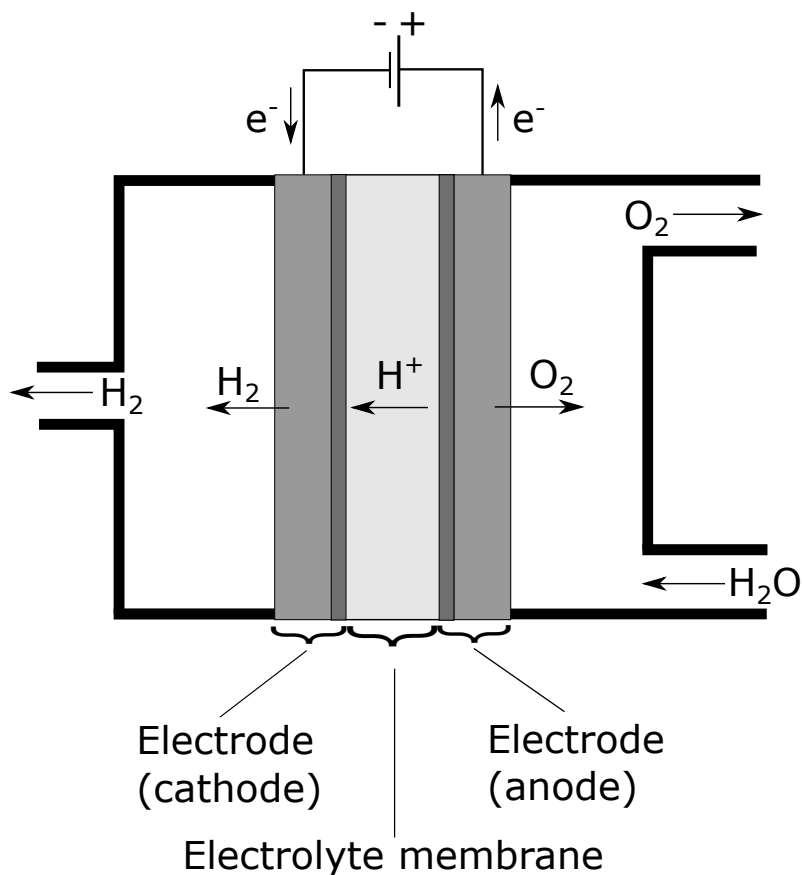


Figure 2.9: Simplified sketch of a PEM electrolyser cell

Membrane electrode assembly

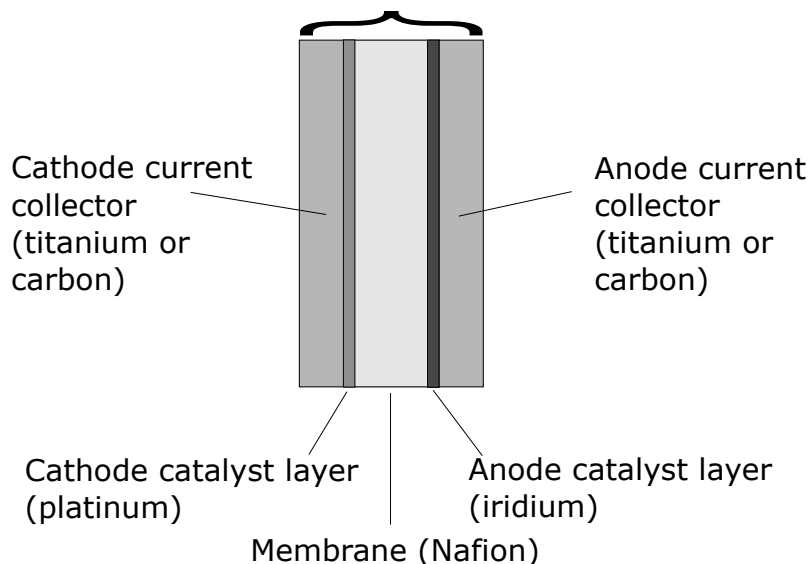


Figure 2.10: Simplified sketch the MEA used in electrolyzers. Typical materials applied are written in parentheses

have to overcome the voltage losses by compensating for an increased voltage. The input voltage for a PEM electrolyser is therefore given by:

$$V_{EL} = V_{OC,EL} + V_{act,EL} + V_{ohmic,EL} + V_{conc,EL} \quad (2.53)$$

where $V_{OC,EL}$ is the open circuit voltage obtained at zero current, and $V_{act,EL}$, $V_{ohmic,EL}$ and $V_{conc,EL}$ are the activation, ohmic and concentration losses, respectively. Hence, the only difference between the fuel cell voltage (equation 2.15) and electrolyser voltage, is the signs of the losses. Indeed, Tribioli et al. (2016) suggest that for reversible fuel cells (a fuel cell that could operate as both a fuel cell and an electrolyser), the losses and OC voltage could be calculated by the exact same equations in both operational modes. The literature differs slightly in how the open circuit voltage and the losses are calculated. The differences are in terms of which degree empirical approaches are applied due to simplicity reasons or lack of input parameters.

Electrolyser Open Circuit Voltage

The open circuit voltage, is the voltage in the electrolyser when the current is zero. As there are no losses in the electrolyser when there is no current, this voltage is often referred to as the reversible voltage. Görgün (2006) claims that this voltage can be calculated by the Nernst equation, an approach which is used by several articles (Lebbal and Lecœuche, 2009; Awasthi et al., 2011; Dedigama et al., 2014). Hence, the open circuit voltage is given by:

$$V_{OC,EL} = E^0 + \frac{RT}{nF} \ln \left(\frac{a_{H_2} a_{O_2}^{1/2}}{a_{H_2O}} \right) \quad (2.54)$$

where a_{H_2} , a_{O_2} and a_{H_2O} again are the chemical activities of hydrogen, oxygen and water, R is the universal gas constant, T is the cell temperature, n is the stoichiometric coefficient, F is Faraday's constant and E^0 is the standard potential given by:

$$E^0 = \frac{\Delta \hat{g}^0}{nF} \quad (2.55)$$

$\Delta \hat{g}^0$ is further the Gibbs free energy of reaction 2.52 given at standard conditions. Similar as for fuel cells, the activities a_{H_2} , a_{O_2} and a_{H_2O} are difficult to determine, and empirical configurations are typically applied to equation 2.54. For simplicity, the same approach which was used for fuel cells in section 2.1.4 (equation 2.11) is later in this work applied also for electrolysers.

Losses

Lebbal and Lecœuche (2009) suggest applying the following equations for calculations of the activation, ohmic and concentration losses, respectively:

$$V_{act,EL} = \frac{RT}{\alpha nF} \ln \left(\frac{i}{i_0} \right) \quad (2.56)$$

$$V_{ohmic,EL} = ir_{ohmic} \quad (2.57)$$

$$V_{conc,EL} = \frac{RT}{nF} \left(1 + \frac{1}{\alpha}\right) \ln \left(\frac{i_L}{i_L - i}\right) \quad (2.58)$$

These are the same equations suggested in section 2.1.4 for the equivalent losses in fuel cells, and the parameters also have the same physical interpretation. Lebbal and Lecœuche (2009) also suggest using equation 2.21 for calculation of the area specific ohmic resistance, r_{ohmic} . The approach of employing these equations for the losses was also used in 2006 by Görgün and later by García-Valverde et al. in 2012. Similarly as for a fuel cell, the voltage can be plotted towards current density in a polarization curve, which is shown in figure 2.11.

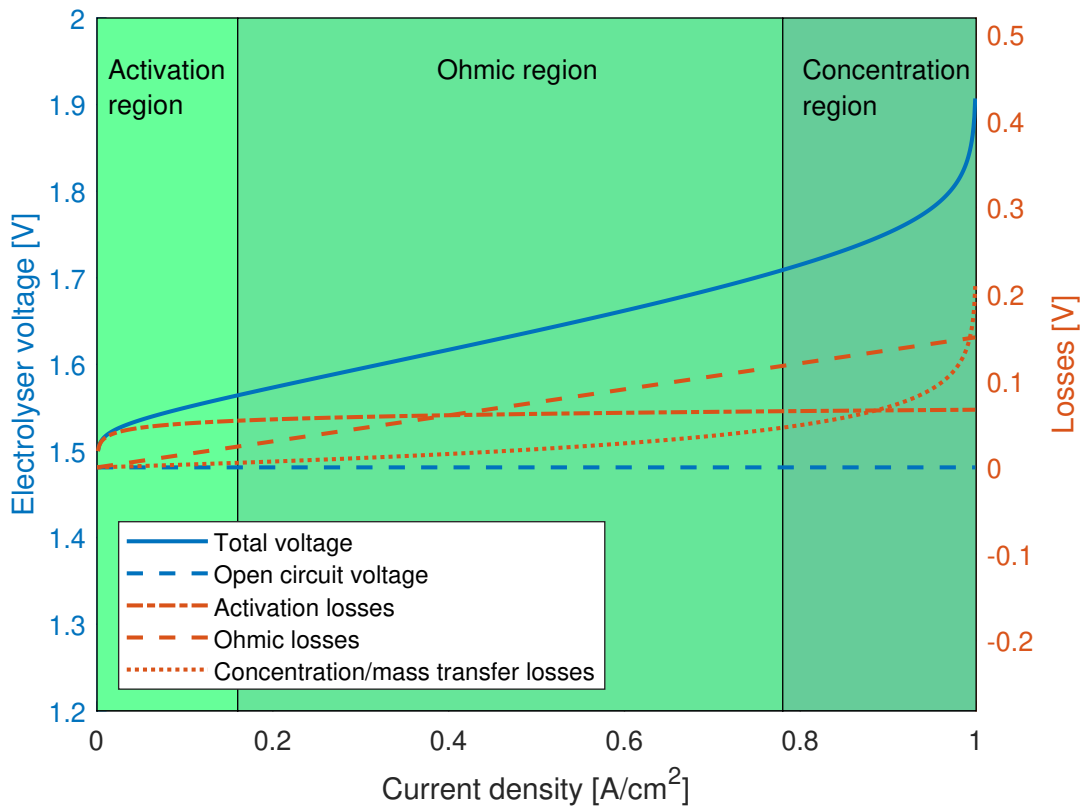


Figure 2.11: Example of polarization curve including losses for an electrolyser

2.2.4 Electrolyser Dynamics

Due to the fact that PEM electrolyzers are essentially very equal to PEM fuel cells, it is reasonable to believe that they will obey many of the same dynamic behaviours. However, far less research have unfortunately been conducted on electrolyser modelling than on fuel cell modelling. There is therefore in this work not found any sufficient models

for electrolyser dynamics. Instead, the dynamic behaviours of electrolyser systems are to some degree accounted for by modelling of transients in balance of plant equipment described in section 2.4.

2.2.5 Electrolyser efficiency

The electrolyser efficiency can in the same way as fuel cell efficiency be divided into voltage and current efficiency:

$$\eta_{EL} = \eta_{EL,V} \cdot \eta_{EL,F} \quad (2.59)$$

Voltage Efficiency

The electrolyser voltage efficiency can be defined as the ratio between the energy stored in the products and the energy used by the electrolyser. The electric power input of an electrolyser can be calculated in the same way as the electric power output of a fuel cell:

$$P_{EL} = IV_{EL} \quad (2.60)$$

The energy stored in the products of an electrolyser is the amount of energy which is released from the reactants in a fuel cell. Hence,

$$P_{stored,EL} = P_{total,FC} = \Delta\hat{h} \frac{I}{nF} \quad (2.61)$$

Thus, for a similar approach as for fuel cells, the electrolyser voltage efficiency can be derived as:

$$\eta_{EL,V} = \frac{P_{stored,EL}}{P_{EL}} = \frac{\Delta\hat{h} \frac{I}{nF}}{IV_{EL}} = \frac{\Delta\hat{h}/nF}{V_{EL}} \quad (2.62)$$

Again, it can be discussed whether the higher or lower heating value should be used for $\Delta\hat{h}$. However, Selamet et al. (2011) assert that most scientific researches calculate the electrolyser efficiency based on the higher heating value.

Current Efficiency

Also in electrolysers, there will in reality be a diffusion of hydrogen and oxygen through the electrolyte membrane, in addition to internal currents. This will contribute to a lower hydrogen production than what is theoretically possible to achieve given by the current and voltage. The current (Faradaic) efficiency associated with this is suggested by Barbir (2005) to be:

$$\eta_{FC,F} = \frac{i - i_{loss}}{i} \quad (2.63)$$

Similar as for fuel cells, it is for electrolysers stated in Barbir (2005) that the cross over of gases and internal currents will have a very small effect except at low current densities.

2.2.6 Waste heat

Due to the irreversibilities, electrolyzers will also generally release waste heat. With reference to the terms outlined in the previous section, the heat will be equal to the difference between the electric power input to the electrolyzer and the energy stored in the hydrogen produced:

$$\dot{Q}_{EL} = P_{EL} - P_{stored,EL} \quad (2.64)$$

In terms of voltage efficiency, equation 2.64 can be rewritten as:

$$\dot{Q}_{EL} = P_{EL} (1 - \eta_{EL,V}) \quad (2.65)$$

2.3 Hydrogen Stored as Compressed Gas

A method for storing hydrogen is by compressing the gas and storing it in cylindrical tanks. This is a rather simple method, where the hydrogen can be stored at an indefinite time with no purity limits. There are also several other methods for storing hydrogen, with different features. The general distinction between the methods is made upon whether the hydrogen interacts with the storage medium or not (Zohuri, 2019; Sherif et al., 2016). When stored as a compressed gas, the hydrogen will desirably not react with the material in the storage tank. Other examples of such physical storage is hydrogen stored as a cryogenic liquid, where the hydrogen exhibit a high volumetric density Dicks and Rand (2018). Oppositely, hydrogen stored in metal hydrides is an example of a storage method where the hydrogen reacts with the storage material. This particular storage method offer the advantage of safety, as it does not require any high pressures (Boudellal, 2018). However, for simplicity, only compressed gas storage will be considered further in this work.

2.3.1 Practical Aspects

At atmospheric pressure and temperature, hydrogen possesses a high specific energy, while a very low volumetric energy density. This means that when storing energy in hydrogen, the gas would be very light weight, yet occupy a large volume. This is inconvenient for applications where physical footprint is a critical parameter. By compressing the gas, the volumetric energy density will increase. Typical storage pressures vary between 20 and 70 bars. Unfortunately, the compression process is quite energy consuming, and often require energy between 5 and 15% of the higher heating value when using conventional compressor technology (Dicks and Rand, 2018).

2.3.2 Equation of State for Gaseous Hydrogen

An equation of state for a gas, is a mathematical relationship between different properties of the gas, for example pressure, temperature and specific volume. The equation of state

for compressed gaseous hydrogen is discussed in Klell (2010). The discussion is summarised below.

A gas is termed ideal, if it follows the assumptions that the gas molecules are infinitesimally small, round and hard spheres which occupy a negligible volume. Further, there must not exist any forces between the molecules except the ones occurring during collisions. The gas will then obey the ideal gas law given by:

$$PV = NRT \quad (2.66)$$

where P is the gas pressure, V is the volume, N is the amount substance, R is the universal gas constant and T is the gas temperature.

However, the assumptions for the ideal gas law are not valid for gases at all conditions. A method of evaluating the assumptions is to calculate the compressibility factor:

$$Z = \frac{PV}{NRT} \quad (2.67)$$

It can be noticed that a compressibility factor of 1 would turn equation 2.67 into the ideal gas law (equation 2.66), and any deviations from 1 would imply that the gas does not perfectly follow the assumptions. For a given pressure, volume and temperature, it can be shown that the compressibility factor is the ratio between the mass calculated by the ideal gas law and the real mass in the system:

$$Z = \frac{m_{ideal}}{m_{real}} \quad (2.68)$$

Conveniently, the compressibility factor has already been found experimentally for several conditions and is plotted in charts. One such chart is redrawn in figure 2.12. By use of equation 2.68, figure 2.12 can therefore be used to estimate the errors the ideal gas law gives for calculations of the mass. According to the figure, the deviation is approximately 20% at 300 K and 300 bar, while at 300 K and 600 bar the deviation is approximately 40%. At low pressures, the error is much smaller. By applying the ideal gas law, it must therefore first be determined which accuracy is demanded for the calculations.

If the ideal gas law is found insufficient, Klell (2010) suggests the following modified correlation, termed the van der Waals equation. This accounts for intermolecular forces and molecular volume:

$$\left(P + \frac{a}{(V/N)^2} \right) \left(\frac{V}{N} - b \right) = RT \quad (2.69)$$

where $a = 0.025 \text{ m}^6 \text{ Pa/mol}^2$ and $b = 2.66 \cdot 10^{-5} \text{ m}^3/\text{mol}$ for hydrogen. Figure 2.13 shows the mass plotted against pressure for a volume of 1 m^3 at 300 K , using the ideal gas law and van der Waals equation, respectively.

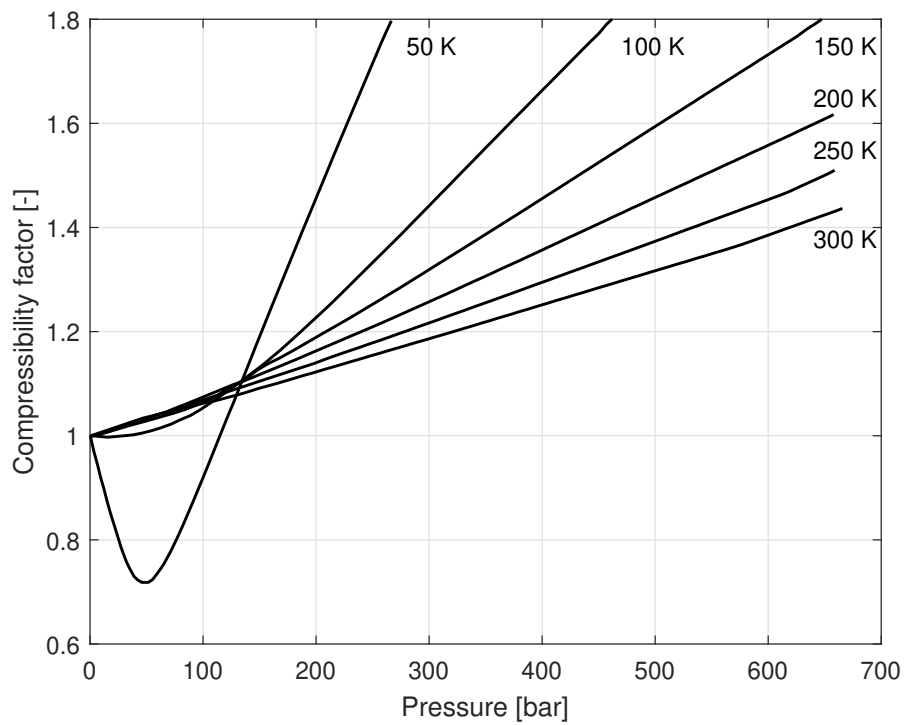


Figure 2.12: Compressibility chart for gaseous hydrogen, redrawn from Klell (2010)

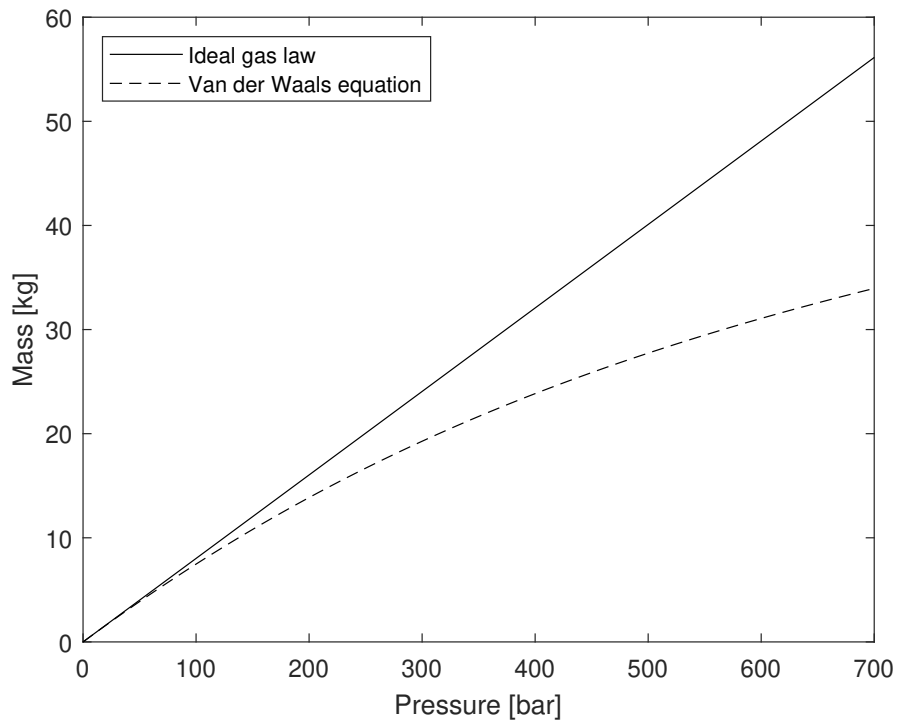


Figure 2.13: Mass calculated by the ideal gas law and the van der Waals equation, for a volume of 1 m^3 at 300 K

2.4 Balance of Plant Components

In order to operate fuel cell and electrolyser stacks, a set of supporting systems are required. The components comprising these system are commonly referred to as Balance of Plant (BoP) components. These systems also accomplish that the fuel cells and electrolysers are run at the desired optimized conditions. This section will first shortly outline the duties of the BoP components fuel cell and electrolyser systems. Further it will describe the most typical BoP components implemented in existing systems.

Figure 2.14 shows the requirements of a fuel cell stack, and is based on chapter 9 in Barbir (2013). Hydrogen and air have to be fed to the fuel cell at certain temperatures, pressures and humidity levels. The product water must further be removed. Moreover, the waste heat produced in the process needs to be removed in adequate rates. The DC-electricity produced must also be treated to be of the demanded quality. To increase the fuel utilization, many systems integrates a re-circulation loop of hydrogen from the cathode to the anode. Hydrogen may occur at the cathode due to diffusion of hydrogen through the electrode membrane or unwanted flow of hydrogen through holes as result of inaccurate machining. Similarly, figure 2.15 shows the required operating conditions for electrolysers, and is based on chapter 4 of Boudellal (2018). For simplicity, it is only considered hydrogen storage as compressed gas in this work. Storing hydrogen in different forms like liquefied gas or metal hydrides would require different BoP components.

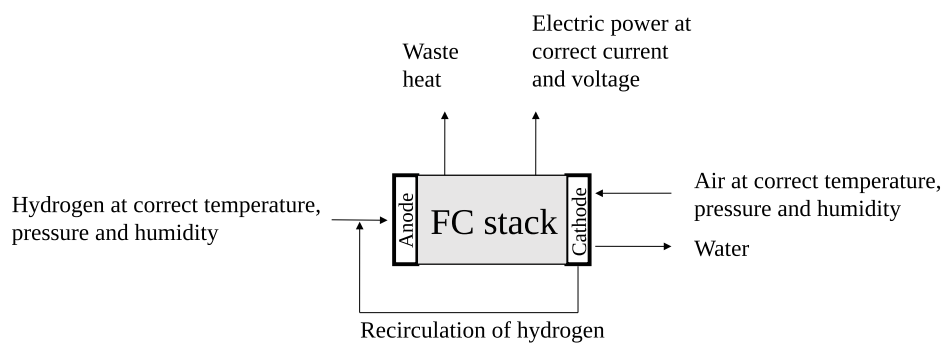


Figure 2.14: Material and energy flows in and out of fuel cell stacks

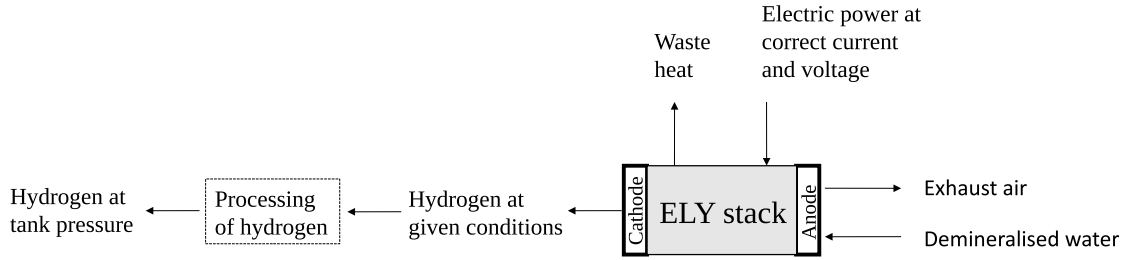


Figure 2.15: Material and energy flows in and out of electrolyser stacks

2.4.1 Air Compression Unit

Compressors can be used to elevate the pressures of gas streams. The role of compressors in fuel cell systems is often very essential, and is described in chapter 9 of Barbir (2013). The description is summarised below.

In fuel cell systems, the pressure of the inlet hydrogen and air streams will have an important significance on the fuel cell performance. It is therefore crucial that the inlet gases are compressed to the desired pressure. In many applications, hydrogen is stored at a higher pressure than the inlet pressure to the fuel cell, hence the pressure of the hydrogen stream has to be lowered in an expander or similar device and not compressed to a higher pressure. On the other side, the air stream is normally initially at atmospheric pressure, and must in most applications be pressurised. This pressure rise is commonly obtained by a compressor which increases the gas pressure by applying a mechanical work. The compressor is run by an electric motor, which therefore represents a power loss or a parasitic load. If the fuel cell is operated at atmospheric inlet pressure on the air stream, the compressor could be replaced by a fan or a blower to feed the fuel cell stack.

For an adiabatic compressor working with ideal gases, the power consumption and outlet temperature can be calculated by:

$$W_{comp} = \frac{\dot{m}c_p T_{in}}{\eta_{comp}} \left[\left(\frac{P_2}{P_1} \right)^{\frac{\kappa-1}{\kappa}} - 1 \right] \quad (2.70)$$

$$T_{out} = T_{in} + \frac{T_{in}}{\eta_{comp}} \left[\left(\frac{P_2}{P_1} \right)^{\frac{\kappa-1}{\kappa}} - 1 \right] \quad (2.71)$$

In these equations \dot{m} is the mass flow, c_p is the specific heat capacity, T_{in} is the inlet temperature, η_{comp} is the compressor efficiency, P_{in} is the inlet pressure, P_{out} is the outlet pressure and κ is the heat capacity ratio. Barbir (2013) validates that the assumptions of adiabatic compression and ideal gas are valid for the compression of air up to normal fuel cell operating pressures.

2.4.2 Hydrogen Compression Unit

The hydrogen compression unit is responsible of compressing the outlet hydrogen from the electrolyser, to the storage pressure. Sdanghi et al. performed a review of state of the art technology for hydrogen compression in 2019. The compressors were divided into two categories; Mechanical compressors and non-mechanical compressors. In this work, mechanical compressors will primarily be treated. Additionally, in the collaboration in the HES-OFF project, electrochemical compression has been an interesting discussion topic. Therefore, a section is also dedicated to the basic principles of this.

Mechanical Compression

Mechanical compressors are based on the principle of compressing gas by applying a mechanical work. For hydrogen compression, the most common category of compressors is positive displacement compressors. Here, the compression is obtained by mechanically reducing the volume of a chamber containing hydrogen. The compression can be performed by only one compressor (single-stage), or by several compressors arranged in series (multi-stage). (Sdanghi et al., 2019)

The specific mechanical work required to compress a gas at the instantaneous specific volume v from pressure p_1 to p_2 is given by (Klell, 2010):

$$w = \int_{p_1}^{p_2} v dP \quad (2.72)$$

In the modelling of the hydrogen compressor work, it must therefore be determined which equation of state is to be used. This depends on the accuracy demanded. It was mentioned in section 2.3.2 the ideal gas law gives relatively large errors when applied to high pressure hydrogen. Nevertheless, some learning books (Klell, 2010; Larminie and Dicks, 2003) suggest to use the ideal gas law in the calculation of compressor work (equation 2.72). This approach yields the following integral:

$$w = \int_{p_1}^{p_2} \frac{RT}{M_m P} dP \quad (2.73)$$

Dicks and Rand (2018) state that the hydrogen compression process will probably be implemented as multi-stage process. In that case, it is written in Burheim (2017) that the compression process is close to isothermal. The specific compression work can then be calculated as:

$$w = \frac{RT}{M_m} \ln \left(\frac{P_2}{P_1} \right) \quad (2.74)$$

To obtain the overall ideal compressor power, the compression work is multiplied with the mass flow:

$$W_{compressor,ideal} = \dot{m} \cdot w \quad (2.75)$$

All real compressors will further be affected by certain losses, represented by the compressor efficiency η_{comp} . Sdanghi et al. (2019) state that this efficiency typically lies in the range of 50-85% for mechanical compressors. By means of the efficiency and equation 2.74 and 2.75, the real compressor power can be given by:

$$W_{compressor} = \frac{1}{\eta_{comp}} \dot{m} \cdot \frac{RT}{M_m} \ln \left(\frac{P_2}{P_1} \right) \quad (2.76)$$

Electrochemical Compression

Electrochemical compressors are described in Sdanghi et al. (2019) as an innovative device with several advantages. The following paragraphs summarises the brief description.

Electrochemical compressors are very similar to PEM fuel cells and electrolyser, and consist of an electrolyte membrane surrounded by electrodes (figure 2.16). Low pressure hydrogen is fed to the compressor anode, and split into protons and electrons. The protons flow through the membrane, while the electrons are forced through an external circuit due to an electric driving force. At the cathode, the protons and electrons will reform to gaseous hydrogen, where the pressure depends solely on the voltage supplied to the compressor.

In terms of modelling, the electrochemical compression follows the same principles as fuel cells and electrolyzers. The voltage is determined by the Nernst equation, and modified according to different losses. The current and mass flow are correlated by Faraday's law.

Sdanghi et al. (2019) refer to research showing that electrochemical compression can be much more energy efficient than mechanical compression at moderate discharge pressures (less than approximately 20 bar). At a discharge pressure up to 20 bar, an electrochemical compressor showed to use approximately 70% less energy than a conventional mechanical compressor. However, at higher pressures, the electrochemical compressors seem to suffer from large diffusion rates of hydrogen through the electrolyte membrane, resulting in severe losses. It was therefore concluded that the technology is not yet convenient for very high discharge pressures.

Due to time limitations, electrochemical compressors will not be treated further in this work. Neither will such devices be implemented in the developed model presented later. However, a more comprehensive analysis is suggested as further work for the modelling activity in framework of the HES-OFF project, as this has been discussed as a promising technology.

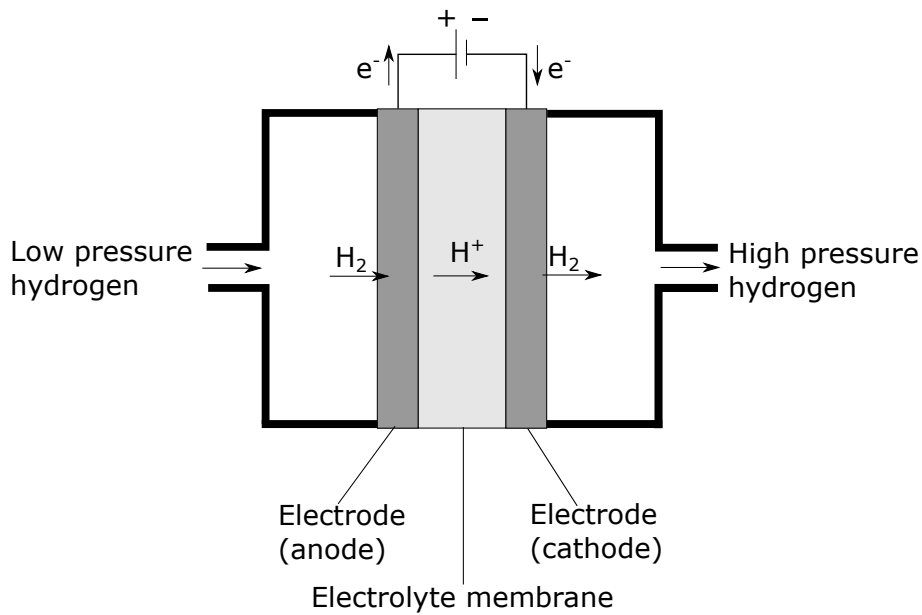


Figure 2.16: Simplified sketch of an electrochemical compressor

2.4.3 Ejectors

Ejectors are devices which use a high pressure gas stream to provide suction and compression of a low pressure stream. These are therefore well suitable to drive the hydrogen re-circulation loop by use of high pressure hydrogen from the storage tank (Barbir, 2013). The ejector technology is well known in the process industry. A description of the working principles can be found in chapter 8 in Coker (2007), and is summarised below.

A general ejector is illustrated in figure 2.17. This consists of a nozzle, suction zone, supersonic diffuser, diffuser throat and subsonic diffuser. High pressure gas (primary flow) enters the nozzle and is accelerated to supersonic speed because of the convergent-divergent design. At the end of the nozzle, this flow will be of the same low pressure as the secondary flow. In the suction chamber, the high velocity primary flow is mixed with the slow secondary flow. In the mixing, the primary flow will be decelerated while the secondary flow will be accelerated. This results in a suction of the secondary flow. The mixed flow will be of supersonic speed, and will therefore undergo a deceleration and pressure rise through the three remaining parts. Because the suction of the secondary flow is dependent on the primary flow, the mass flow of the secondary flow can be controlled by controlling the original pressure of the primary flow.

In a fuel cell, ejectors can therefore be placed prior to the stack inlets to drive the hydrogen re-circulation. The primary flow is then the high pressure gas from the storage tanks, while the secondary flow is the hydrogen from the re-circulation loop. The re-circulation is therefore driven by the suction that the secondary flow experiences in the ejector. This is shown in figure 2.18, which is redrawn from Barbir (2013). By use of ejectors, the

hydrogen re-circulation is therefore driven for free, because the high pressure hydrogen in the storage tanks normally has to be expanded before entering the stacks anyway.

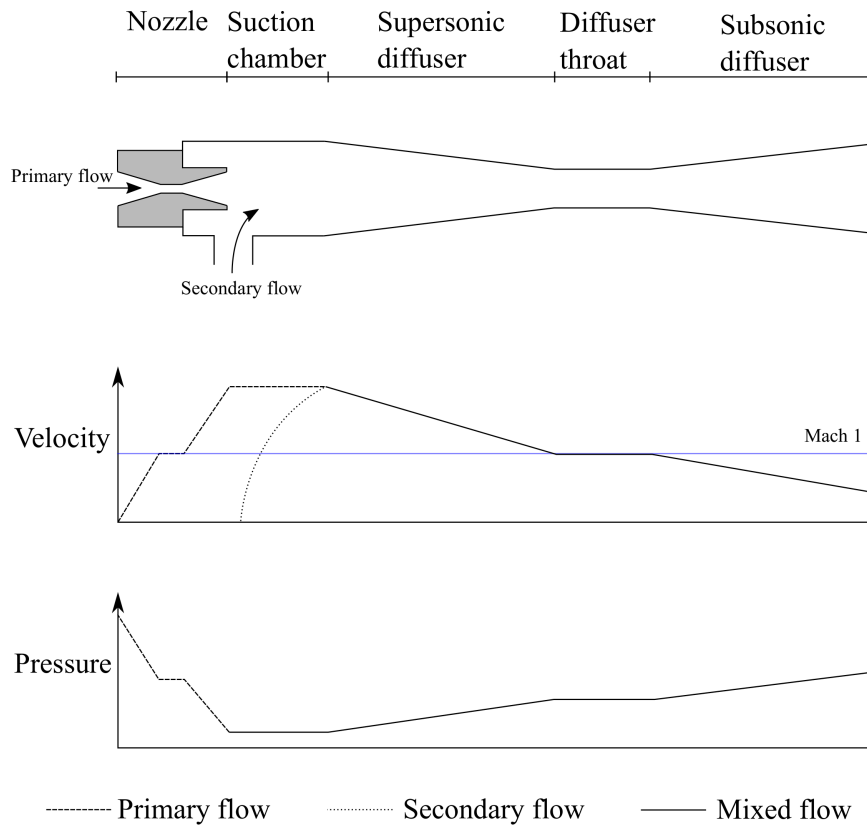


Figure 2.17: Sketch of an ejector with pressure and velocity diagrams. Redrawn from Coker (2007)

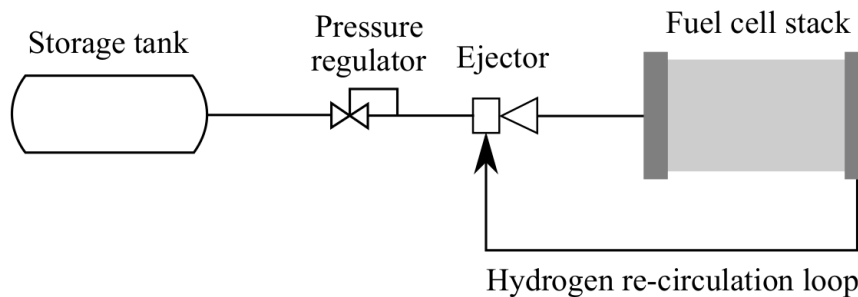


Figure 2.18: Hydrogen supply system with ejector. Redrawn from Barbir (2013)

2.4.4 Heat Exchangers

Heat exchangers are devices used to exchange heat from one medium to another. In fuel cell and electrolyser systems there are several components which need heating or cooling to maintain a somewhat constant temperature. As it has been shown in the previous sections, the temperature have several impacts on the fuel cell and electrolyser performance. Heat exchangers can therefore play an important role in such systems. Stacks, compressors, pumps and other units may need cooling, while the gas flow may need heating. To save energy and increase the overall efficiency, Barbir (2013) chapter 9 states that it is common to transfer heat between different components in systems. The gas streams can for example be heated by the waste heat from the fuel cells, and vice versa. In this way, the need for external heat sources is reduced.

Barbir (2013) further shows that thermal management systems can be designed in several ways. Moreover, any textbook of basic heat and mass transfer can show that heat exchangers can be designed in a variety of ways. All this is beyond the scope of this work. Heat exchangers will rather be modelled by the following simple expression for heat transfer, which can be derivated from the theory in any textbook of basic thermodynamics, for example Moran et al. (2015):

$$Q = \dot{m} \cdot c_p | (T_{in} - T_{out}) | \quad (2.77)$$

where \dot{m} is the mass flow of the heated/cooled medium, c_p is the specific heat capacity of the medium, T_{in} is the inlet temperature of the medium and T_{out} is the outlet temperature of the medium. To obtain equation 2.77, it is assumed constant pressure through the heat exchanger and negligible changes in kinetic and potential energy.

2.4.5 Humidifiers

Humidification devices are normally installed various places in fuel cell systems to obtain good hydration conditions in fuel cells. This is important, as a good hydration will lower the ohmic losses in the fuel cell, while at the same time contribute to less degradation (section 2.1.4 and 2.5.1). The humidity is increased by adding water vapor to the system (see equation 2.20). This can be achieved by hydrating the inlet gas streams to the fuel cell stacks. Hydration of the hydrogen stream will prevent electroosmotic drag from drying out the anode side of the membrane. Hydration of the air stream will prevent excess of dry gas in the cathode, which can remove water at a higher rate than what is generated by the fuel cell reaction and dry out the membrane Barbir (2013). The humidification of the gas streams can be performed in a variety of methods. Among these are bubbling, direct water injection and use of mass exchangers. Humidification can also be obtained without any humidification device, but rather by special operating strategies which will self-humidify the fuel cell. A description of these methods can be found in Barbir (2013) chapter 3, and is summarised in the following paragraphs.

Bubbling

In a bubble humidifier, gas is bubbled out of a pipe lowered in heated liquid water. The gas fed into the water will rise to the liquid surface and in this process be humidified controlled by the temperature of the water. The humidifier must be designed such that the outlet gas stream does not carry water droplets. Due to its large sizes and difficulties of designing an efficient device, this type of humidifier is rarely used in commercial fuel cell systems, but rather in laboratory test rigs.

Direct Water Injection

Humidification by direct water injection, is a method where water is sprayed into the gas streams as a fine mist. The large contact area constituted by the droplets will ease evaporation of the water. The heat of evaporation has to be supplied to the humidifier. This heat is often of a small magnitude, and is normally taken from the heat loss caused by the fuel cells or compressors. The water stream could eventually be injected as steam to eliminate the need for additional heat supply, but this would further require the availability of steam.

Mass exchangers

A mass exchanger is a device that can transfer mass from one medium to another. In fuel cell systems, such units can exchange water from the cathode exhaust to the inlet air stream. This is obtained through a water-permeable medium which can be either a porous plate or a membrane such as Nafion.

Self Humidification

By short-circuiting the stacks, the membranes in the fuel cells can be self-humidified without humidifying the gas streams. The short-circuiting generates additional water in the fuel cell reaction on the cathode side, which will diffuse through the membrane and make it humid. By use of this method, there is therefore no need for external humidifiers.

2.4.6 Turbines

If air is supplied in excess to a fuel cell, Barbir (2013) explains that turbines may be used to harvest energy from the exhaust air. The same book shows that the energy which can be extracted by expansion in these turbines from fuel cell exhaust pressure, P_{out} , to ambient pressure, P_0 , is given by:

$$W_{exp} = \dot{m}_{air,out} \cdot c_p \cdot T_{out} \left[1 - \frac{P_0}{P_{out}}^{\frac{k-1}{k}} \right] \quad (2.78)$$

The energy from these turbines can for example be used to run the air compressors. This was done in the EVERYWHERE project, where the aim was to develop a 100 kW single

stack fuel cell system by use of the PowerCell S3 stack. Here, the turbine was directly mounted to the air compressor and therefore worked as a turbocharger to the compressor. It was asserted that this turbine could produce almost half of the energy consumed by the air compressor (PowerCell Sweden AB, 2018). However, to model the energy produced by these turbines in further detail, it is required to know the utilization of air fed to the fuel cell and conditions of the exhaust. These are numbers which can be difficult to access for different stacks without performing own test.

2.4.7 Hydrogen Purification System

The gaseous hydrogen produced by electrolyzers has to be purified before it is being stored and further reused as fuel in fuel cells. This is described in Boudellal (2018), and summarised below.

In the electrolyzers, a certain amount of oxygen will diffuse through the electrolyte membrane and mix with the hydrogen produced at the cathode. Moreover, due to the humid conditions in an electrolyser, the hydrogen gas produced will contain a certain amount of water. Therefore, the hydrogen must be both deoxidised and dried. These processes can be obtained in two separate units (deoxidiser and dryer) or as one combined purification unit.

Regardless of how the purification is obtained, García-Valverde et al. (2012) suggest that the purification system can introduce a dynamic behaviour to the electrolyser system. The purification will take a certain amount of time, and under variations in production, this can be observed to induce a time lag to the mass flow. It is further proposed that this time lag can be modelled as a first order delay, where the time constant has to be found experimentally. The time lag can be represented by a Laplacian block diagram, and is redrawn from García-Valverde et al. (2012) in figure 2.19.

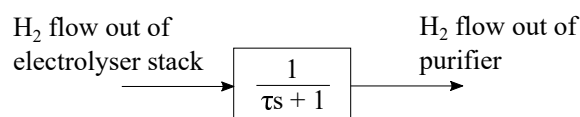


Figure 2.19: Laplacian block diagram of the time delay due to the purification system

2.4.8 Power Electronics

Power electronics is a collective noun representing equipment which controls and converts electricity to a desired condition. In fuel cell systems this is often employed to transform intermittent direct current (DC) to stable alternating current (AC). Similarly, power electronic devices are used to transform AC power to varying DC power in electrolyser systems. It is important to emphasise that power electronics is a comprehensive subject, and a detailed analysis would be far beyond the scope of this work. The following section will therefore only touch slightly into the main components of power electronics

used in fuel cell and electrolyser systems. In the end, it will give a suggestion for how power electronics can be modelled very simple in terms of efficiency.

Buck and Boost Converters

Buck and boost converters are components which can convert DC to respectively lower or higher voltage, and is described briefly in Barbir (2013) chapter 9. The same book provides a graphical presentation of how these converters can be exploited in fuel cell systems, and is redrawn in figure 2.20. Because the components converts DC to another DC, these components are commonly marked DC/DC in system drawings.

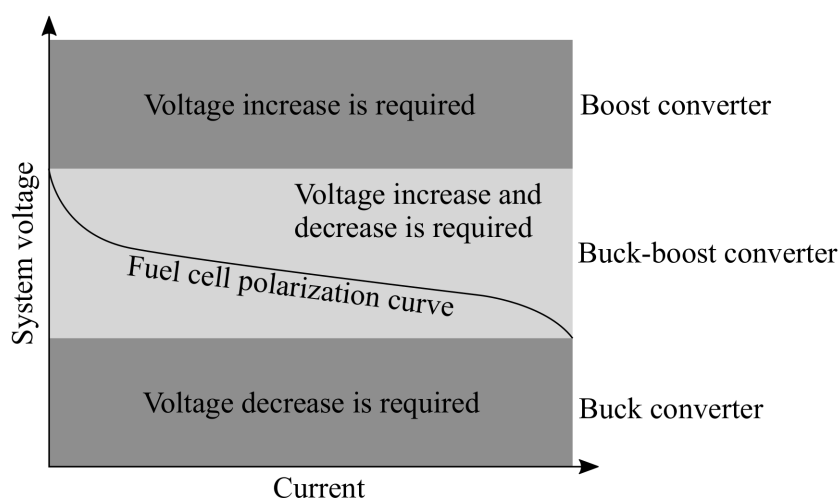


Figure 2.20: Usage of buck and boost converters in fuel cell systems. Buck converters are used to lower the voltage from the fuel cell output voltage. Boost converters are used to increase the voltage. Buck-boost converters can serve both duties. Redrawn from Barbir (2013).

Inverters and rectifiers

Inverters change direct current to alternating current. This is accomplished by electronic switches turning on and off the DC electricity to create approximate a sine wave AC output (Barbir, 2013). Rectifiers change alternating current to direct current, and have therefore the opposite duty compared to inverters (Bessarabov and Millet, 2018).

Efficiency of Power Electronics

The losses associated with the power electronics can be represented by efficiency parameters. O’Hayre et al. (2016) claims that the overall efficiency of the power electronics is in the range of 80-95% in fuel cell systems. This assumed an inverter efficiency of 85-97%. Barbir (2013) asserts that this number should be lower (70-90%), which results in a

correspondingly lower overall power electronics efficiency. It is in the same book argued that the efficiency will vary slightly with the current input to the system.

2.4.9 Other BoP Components

In addition to the components mentioned in the previous sections, there are several other components in fuel cell and electrolyser systems. The electrolysers and the humidifiers might require demineralised water as inputs (Boudellal, 2018; Barbir, 2013). If this is not available, demineralisation equipment is needed. Further, several pumps may be needed to drive the water management systems and other fluid streams. Fans and blowers are also components which are commonly installed in fuel cell and electrolyser systems to provide cooling or to drive gas flows (Barbir, 2013). Different types of valves are also extensively employed in the systems, especially for flow control (Boudellal, 2018; Larminie and Dicks, 2003).

2.5 Degradation

For long-term running fuel cell and electrolyser systems, degradation is an important phenomenon. The systems are likely to be affected differently depending on which operating conditions they are exposed to. The impacts of various conditions are therefore crucial to be aware of when deciding both design and loading strategies for a system, in order to maintain the best performance for a system over a prolonged time. This section will outline important aspects about degradation which are considered to be important for the fuel cell and electrolyser stacks in the HES-OFF system. It is important to emphasise that the BoP components also will be degraded, but this will not be considered in this work as a full analysis of all the components would be too comprehensive.

2.5.1 Degradation in Fuel Cells

The open literature describes several operating conditions which will contribute to reduced performance and shorter lifetimes of fuel cell stacks. This section gives a review of four operating conditions which are considered to be the most important contributors to fuel cell degradation in framework of the HES-OFF project. Afterwards, it will present a selection of degradation rates which have been reported for fuel cells operated under various conditions for a prolonged time.

Load Variations

The fuel cells in the HES-OFF system are demanded to continuously adjust the load according to the demand of the offshore installation. This means that the fuel cells have to be exposed to voltage variations which is stated by Borup et al. (2007) to have impacts on the fuel cell performance. The article indicates that the effects of load variations will be particularly evident on the cathode electrode, and it claimed that this could be explained by the kinetics of the hydrogen oxidation reaction and oxygen reduction reaction. During the

variations, there will be an accumulation of oxide coverage over the platinum and carbon in the cathode electrode, while at the same time the dissolution of platinum will increase. This will negatively affect the fuel cell performance, as it reduces the cell active area. Along with these effects, it is also mentioned in the article that the load variations will negatively affect the electrode's ability to remain hydrated at the desired level. de Bruijn et al. (2007) supports in their review of several experimental studies, that a faster degradation of the cathode was observed under potential cycling rather than constant load conditions. Furthermore, it was found that the degradation effect was amplified with higher maximum voltages during the cycling.

Start/stop Cycling

Start/stop cycles will contribute to degradation of fuel cells, and a description of this can also be found in Borup et al. (2007). When a fuel cell is shut down for a prolonged time, air from the cathode will diffuse into the anode and fill the surrounding gas chambers. When the fuel cell is started again and new hydrogen is supplied to the anode, the air will immediately block the hydrogen from reaching the electrode areas the farthest away from the anode inlet. There will therefore be some points with local fuel-starvation at the anode until the unwanted oxygen has disappeared. Borup et al. (2007) refer to a paper by Reiser et al. (2005) that propose that a phenomenon called the reverse-current mechanism will occur in these points. This phenomenon is characterised by currents going from the positive electrode to the negative electrode, thus opposite of the normal current in the fuel cell. The only reactions which can sustain this current direction in the fuel-starved regions on the negative electrode are either evolution of oxygen or corrosion of carbon. The corrosion of carbon is associated with degradation of the fuel cell, as it will reduce the active area of the cathode electrode.

To minimise the degradation effects related to start/stop cycles, Borup et al. (2007) assert that startup of fuel cells must follow different procedures. The most effective strategy, is to implement a voltage control during the startup, which means that the fuel cell voltage is kept at a low level soon after hydrogen is introduced to the anode. Perry et al. investigated this effect in 2006, and found that the performance decrease of a certain fuel cell was $4 \mu\text{V}/\text{cycle}$ when the cell voltage was kept below 0.080 V during startup, rather than $100 \mu\text{V}/\text{cycle}$ when each cell was kept at approximately 0.905 V.

Humidity and Temperature

The humidity in the fuel cell will not only affect the fuel cell performance through the membrane conductivity as described in section 2.4.5, but also through degradation of the MEA. It is described in Barbir (2013) chapter 11, that the electrolyte membrane will swell extensively when hydrated. This will cause significant stresses in the membrane-electrode assembly. In the case of dry conditions, the degradation will be amplified as the ductility of the materials will decrease. Varying relative humidity will be particularly dangerous for the MEA, as it potentially can cause fatigue fractures of the structure. The humidity in a fuel cell is very dependent on the operating temperature, as a high temperature will

vaporise the water stored in the MEA and dry out the cell. To minimise the degradation, it is therefore important to maintain the fuel cell at a fairly constant temperature where it is not dried out.

Freeze-Thaw Cycles

Regarding that hydrogen fuel cells comprise a lot of water, subfreezing conditions can potentially have large impacts on the fuel cells. Borup et al. (2007) reviewed several studies in order to investigate permanent changes due to subfreezing conditions. A number of studies have focused on so-called freeze-thaw cycles, which are cycles where the fuel cells are frozen and then thawed. Both Borup et al. (2007) and de Bruijn et al. (2007) found that the earlier literature disagrees on the degradation effect caused by such cycles. Certain articles report severe degradation rates for fuel cells subjected to such exposures. Other studies confirm the opposite, where no compelling degradation rates are found during these cycles. However, both Borup et al. and de Bruijn et al. suggest that the preparation of the fuel cells before freezing is important for how significant consequences the freeze-thaw cycles will cause.

During shutdown of fuel cells, Borup et al. (2007) explain that it is common to either dry out the cells by purging with clean gas, or replacing the water current in the fuel cell with a nonfreezing solvent such as ethylene glycol. This will possibly contribute to reducing the degradation during freeze-thaw cycles. de Bruijn et al. (2007) refer to studies showing that the electrodes will be particularly impacted, but with these preparations before freezing, the degradation rates can be limited to 0.1-0.3 mV per freeze-thaw cycle. However, this should be considered against the fact that other studies find almost negligible effects of freeze-thaw cycles.

Due to the lack of consistency in the open literature, it is difficult to conclude upon and quantify the effects of freeze-thaw cycles. Nevertheless, the phenomena should probably be taken into consideration when designing fuel cell systems operating in subfreezing conditions, as it appears that there might be permanent effects related to this operational condition.

Reported Degradation Rates During Typical Operation

During operation, fuel cells can be exposed to a variety of factors that will contribute to degradation. There will also be a certain degradation under constant ideal operation. Additionally, some components such as the bipolar plates have shown to experience significant degradation, while this has not been well documented to have any correlation with particular operating conditions (de Bruijn et al., 2007). The accumulated degradation effects may therefore be better described as average rates over a prolonged time frame. A selection of reported degradation rates for different fuel cell projects are listed in table 2.1.

Fuel cell name	Application	Reported degradation	Source
Evo2 (PowerCell S3)	Automotive	22 $\mu V/h$	AUTO-STACK CORE (2018)
Ballard stacks in general	Most applications	2-10 $\mu V/h$	Knights et al. (2004)
Nedstack XXL	Stationary	3 $\mu V/h$	Coolegem et al. (2013)

Table 2.1: Reported degradation rates on different fuel cell projects

2.5.2 Degradation in Electrolysers

Electrolysers will also experience a degradation over time, which will depend on the operating conditions that the electrolysers are exposed to. Knowledge about this field is critical to extend the lifetime of electrolyser systems, which has been addressed as one of the biggest challenges for realising a wide marked implementation. Frensch et al. (2019) report that there has unfortunately been conducted relatively little research on this field. There is particularly a lack of knowledge of how dynamic conditions will affect the electrolyser durability and lifetimes. Buttler and Spliethoff (2018) also conclude upon this, and state that systematic studies are necessary to quantify the impact of different operating conditions. Despite the insufficiency of conducted research on electrolyser degradation, some studies are performed on this field indicating different correlations between certain operating conditions and degradation. This section attempts to summarise these findings.

Temperature

High operating temperatures will likely cause severe degradation of the electrolyser membrane. As the Nafion membrane contains Fluorine, degradation of this can be observed by emission of this element. This can be measured by the Fluorine Release Rate (FRR). Feng et al. (2017) found in a review of previous studies that FRR increases with approximately two orders of magnitude when the operating temperature is increased from 55 °C to 150 °C. Frensch et al. presented later in 2019 a study backing up these results, where the FRR was found to increase by one order of magnitude when the temperature was elevated from 60 °C to 90 °C. The dissolution of the membrane will actually increase the electrolyser performance, due to a lower ohmic resistance when the membrane thickness decreases. However, the negative effect is that the electrolyser will eventually malfunction as the thin membrane will allow higher rates of gas cross over, and at the end pinholes will develop. The two studies also suggest that increased temperatures will accelerate passivation of Titanium used in the bipolar plates of the electrolysers. This will contribute to a decrease in electrolyser performance and structural deterioration in the long term. The joint effects was measured as a degradation rate by Frensch et al. (2019). It was found that the degradation rates were 1.2 and 3.0 $\mu V/h$ at 60 °C and 80 °C, respectively. At 90 °C the degradation rate was measured to 183 $\mu V/h$, hence a significant increase. In all cases, the electrolyser was operated at a current density of 2 A/cm^2 , which was considered as high

for that particular electrolyser.

High Current Density

Research show that it is reasonable to believe that the degradation will increase when an electrolyser is operated at high current density. Feng et al. (2017) refer to studies suggesting that high current density will accelerate dissolution of the catalysts. One of these studies is Lettenmeier et al. (2016), which found a significant increase in dissolution of Iridium from the anode at high current densities. The impact on the electrolyser performance of this phenomenon seems however difficult to determine. Lettenmeier et al. (2016) assert that high current densities do not lead to any particular performance decrease. On the other hand, Rakousky et al. (2017) showed a different causality. At high current density (2 A/cm^2) an average degradation rate of $194 \mu\text{V/h}$ was measured, while at low current density (1 A/cm^2) no significant voltage degradation was measured. In the experiment, two equal electrolyser cells were operated at their respective currents, while maintained at $80 \text{ }^\circ\text{C}$. The voltages measured through the experiment are reprinted in figure 2.21. It can be observed that the voltage at the electrolyser anode is the dominating contributor to the increase in overall electrolyser voltage. This is interesting, regarding that the previous mentioned studies reported particularly high dissolution from the anode electrodes.

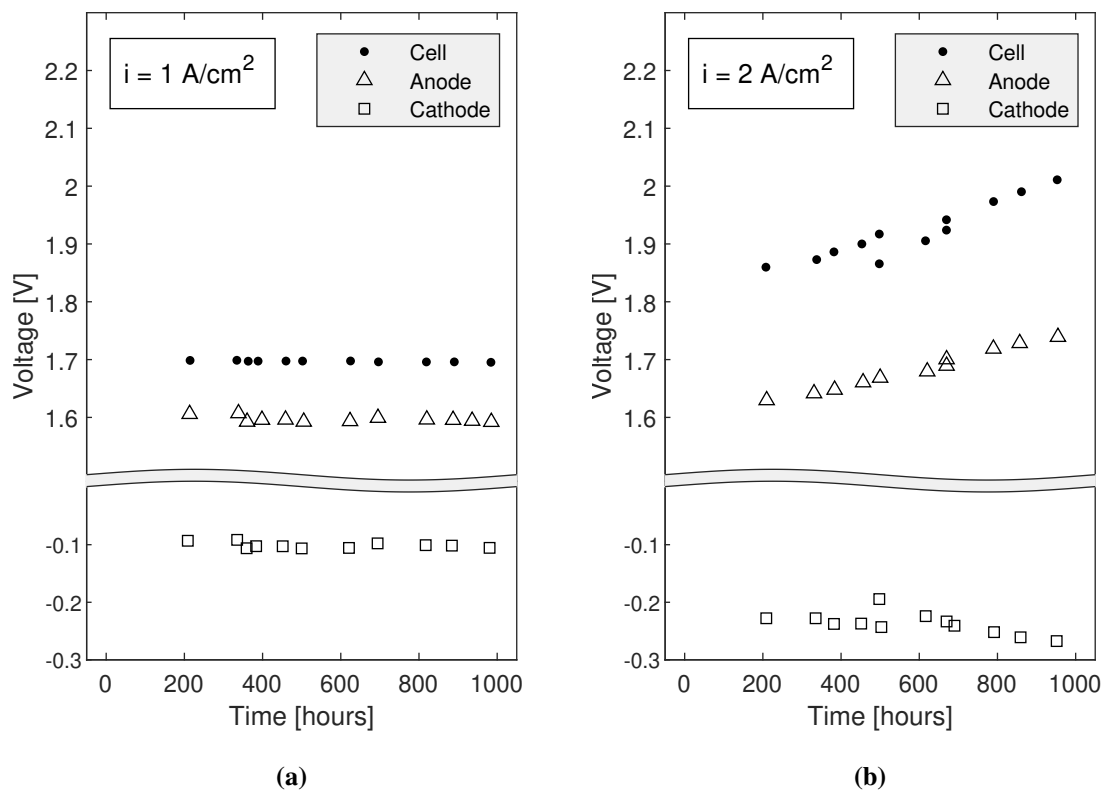


Figure 2.21: Constant operation at (a) 1 A/cm^2 and (b) 2 A/cm^2 . Redrawn from the results of Rakousky et al. (2017).

Load Cycling

It has also been suggested that load cycling will accelerate electrolyser degradation. Yet, a correlation has this far not been confirmed. According to the review of Buttler and Spliethoff (2018), several manufacturers report that load cycling has no significant effect on the lifetime of their PEM electrolysers. During the experiments of Rakousky et al. (2017) mentioned in the previous paragraph, it was also tested to operate cells dynamically between high and low current densities. The results showed lower degradation rates for dynamic loading compared to constant operation at high current density. However, this was explained by the reason that the electrolyser was operated for a shorter time at high current densities during dynamic loading, and as this was especially severe, the accumulated degradation would therefore be less. At the same time, the degradation was larger than operation on low current densities. It may therefore appear that dynamic load itself is not a source of degradation, but it may cause increased degradation as it may imply occasionally operation with high current density.

Reported Degradation Rates

Similar to fuel cells, some studies and manufacturers provide average degradation rates for systems which have been tested for a long time. Such rates are presented in table 2.2. Unfortunately, as it was mentioned in above, the electrolyser technology suffers from lack of research on behaviours during various loading strategies. This might be explained by the fact that commercial electrolysers in operation today, have generally less daunting operating profiles than fuel cells. The tests presented in table 2.2 have therefore been performed in almost steady state, which can explain why the degradation rates are extremely low. This applies especially by the number given by Proton Onsite, where there were no detectable voltage decay during the 20 000 hour test period.

Electrolyser	Application	Reported degradation	Source
Self-made for research	Stationary	$1.5 \mu V/h$	Selamet et al. (2011)
Giner ELX stack	Stationary	$1 \mu V/h$	Hamdan and Harrison (2019)
Proton site	On- Stationary	$\sim 0 \mu V/h$	Anderson (2016)

Table 2.2: Reported degradation rates for different electrolysers

2.6 Weight and Footprint of Commercial Systems

In order to perform the weight and footprint assessment later in the thesis, there has been conducted a brief state-of-the-art analysis of commercial fuel cell and electrolyser technology. Such data can typically be acquired through datasheets or white papers provided by the manufacturers. However, throughout this work and from discussions with partners in the HES-OFF project, it has been identified that manufacturers often are cautious with providing data for their products. The analysis therefore frequently suffers from lack of information to give representative data for the technologies. The results of the analysis are presented in this section.

2.6.1 Fuel Cell Stacks

Fuel cells stacks are currently available for a large range of applications. Data for various stacks is presented in table 2.3. In this table, there is presented calculated ratios between stack powers and stack weights, as well as stack powers and stack volumes. It is also attempted to categorise the stacks according to their intended application. However, this categorisation is quite inaccurate as some stacks are suggested in a large scale of applications. The most typical applications are therefore listed. Figure 2.22 and 2.23 graphically show the numbers listed in table 2.3.

It can be noticed that the stacks intended for the automotive industry exhibit the largest power/weight and power/volume ratios. These are applications where weight and footprint typically are crucial parameters. It could also be reasonable to believe that Unmanned Aerial Vehicles (UAVs) would require high power/weight ratio, as weight is critical for the flying time. However, the relatively low number for the Aerostak stack listed in table 2.3 can be explained by the fact that the stack is very small and better mass optimisation is difficult to obtain at this level.

Stack	Application	Capacity [kW_e]	Power/weight [kW/kg]	Power/volume [kW/m³]
PowerCell S3 ¹	Automotive, maritime	49-125	2.9	3359
Toyota (Mirai) stack ^{2,3}	Automotive	114	2.0	3100
Ballard FCgen 1020 ACS ⁴	Backup power, automotive	0.45-3	0.2	211
Ballard FCgen LCS ⁵	Automotive	50	1.7	1776
Ballard FCvelocity 9SSL ⁶	Automotive	3.8-21	1.2	1525
Nedstack FCS 13-XXL ^{7,8}	Stationary, maritime	13.6	0.3	399
Nedstack FCS 10-XXL ^{9,10}	Maritime propulsion	10.6	0.3	376
Nedstack FCS 7-XXL ^{11,12}	Backup power	6.8	0.3	331
PowerCell S2 ¹³	Backup power	3-35.5	2.7	316
Aerostak ^{14,15}	UAVs	0.3-1.7	0.6	183

Table 2.3: Data for fuel cell stacks. Highest power/weight and power/volume ratios among stack configurations are listed

¹PowerCell Sweden AB (2020d)

²Toyota Motor Corporation (2020)

³Toyota Motor Corporation (2019)

⁴Ballard Power Systems Inc. (2020a)

⁵Ballard Power Systems Inc. (2020b)

⁶Ballard Power Systems Inc. (2020c)

⁷Nedstack fuel cell technology B.V. (2020d)

⁸Nedstack fuel cell technology B.V. (2020f)

⁹Nedstack fuel cell technology B.V. (2020c)

¹⁰Nedstack fuel cell technology B.V. (2020g)

¹¹Nedstack fuel cell technology B.V. (2020e)

¹²Nedstack fuel cell technology B.V. (2020b)

¹³PowerCell Sweden AB (2020c)

¹⁴HES Energy Systems (2020b)

¹⁵HES Energy Systems (2020a)

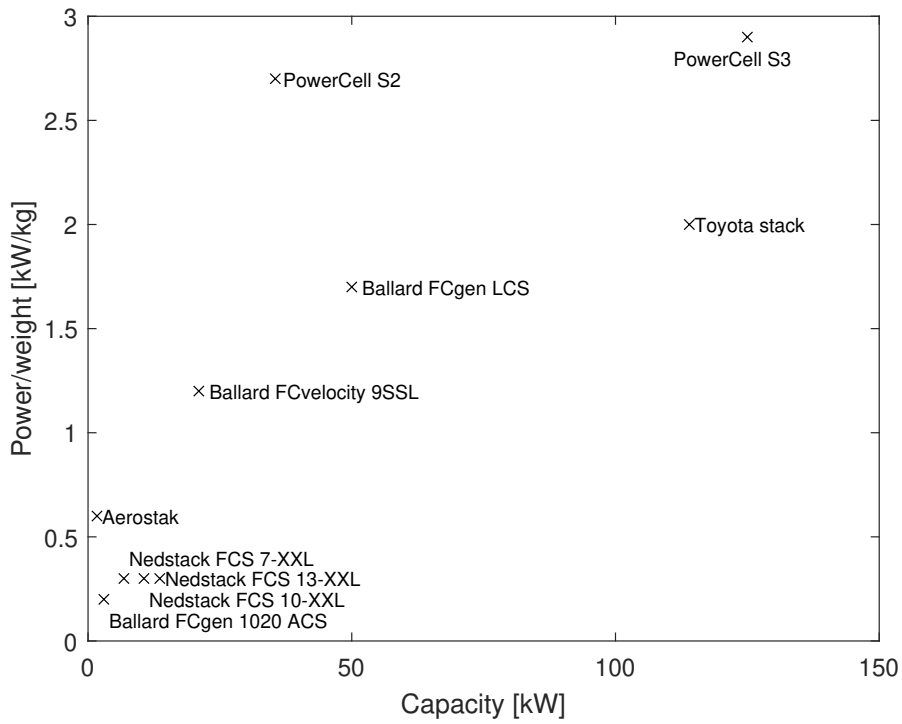


Figure 2.22: Power/weight ratios for fuel cell stacks plotted towards capacity

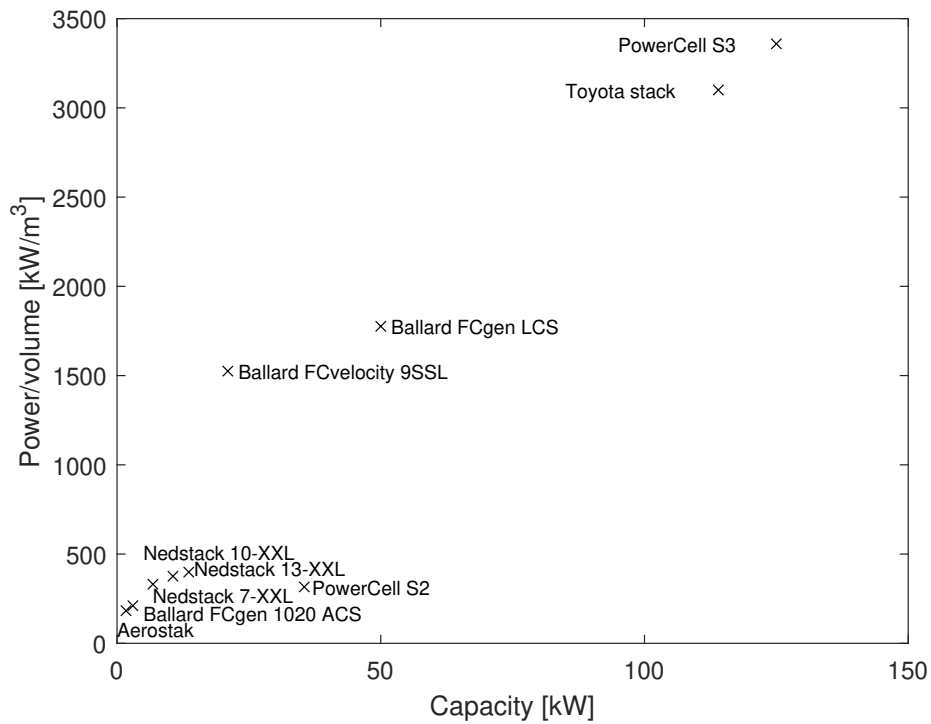


Figure 2.23: Power/volume ratios for fuel cell stacks plotted towards capacity

2.6.2 Fuel Cell Systems

Various manufacturers provide full fuel cell systems including both cell stacks and BoP components. Examples of such systems are listed in table 2.4. For stationary power production, Nedstack Fuel Cell Technology B.V. and Hydrogenics Corporation provide systems in the MW-range stored in 40ft containers (Nedstack fuel cell technology B.V., 2020a; Hydrogenics Corporation, 2020a). For more motive applications, systems in the kW-range are available (PowerCell Sweden AB, 2020b; Hydrogenics Corporation, 2020b; Ballard Power Systems Inc., 2020d; Swiss Hydrogen SA, 2020). The systems are listed with their associated capacities and calculated power/weight and power/volume ratios. It should be noted that the systems do not have the same outputs, and therefore not necessarily the same amount of system components. The numbers are consequently not fully comparable.

System	Application	Capacity [kW _e]	Power/weight [kW/kg]	Power/volume [kW/m ³]
Nedstack CHP-FCP-1000 ¹	Stationary	>1000	0.034	13
PowerCell MS-100 ²	Automotive, maritime	100	0.59	357
Hydrogenics HYPM-HD 180 ³	Bus, rail	198	0,28	167
Hydrogenics MW platform ⁴	Stationary	>1000	0,031	13
Ballard FCveloCity HD ⁵	Automotive	100	0,36	197
Swiss Hydrogen HY-REX 100 ⁶	Automotive	100	1,0	371

Table 2.4: Data for fuel cell systems. Highest power/weight and power/volume ratios among stack configurations are listed

¹Nedstack fuel cell technology B.V. (2020a)

²PowerCell Sweden AB (2020b)

³Hydrogenics Corporation (2020b)

⁴Hydrogenics Corporation (2020a)

⁵Ballard Power Systems Inc. (2020d)

⁶Swiss Hydrogen SA (2020)

For some systems it is also provided information of which and how many stacks are employed. This makes it possible to calculate how much stacks contribute to the overall system weight and volume. Such information is presented in table 2.5. For the Nedstack containerised system intended for stationary power production, the stacks contribute to only 17% of the system weight and 5.3% of the system volume. The automotive industry has shown that it is possible to make much more compact systems, where the stacks in the HY-REX 100 system contribute to 44% of the system weight and 14% of the system volume. It should be emphasised that the systems have different purposes and accordingly different system components. Yet, it may be reasonable to think that there is a potential for mass and weight optimisation for the stationary system, if this is desired.

System	Application	System Capacity [kW_e]	Stack used	Weight% stacks	Volume% stacks
CHP-FCP-1000 ^{1,2}	Stationary	>1000	13-XXL	17	5.3
MS-100 ^{3,4}	Automotive, maritime	100	S3	25	13
HY-REX 100 ^{4,5,6}	Automotive	100	S3	44	14

Table 2.5: Data for fuel cell systems where information about the installed stacks is also provided. Highest power/weight and power/volume ratios among stack configurations are listed.

¹Source regarding system information: Nedstack fuel cell technology B.V. (2020a)

²Source regarding the installed stack: Nedstack fuel cell technology B.V. (2020d)

³Source regarding system information: PowerCell Sweden AB (2020b)

⁴Source regarding the installed stack: PowerCell Sweden AB (2020d)

⁵Source regarding system information: PowerCell Sweden AB (2020a)

⁶Source regarding system information: Swiss Hydrogen SA (2020)

2.6.3 Electrolyser Stacks

It may seem like the electrolyser market is more focused on providing full electrolyser systems rather than single stacks. Therefore, it is difficult to procure data of electrolyser stacks, in the same way as what was obtained for fuel cell stacks in table 2.3. Nevertheless, to get a sense of the dimensions of electrolyser stacks, data can be found for the Proton OnSite M-Series 250 kW stack in the book by Bessarabov and Millet (2018). This stack weights 295 kg and its dimensions are 49x61x89 cm. By use of these numbers, it can be calculated that the stack exhibits a power/weight ratio of 0.85 kW/kg and a power/volume ratio of 940 kW/m^3 .

2.6.4 Containerised Electrolyser Systems

Through this work, it has been found that electrolyser systems are currently commercially available frequently as containerised systems intended for stationary hydrogen production. This is a statement which has been confirmed by the industry partners in the HES-OFF project. Such systems are listed in table 2.6. Unfortunately, it has proved to be difficult to procure the weights of the systems. However, the 1.4 MW H-TEC ME 450/1400 system is listed to have a weight of 25 tonnes. Further, averagely approximately one 40 ft container is demanded to house a system with production capacity of $200 \text{ Nm}^3/\text{h}$. Additionally, smaller cooling equipment must often be included.

Electrolyser System	Capacity [MW]	Capacity [Nm^3/h]	Housing	Weight [Tonnes]
NEL MC200 ¹	1	207	2 x 40ft containers	-
NEL MC400 ¹	2	413	2 x 40ft containers	-
ITM HGas2SP ²	1.34	250*	2 x 30ft containers	-
ITM HGas3SP ³	2	375*	2 x 40ft containers	-
Giner ELX ⁴	1	200	1 x 40ft container	-
Areva H2Gen E200 ⁵	1.6	200	1 x 40ft container	-
H-TEC ME 450/1400 ⁶	1.4	210	1 x 40ft container	25

Table 2.6: Data for commercial containerised electrolyser systems. *Ideal gas law is used to calculate volumetric flow rate.

¹Nel ASA (2020)

²ITM Power (2020a)

³ITM Power (2020b)

⁴Giner ELX (2020)

⁵Areva H2Gen (2020)

⁶H-TEC SYSTEMS GmbH (2020)

2.7 Developed Matlab Simulink[®] implementations

According to objective 2 presented in section 1.2.3, it should be performed a search for already developed models integrated in the Matlab Simulink[®] environment. In that context, two fuel cell stack models have been found and are presented in the following section.

2.7.1 Nehrir and Wang Simulink Model (NW Model)

As an attachment to the Nehrir and Wang (2009) book, there is provided a Matlab Simulink[®] file where it is suggested a model implementation of a 500 W PEM fuel cell stack. As an alternative to developing an own model, this model can possibly be tuned to fit different stacks. However, as it will be presented, the model relies on several empirical approaches which can make it difficult to use this model generically to fit arbitrary stacks. This section will therefore present the model in detail, and discuss the difficulties with adapting the model.

Modelling Approach

The model models a fuel cell stack, and the presented model is tuned to the 500 W SR-12 PEM stack manufactured by Avista Labs. In terms of the model classification chart in figure 1.2, the model is a dynamic model which comprise one spatial dimension. The model focuses on single cells which are scaled up to represent the entire stack. These are modelled within the electrical, fluidic and thermal domain, with use of both analytical, semi-empirical and empirical equations. The thermal model is implemented as a separate

unit, which continuously calculates the overall stack temperature and heat loss. Since this is beyond the scope of this work, the thermal model is not presented and the stack temperature is rather represented as a constant input parameter. The model outputs are stack voltage and power. The input to the model is a varying current which represents the loading of the stacks. In addition, a set of constant input parameters which are listed in table 2.7 are needed.

Assumptions

To perform the modelling, the following set of assumptions is applied and listed in the book:

1. One-dimensional treatment of flow and distribution of gas species inside the fuel cells
2. Ideal and uniformly distributed gases
3. Constant pressures in the fuel cell gas flow channels
4. The fuel is humidified hydrogen, and the oxidant is humidified air. Further aspects of the humidity are not considered.
5. The effective water vapor pressure is 50% of the saturation pressure at the anode, and 100% of the saturation pressure at the cathode.
6. The fuel cell operates below 100°C and the reaction product is in liquid phase
7. Thermodynamic properties are evaluated at average stack temperature, temperature variations across the stack are neglected and the overall specific heat capacity of the stack is assumed to be constant.
8. Parameters for individual cells are lumped together to represent a fuel cell stack

Governing equations

The NW model applies mostly common equations, and some of these equations have already been presented in section 2.1. However, for certain calculations the model uses more special approaches which are not found in very many other models. This section will outline the entire approach.

Equations already outlined in section 2.1:

The overall dynamic fuel cell voltage is modelled by the reversible voltage and subtraction of different losses. The losses considered are the activation losses, ohmic losses and concentration losses, as well as the dynamic voltage drops caused by the mass transfer delay and the double layer charge effect. The implementation of the two last losses have already been discussed in section 2.1.6 and 2.1.6. The overall dynamic voltage is therefore given by:

$$V_{out} = E_{OCV} - V_{act,1} - V_C - V_{ohmic} \quad (2.41)$$

In section 2.1.6 and 2.1.6, it was presented the following equations, which are also used in the NW model:

$$E_{OCV} = E_{Nernst} - V_d = E_{Nernst} - \lambda_e I \left(1 - \frac{1}{\tau_e s + 1} \right) \quad (2.33)$$

$$V_C = \left(I - C \frac{dV_C}{dt} \right) (R_{act,2} + R_{conc}) \quad (2.40)$$

$$V_{act} = \underbrace{\eta_0 + (T - 298) \cdot a}_{V_{act,1}} + \underbrace{T \cdot b \ln I}_{V_{act,2}} \quad (2.39)$$

Additional equations special for the NW model

In addition to the equations listed above, the NW model applies several other semi-empirical correlations. The Nernst voltage is calculated by:

$$E_{Nernst} = E_{0,cell}^o - k_E(T - 298) + \frac{RT}{2F} (a_{H_2} \cdot a_{O_2}^{0.5}) \quad (2.79)$$

k_E is here an empirical constant. The activities of the gases, a_{H_2} and a_{O_2} , are strictly the activities where the half reactions occur, and Nehrir and Wang (2009) argue that this is on the interfaces between the electrodes and the membrane. The activities here will be different than the activities at the inlets of the fuel cells, as the gases has to diffuse through the electrodes. Therefore, the NW model employ the following correlations to calculate the gas activities at the electrode-membrane interface:

$$a_{H_2} = 0.5 P_{H_2O}^{sat} \left(\frac{1}{x_{H_2O}^{ch,a} e^{\frac{RTl_a i}{2FP_a D_{H_2O,H_2}}} - 1} \right) \quad (2.80)$$

$$a_{O_2} = P_{H_2O}^{sat} \left(\frac{1}{x_{H_2O}^{ch,c} e^{\frac{RTl_c i}{2FP_c D_{H_2O,O_2}}} - 1} \right) \quad (2.81)$$

Here, $P_{H_2O}^{sat}$ is the saturation pressure of water at the given average stack temperature. l_a and l_c are the widths of the anode and cathode electrodes, while P_a and P_c are the inlet pressures to the anode and cathode chambers. D_{H_2O,H_2} and D_{H_2O,O_2} are the effective binary diffusivities of water molecules in pair with gaseous hydrogen and oxygen. $x_{H_2O}^{ch,a}$ and $x_{H_2O}^{ch,c}$ are the mole fractions of water at the anode and cathode inlets, and is calculated by:

$$x_{H_2O}^{ch,a} = \frac{P_{H_2O}^{sat}}{P_a} \quad (2.82)$$

$$x_{H_2O}^{ch,c} = \frac{P_{H_2O}^{sat}}{P_c} \quad (2.83)$$

The saturation pressure of water is further calculated by:

$$P_{H_2O}^{sat} = (-40529.45 + 401.9403 \cdot T - 1.334303 \cdot (T^2) + 0.001483784 \cdot (T^3)) / 760 \quad (2.84)$$

To calculate the concentration losses (represented as the concentration resistance), the NW model apply the following equation:

$$V_{conc} = 2.6 \frac{RT}{nF} \ln \left(1 - \frac{i}{i_L} + 1 \cdot 10^{-100} \right) \quad (2.85)$$

The ohmic losses are as normally calculated as the product of current and ohmic resistance. However, the ohmic resistance is calculated by:

$$R_{ohm} = R_{ohm0} + k_{RI}I + k_{RT}T \quad (2.86)$$

Here, R_{ohm0} , k_{RI} and k_{RT} are empirical constants. The ohmic resistance has therefore a linear relationship to the current, which means that the ohmic losses are proportional to the square of the current. This contradicts the more traditional understanding that the ohmic losses have a linear dependency on the current, which was described in section 2.1.4.

Summary of Input Parameters Needed

From the equations listed in the previous section, it can be seen that adaption of the NW model requires procurement of several parameters. All the parameters are listed in table 2.7, and with a comment on how these typically can be acquired. The values for diffusivities and electrode thicknesses are not provided explicitly in the model.

Conclusion

The NW shows to employ several semi-empirical and empirical equations which introduces numerous input parameters. The summary in table 2.7 further displays that nine of these input parameters most probably have to be obtained empirically. Additionally, many of these do not have an intuitive physical meaning, but are empirical constants which therefore need to be tuned according to experimental data. It is therefore concluded that the NW model is quite difficult to adapt as a generic model which can represent arbitrary stacks. However, the model implements some interesting approaches and it can be used as inspiration when developing own models.

2.7.2 Simulink® Simscape™ Library Fuel Cell Stack Block

In the Simscape™ Library in the Simulink® environment, it can be accessed a block named Fuel Cell Stack. This block is described to implement a generic model for the most popular types of fuel cell stacks (The MathWorks Inc). In the following, this block is referred to as the Simscape FC block.

Symbol	Physical meaning	How to obtain	Value in NW
$E_{0,cell}^o$	Rev. cell voltage at standard cond.	Tabulated	1.229V
λ_e	Empirical constant	Empirically	$3.33 \cdot 10^{-3} \Omega$
τ_e	Time const. for mass transport delay	Empirically	80 s
C	Capacitance of charge double layer	Empirically	4 F
η_0	Empirical constant	Empirically	1.272 V
a	Empirical constant	Empirically	$9.597 \cdot 10^{-6}$
b	Empirical constant	Empirically	$9.274 \cdot 10^{-5}$
T	Operating temperature	Datasheets	273 – 373 K
I_L	Limiting current	Datasheets	25 A
l_a	Thickness of anode electrode	Manufacturer	–
l_c	Thickness of cathode electrode	Manufacturer	–
P_a	Anode inlet pressure	Datasheets	1.5 atm
P_c	Cathode inlet pressure	Datasheets	1.0 atm
D_{H_2O,H_2}	Binary diffusivity	Tabulated	–
D_{H_2O,O_2}	Binary diffusivity	Tabulated	–
R_{ohm0}	Empirical constant	Empirically	0.02054 Ω
k_{RI}	Empirical constant	Empirically	$3.9 \cdot 10^{-5} \Omega/A$
k_{RT}	Empirical constant	Empirically	$4.94 \cdot 10^{-5} \Omega/K$

Table 2.7: Input parameters used in the NW model

The Simscape FC block is tuned in the dialog box of the block. Here, the user has to select the model detail level and one can choose between applying a detailed or simplified model. By selecting the simplified model, the model is tuned by providing the following information about the fuel cell stack:

- Voltage at 0 A and 1 A
- Current and voltage at nominal
- Current and voltage at maximum operating point

By selecting the detailed model, the model will be further tuned according to the following data which have to be provided:

- Number of cells
- Nominal stack efficiency (based on LHV)
- Operating temperature
- Nominal Air flow rate
- Nominal supply pressure
- Nominal composition of hydrogen in fuel stream and oxygen and water in air stream

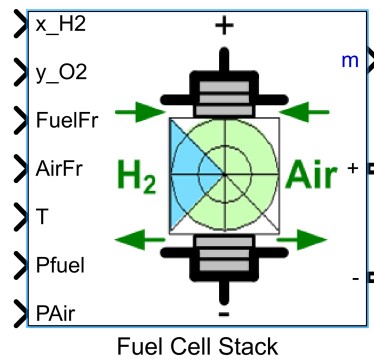


Figure 2.24: Screenshot of the Fuel Cell Stack Block accessed in the Simscape™ library in the Simulink® environment. (Referred to as the Simscape FC block in the text)

As an option in the detailed model, a polarization curve is plotted for the fuel cell stack by means of the provided data.

Figure 2.24 depicts the Simscape FC block as it appears in the Simulink block diagram. The output of the block is a signal bus denoted “m”, which contains several values, among these is the stack voltage. The block has a positive and negative pole representing the poles of the fuel cell stack. To make the block function, a implementation representing power electronics has to be coupled to these poles. Further, the detailed version of the model allows for controlling the following parameters:

- Fuel composition (x_{H2} [%])
- Oxidant composition (y_{O2} [%])
- Fuel flow rate (FuelFr [lpm])
- Air flow rate (AirFr [lpm])
- System Temperature (T [K])
- Fuel supply pressure (Pfuel [bar])
- Air supply pressure (PAir [bar])

By selecting to control the fuel and air flow rate, the block allows for specification of dynamic parameters through the dialog box by means of three inputs:

- Fuel Cell response time [seconds]
- Peak O_2 utilization [%]
- Voltage undershoot [V] at peak O_2 utilization

If these fields are not specified, the block will use default parameters which are a response time of 1 second, peak O₂ utilization of 80% and a voltage undershoot value of 10 V (The MathWorks Inc).

For illustration of how the model can be tuned, the block contains options for presetting the values to model different example stacks. The most well-documented preset is described in the documentation of the block, and is tuned to the 6 kW NedStack PS6 stack (The MathWorks Inc). This preset is accessed in the dialog box of the block under the name PEMFC - 6 kW - 45Vdc.

Modelling of the HES-OFF system

This chapter presents the modelling of the HES-OFF hydrogen energy storage system. Firstly, the assumed design of the system is presented. This comprise an outline of which system components are embedded and a description of the fuel cell and electrolyser characteristics and organisation. Secondly, the developed model of the system is described. Finally, it is outlined a method to evaluate the fuel cell part of the developed model by benchmarking with the Simscape FC block.

3.1 Assumed System

To perform the modelling of the HES-OFF system, it is first of all necessary to assume a design of the system. However, it must be emphasised that within the framework of the HES-OFF research project, the design is still under investigation. Therefore, the design presented in this work is only an assumed design for the purpose of this work, and is not an official design stated on behalf of the HES-OFF research project.

It is assumed in this work that the system should have both total fuel cell and total electrolyser capacity on 2 MW. The value of 2 MW has been selected for the purpose of this work, but can easily be adjusted within the model by changing the capacity of each stack or changing the number of stacks in the system. The following section presents the overall design of the assumed system.

3.1.1 System layout

In section 2.4 it was described which BoP components PEM fuel cell and electrolyser systems running on pure gaseous hydrogen typically need. This has been taken into account for the HES-OFF hydrogen energy storage system, and an assumed system layout is presented in figure 3.1.

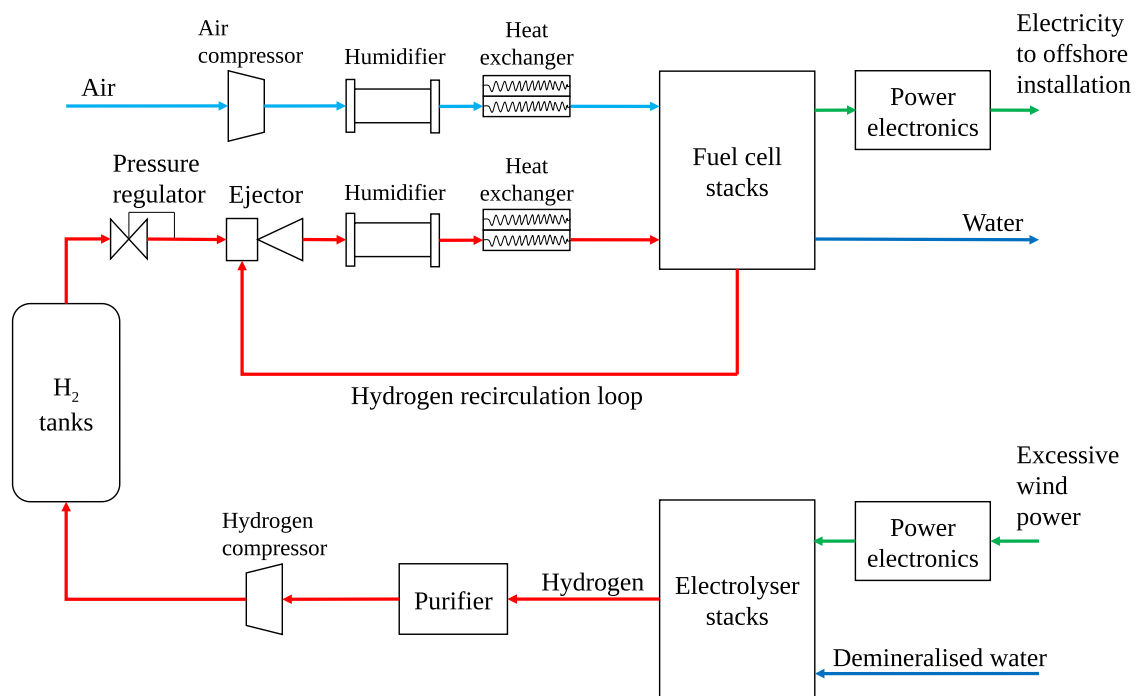


Figure 3.1: Simplified system drawing of the suggested and modelled HES-OFF hydrogen energy storage system

The system will comprise several fuel cell and electrolyser stacks to obtain the required capacity, and all these stacks are represented with respective blocks in figure 3.1. It is assumed that both the air stream and the hydrogen stream entering the fuel cell must be processed using humidifiers and heat exchangers. In addition must the air stream be pressurised, which is obtained by a mechanical compressor. The re-circulation of unused hydrogen in the fuel cells is solely run by an ejector system which uses high pressure gas from the storage tank as the primary flow. The electricity produced by the fuel cells is processed to the desired conditions by use of power electronics. Similarly, the electric input power to the electrolyser is processed from given conditions, to the type of electricity consumed by the electrolyser. The outlet hydrogen from the electrolyser is purified and further compressed with a mechanical compressor and stored in storage tanks. As it was discussed in section 2.4.2, electrochemical compression has been discussed as an interesting alternative to fulfill the duty of hydrogen compression. Yet, due to time limitations in this work and the relative simple nature of mechanical compressors, the hydrogen compression is therefore modelled to be performed by mechanical compressors.

It must be emphasised that this is a simplified design to show the integration of important components in the system. Even though different components are only represented by one icon, a real system would probably require a larger quantity of certain components (e.g. many ejectors and not only the one which is depicted). Moreover, it is outlined in chapter 2.4 other components which are typically installed in fuel cell and electrolyser systems than the ones included in figure 3.1. However, these are not included, because it is assumed that they are not strictly needed or can be neglected in the modelling of the system.

3.1.2 Fuel Cell Stacks

Stack Characteristics

The fuel cell stacks in the assumed system are considered to be the PowerCell S3 stack, manufactured by the Swedish manufacturer PowerCell Sweden AB. This is a 125 kW PEM stack (PowerCell Sweden AB, 2020d), and 16 stacks are therefore required to fulfill the requirement of 2 MW output electric power from the entire system. A polarization curve for the fuel cell can be found in a datasheet provided by the manufacturer (PowerCell Sweden AB, 2020d), and is replotted in figure 3.2. In the datasheet, it is stated that this polarization curve was obtained using a fuel stream with a pressure of 2.2 bars and with 70% H_2 in N_2 . In this work, the fuel cells are considered to run on pure hydrogen, but therefore at a correspondingly lower pressure (see table 3.2) to obtain the similar polarization curve.

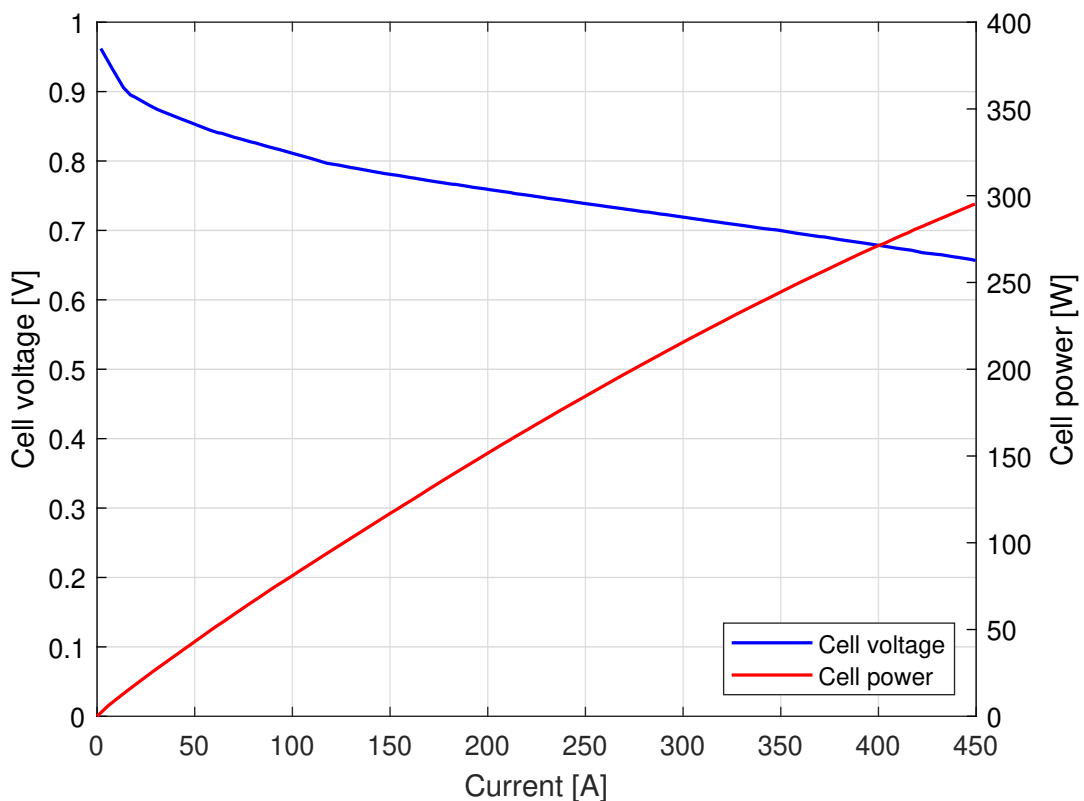


Figure 3.2: Reprinted polarization curve (including cell power) for PowerCell S3 provided by the manufacturer (PowerCell Sweden AB, 2020d)

Modular Organisation

The fuel cell stacks are considered to be organised into 4 modules each containing 4 stacks as illustrated in figure 3.3. This is a common design for big-size fuel cell systems (Ekdunge, 2017) and was also applied by Campanari et al. (2019) in their modelling of a 2 MW PEM fuel cell system. With this modular design, all the stacks within one module are loaded simultaneously, while each of the modules can be loaded differently relative to each other. The advantage with this design, is that the stacks within each module can share many of the same BoP components. The design therefore provides a compromise between flexibility and system cost. The alternatives to the modular design would require to load all stacks either simultaneously or individually. Because of the increased degradation which occurs when stacks undergo dynamic loading (section 2.5), it is inconvenient to load all stacks simultaneously as all stacks then would undergo the dynamic loading. This therefore limits the flexibility of the system. On the contrary, by loading all the stacks individually, some stacks can undergo steady operation while other can be adjusted to fulfill the demand of the total system. However, this would require more BoP components, for example own controllers for each stack. Further, the final operation of the stacks depends on the control system embedded in the fuel cell system. However, because the stack system in reality is a complex system and due to the fact that manufacturers generally are cautious with sharing details about this, detailed control systems and strategies are not included in the modelling activity. Nevertheless, considering the required fidelity of the model, it is reasonable to consider operational procedures and schemes as they are presented in Campanari et al. (2019), where the modules are loaded separately as depicted in figure 3.3.

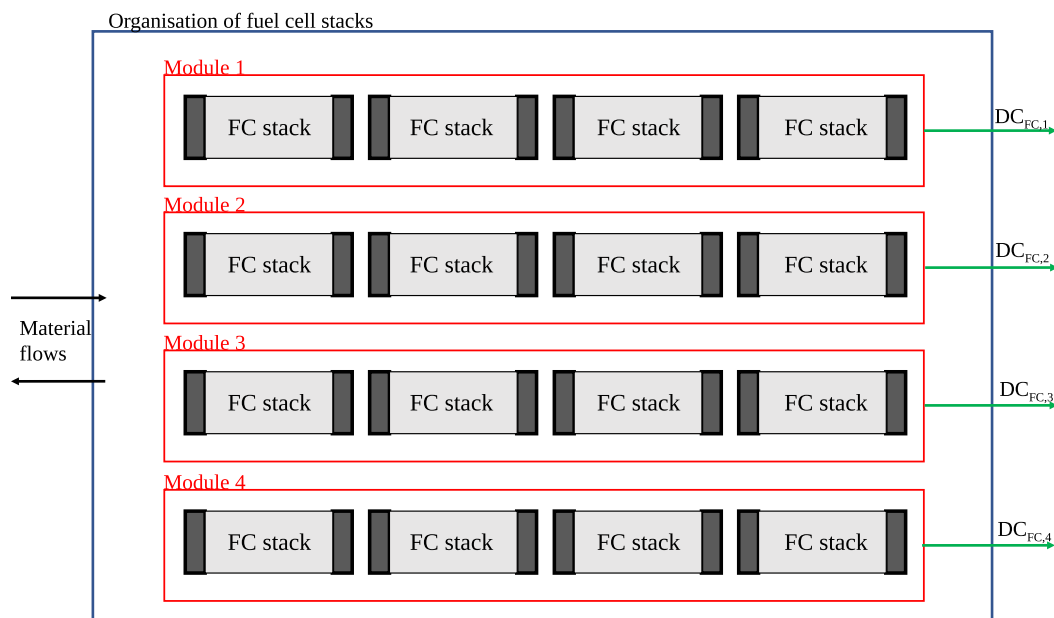


Figure 3.3: Organisation of fuel cell stacks in modules

3.1.3 Electrolyser Stacks

Stack Characteristics

The electrolyser stacks in the assumed system are considered as the Proton OnSite M-series stack, manufactured by the US manufacturer Proton OnSite (owned by the Norwegian Nel ASA) (Bessarabov and Millet, 2018). Data for this stack is presented by the manufacturer through Anderson (2016). This is a 250 kW PEM stack, and eight stacks are therefore required to fulfill the requirement of 2 MW electrolyser capacity for the entire system. A polarization curve for the stacks operating at 13 bar is replotted in figure 3.4. The electrolyser stacks in the HES-OFF system have been tuned with the aim to fit this polarization curve.

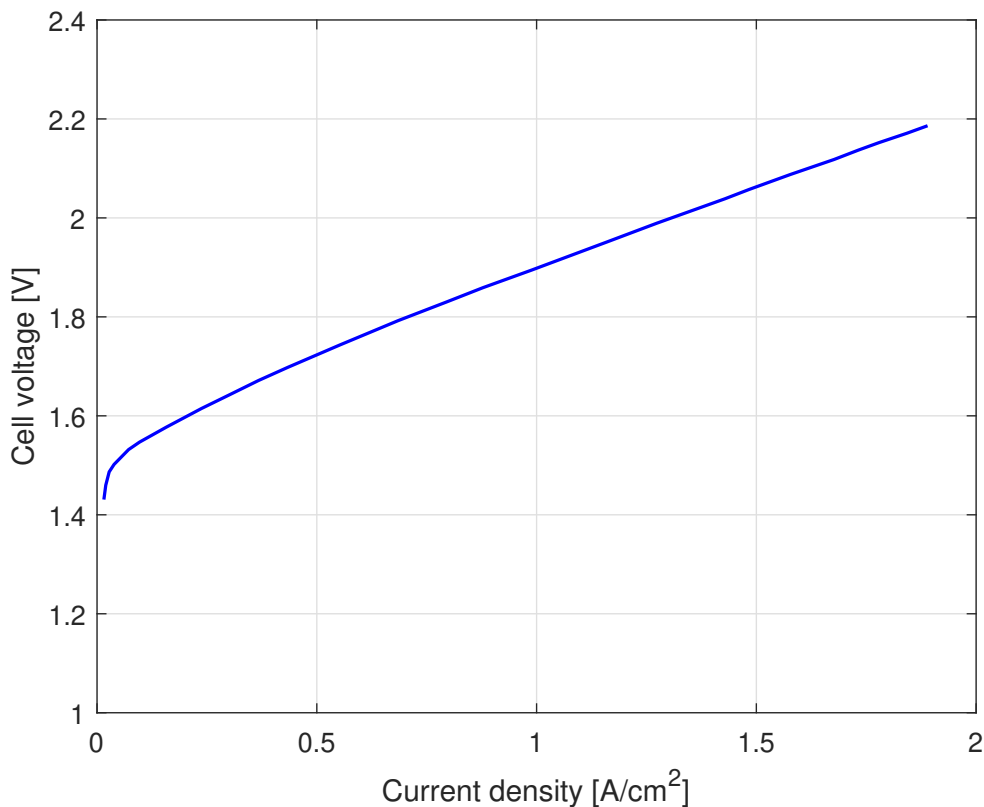


Figure 3.4: Replotted polarization curve for Proton OnSite M-series provided by the manufacturer

Modular organisation

Because of the same argumentation as for the fuel cell stacks, the electrolyser stacks are organised into modules. The configuration comprises two modules including four stacks each, and is shown in figure 3.5.

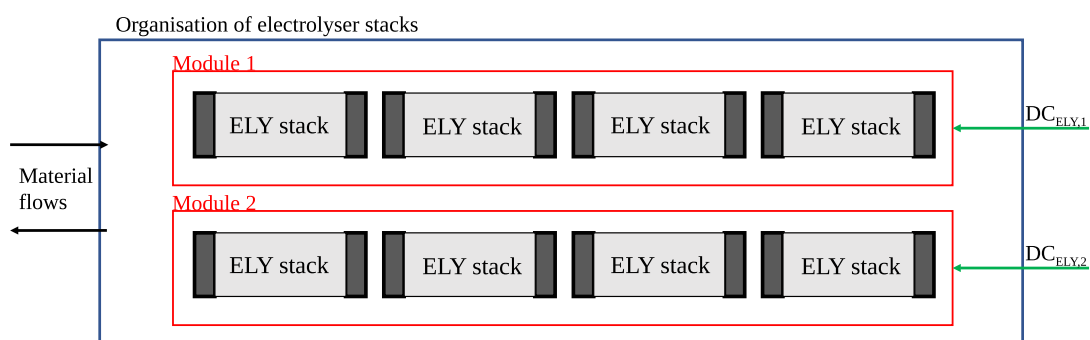


Figure 3.5: Organisation of electrolyser stacks in modules

3.1.4 Balance of Plant Components

Because there is less focus on BoP components in this work, these components are not considered as any specific commercial products. Moreover, the market of BoP components is very wide because components from other industries can be adapted. Therefore, finding designated BoP components to model in this work would be too specific as the purpose of the work is to pave the way for further modelling. Instead, the BoP components are in this work considered by means of typical values which are represented in the literature. The characterisation for the considered BoP components are further described in section 3.2.4.

3.2 Developed Model

3.2.1 Input load

Regarding that the model is intended to be further developed to be implemented in an OPAL-RT platform, it has been decided from the other team-members of the HES-OFF project that the model should have electrical current as the input load. This means that the fuel cells and electrolyzers will be loaded by adjusting the electric current, I .

3.2.2 Modelling Approach

To model the assumed system, an own model based on the equations listed through chapter 2 has been developed. This model is later referred to as the developed model. The fuel cell stacks could possibly be modelled by adapting either the NW model or Simscape FC block outlined in section 2.7. However, the NW model was found insufficient due to its extensive use of unconventional parameters and the Simscape FC block will be used for benchmarking later.

As mentioned, the developed model is based on the equations outlined chapter 2, which were found in the open literature. However, the only phenomenon which it is considered that the open literature do not provide an adequate approach for, is the double layer charge

effect described in section 2.1.6. Here, two approaches are found. The approach by Nehrir and Wang (2009) have an unconventional way to model the activation losses, while the approach by Larminie and Dicks (2003) does not account for concentration losses. It has therefore been developed an own approach as a combination of these two, accounting for both concentration losses and activation losses by means of the equations listed in section 2.1.4. The approach is represented as an equivalent electrical circuit in figure 3.6 and the double layer charge effect is given by the following equation:

$$V_C = \left(I - C \frac{dV_C}{dt} \right) (R_{act} + R_{conc}) \quad (3.1)$$

It follows that the overall fuel cell voltage is given by:

$$V_{FC} = E_{Nernst} - V_d - V_C - V_{ohmic} \quad (3.2)$$

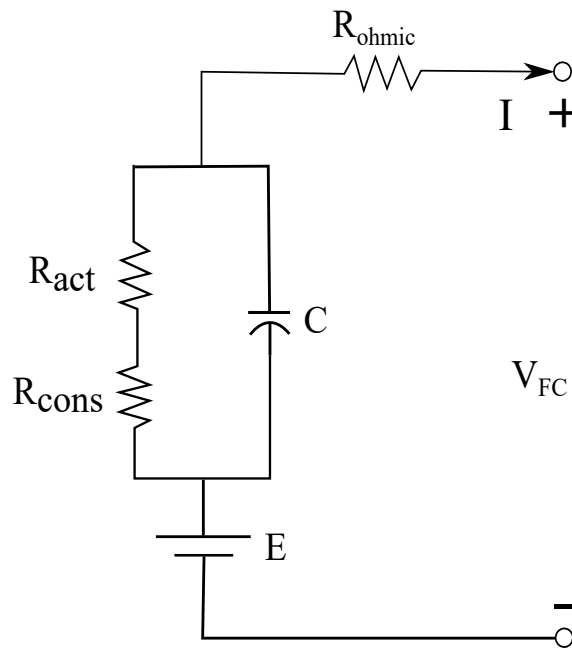


Figure 3.6: Equivalent electrical circuit of the modelled effect by the charge double layer

3.2.3 Further Simplifications

Certain assumptions have already been outlined in this chapter and through the outlining of the equations in chapter 2. Yet, further following simplifications have been applied in the modelling:

- Perfectly controlled humidifiers and heat exchangers are assumed to be applied. This assumption further imply that temperature and humidity conditions are idealized, and the humidifiers and heat exchangers are not considered in the model. This has been found necessary, as the literature review in section 2.4 showed that humidification and heat exchange can be performed in a variety of methods in fuel cell and electrolyser systems, and a general model is difficult to develop. These are assumptions also applied by Gou et al. (2016).
- It is assumed that there are no losses of substances through the system boundaries. The fuel cells and electrolysers are assumed to have no Faradaic losses and eventual hydrogen present at the fuel cell cathode is re-cycled to the anode by the ejectors.
- The fuel cells, electrolysers and all other system components are assumed to not experience any degradation. It was explained in section 2.5 that degradation phenomena in fuel cell and electrolyser systems are quite difficult to model. Moreover, the average degradation rates in table 2.1 and 2.2 imply that simulations must be performed with a very long time frames (years) to observe degradation effects. The simulations in this work will not be performed with such long time frames.
- Power electronics are not considered. It was suggested in section 2.4.8 how the power electronics can be treated simply by means of efficiency losses. However, because this work has a little focus on this field, the treatment of power electronics is left for further work.
- All input parameters except the current are assumed constant. Assumptions for the applied parameters follows in section 3.2.4.
- Parameters for individual fuel cell and electrolysers cells are lumped together to represent stacks. This imply that stack voltages and powers are obtained by multiplying the cell voltages and cell powers with the number of cells.
- The ideal gas assumption is applied in all cases, except for the hydrogen storage tank. It was discussed in section 2.3.2 why the Van der Waals equation gives a better representation of this.

3.2.4 Tuning of Constant Input Parameters

The equations applied in the model require a set of input parameters which have been considered constant. Certain of these parameters are simply physical constants and are listed in table 3.1. Further, there are several parameters which are specific for each fuel cell and electrolyser stack. For the PowerCell S3 and Proton OnSite M-series stack, these have been listed in table 3.2 and 3.3. These parameters have been obtained in three different ways. Certain parameters have been found in manufacturer datasheets or reports from other research projects. Further, a few parameters have been assumed by means of a combination of literature reviews and the best of the author's knowledge after communication with industrial representatives during seminars and meetings. The last set of parameters have been tuned in order to fit given experimental data. The modelling of the BoP components also require a few parameters specific for the equipment. Because no specific commercial BoP components have been selected for the system yet, there have been selected input parameters which can be assumed to be reasonable for this kind of system. These are listed in table 3.4. For all parameters, it is provided a reference footnote with an explanation for the assumed value.

3.2.5 Simulink Implementation

The model of the HES-OFF system was implemented in the Simulink[®] environment, and the dynamic simulations presented in chapter 4 was performed. Steady state diagrams were plotted by use of Matlab scripts. The implementations are further outlined in Appendix A and B.

Parameter	Symbol	Value	Unit	Ref.
Universal gas constant	R	8.314	$J/molK$	¹
Faraday's constant	F	96485	C/mol	1
Gibbs free energy of reaction 2.1	$\Delta\hat{g}_0$	228170	J/mol	2
Higher heating value	HHV	285800	J/mol	1
Specific heat capacity of air	$c_{p,air}$	1.0	$kJ/(kg \cdot K)$	³
Specific heat ratio of air	κ	1.4	-	3
Van der Waals constant	a	0.025	$m^6 Pa/mol^2$	4
Van der Waals constant	b	$2.66 \cdot 10^{-5}$	m^3/mol	4

Table 3.1: Input parameters general for all fuel cell and electrolyser systems

¹O'Hayre et al. (2016)

²Spiegel (2008)

³Moran et al. (2015): Evaluated at $15^\circ C$, ideal gas behaviour assumed

⁴Klell (2010)

Parameter	Symbol	Value	Unit	Ref.
<i>Found explicitly for the S3 125 kW stack</i>				
Cell active area	A_{cell}	300	cm^2	1
Number of cells	N_{cell}	455	-	2
Limiting current	I_L	570	A	3
<i>Assumed to the best of author's knowledge</i>				
Membrane hydration parameter at RH=100%	λ_m	14	-	4
Hydrogen inlet pressure	P_{H_2}	1.54	bar	2
Air inlet pressure	P_{air}	2.0	bar	2
Cell operating temperature	T	68	$^{\circ}C$	5
Membrane thickness	l_m	$5 \cdot 10^{-3}$	cm	6
Capacitance of charge double layer	C	6	F	7
Time constant for gas flows	τ_e	0.25	s	8
Empirical constant in eq. 2.32	λ_e	0.16	Ω	9
<i>Tuned to fit experimental data</i>				
Charge transfer coefficient	α	0.43	-	10
Exchange current density	i_0	$1 \cdot 10^{-5}$	A/cm ²	11

Table 3.2: Input parameters tuned for the PowerCell S3 stack, attempted to fit the experimental data in figure 3.2.

¹AUTO-STACK CORE (2018)

²PowerCell Sweden AB (2020d)

³Haberl (2017)

⁴Figure 2.4

⁵Assumed to be the same as the coolant temperature used in figure 3.2 (PowerCell Sweden AB, 2020d)

⁶Kienitz (2020) indicates that membrane thicknesses are typically the range of 10^{-3} - 10^{-2} cm

⁷Jaouen et al. (2003) reports a volume specific capacitance of $2 \cdot 10^7$ F/m³ for a Carbon/Nafion interface. This was measured for a cathode thickness of 10 μm , and for the active area of 300 cm^2 used in this work, this yields a capacitance of 6 F.

⁸Gou et al. (2016) state that fuel cells can have response times within seconds when perfectly controlled humidifiers and heat exchangers are assumed applied. Li (2005) further supports this by stating that MW fuel cell systems typically have response times within a second.

⁹Data for fitting has not been obtained, and the value used in the NW model 2.7.1 has been applied

¹⁰Must be between 0 and 1, and is typically around 0.5 (O'Hayre et al., 2016)

¹¹Within the range of numbers used in examples in Barbir (2013)

Parameter	Symbol	Value	Unit	Ref.
<i>Found explicitly for M-series 250 kW stack</i>				
Hydrogen outlet pressure	P_{H_2}	13	bar	1
Cell active area	A_{cell}	680	cm ²	2
Number of cells	N_{cells}	100	-	2
<i>Assumed to the best of autho's knowledge</i>				
Membrane hydration parameter at RH=100%	λ_m	14	-	9
Oxygen outlet pressure	P_{O_2}	1	bar	3
Limiting current density	i_L	2.5	A/cm ²	4
Cell operating temperature	T	58	°C	5
Membrane thickness	l_m	0.025	cm	6
Exchange current density	i_0	$1 \cdot 10^{-5}$	A/cm ²	8
<i>Tuned to fit experimental data</i>				
Charge transfer coefficient	α	0.4	-	7

Table 3.3: Input parameters tuned for the Proton OnSite M-series stack, attempted to fit the experimental data in figure 3.4.

¹The hydrogen pressure can be higher for the given stack, but the polarization curve provided by Anderson (2016) and replotted in figure 3.4 is obtained for 13 bar

²Bessarabov and Millet (2018)

³Air is assumed to be released to the atmosphere at approximately 1 bar

⁴Bessarabov and Millet (2018) suggest i_L for electrolyzers to be between 1 - 2.5 A/cm²

⁵Assumed the same as the stack operating temperature, which is 58°C (Bessarabov and Millet, 2018)

⁶Membrane thickness is typically 170 - 250 μm for electrolyzers (Anderson et al., 2013)

⁷Must be between 0 and 1, and is typically around 0.5 (O'Hayre et al., 2016)

⁸Assumed to be the same value as for fuel cells, presented in table 3.2

⁹Figure 2.4

Parameter	Symbol	Value	Unit	Ref.
<i>Assumed to the best of author's knowledge</i>				
Storage tank volume	V_{tank}	30	m ³	1
Storage tank temperature	T_{tank}	15	°C	1
Air compressor inlet temperature	T_{in}	15	°C	1
Storage tank initial mass	$m_{init,tank}$	300	kg	1
Air compressor efficiency	$\eta_{c,air}$	70	%	4
Hydrogen compressor efficiency	η_{c,H_2}	70	%	5
Purifier time constant	τ_p	2.5	s	6

Table 3.4: Parameters tuned for typical BoP components

¹Assumed for the purpose of this work with no further description

²70% is mentioned as a typical air compression efficiency in Barbir (2013)

³Discussed in section 2.4.2

⁴Set to match purifier lag with ramping time (min to max load) of the NEL M-series system (Nel ASA, 2020)

3.3 Evaluation of the Fuel Cell Model by Benchmarking with the Simscape Library Fuel Cell Stack Block

To evaluate the fuel cell stack model implemented to model the HES-OFF system, the model is benchmarked with the SimscapeTM Library Fuel Cell Stack block described in section 2.7.2. In this analysis, the Simscape FC block is operated with the preset values of the 6 kW - 45 Vdc stack. The benchmarking is obtained by tuning the developed model similarly and comparing the outputs. The reason why the model is evaluated by means of a comparison with the Simscape FC block, is because this has been considered as the best feasible alternative. Ideally, the developed fuel cell model should have been compared with experimental data of the PowerCell S3 stack. However, this has been found difficult to obtain, and the model is instead benchmarked with the well-established model - the Simscape FC block.

The polarization curve obtained from the Simscape FC block is plotted in figure 3.7. To approximate this polarization curve with the developed model, some of the similar input parameters can be used. In addition, certain parameters have to be assumed. All the parameters used in the developed model are listed in table 3.5. Note that all the assumed values in table are the same as assumed in table 3.2, except for A_{cell} , I_L and α . The time constant τ_e corresponds 25% of the response time of 1 second which is the default value used in the Simscape FC block.

The Simscape FC block was implemented with assistance from internal forces in the HES-OFF team in order to have current as input load. A more detailed outlining of the implementation can be found in Appendix C.

Parameter	Symbol	Value	Unit
<i>Same as preset values in Simscape:</i>			
Hydrogen inlet pressure	P_{H_2}	1.5	bar
Air inlet pressure	P_{air}	1	bar
Number of cells	N_{cells}	65	-
Cell operating temperature	T	65	$^{\circ}C$
<i>Assumed:</i>			
Exchange current density	i_0	$1 \cdot 10^{-5}$	A/cm^2
Membrane thickness	l_m	$5 \cdot 10^{-3}$	cm
Membrane hydration parameter	λ_m	14	-
Cell active area	A_{cell}	100	cm^2
Limiting current	I_L	270	A
Charge transfer coefficient	α	0.415	-
Capacitance of charge double layer	C	6	F
Time constant for gas flows	τ_e	0.25	s

Table 3.5: Input parameters in the developed model in the benchmarking with the Simscape FC block

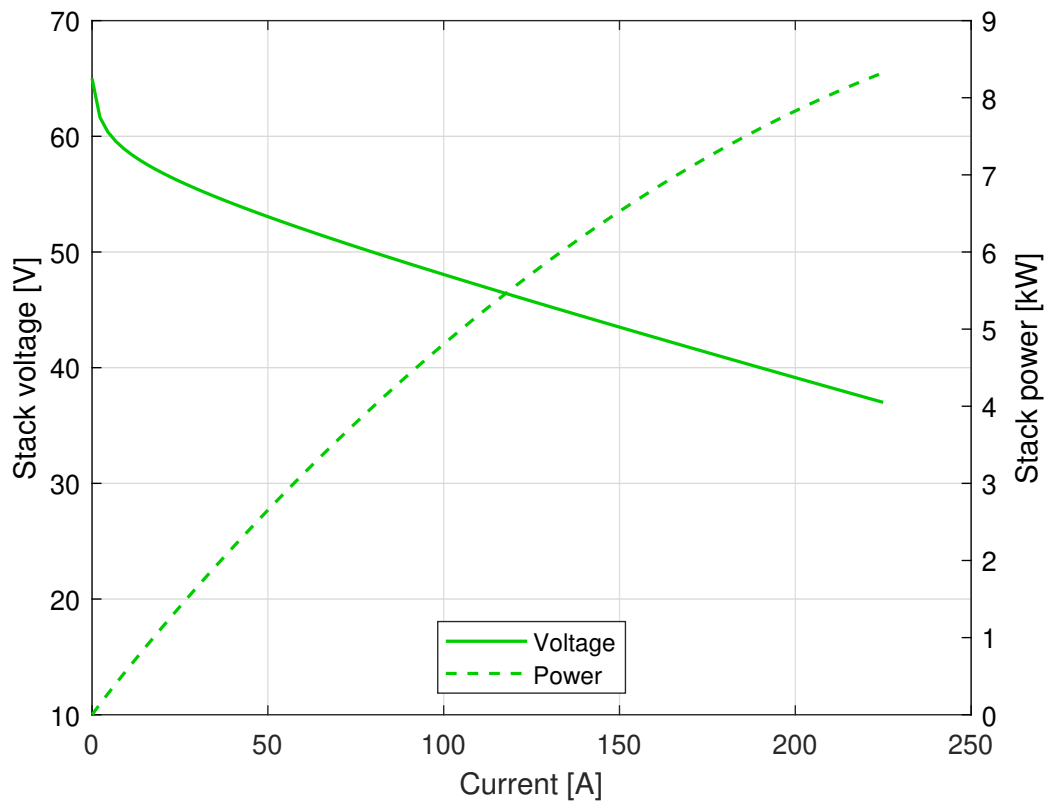


Figure 3.7: Polarization and power curve obtained from the Simscape FC block

Results and Discussion

In this chapter, the results from the work is presented and discussed. Section 4.1 to 4.4 demonstrate the features and capabilities of the developed model by means of different simulations. Further, section 4.5 presents the results of a sensitivity analysis which was performed for certain parameters, followed by section 4.6 which outlines about the benchmarking of the fuel cell model with the Simscape FC block. Section 4.7 considers the weight and footprint of the modelled system, before the chapter is ended with a discussion of the work in section 4.8.

4.1 Demonstration of Fuel Cell Stack Submodel

4.1.1 Steady State Diagrams

The modelled polarization curve of the fuel cell cells is plotted in figure 4.1 by means of the input parameters listed in table 3.1 and 3.2. Additionally, the provided polarization curve from the manufacturer of PowerCell S3 is plotted in the same figure. From the modelled curve, the three characteristic regions (activation, ohmic and concentration region) are identified by visual inspection. The polarization curve is plotted towards current, I , and not the area normalized current density, i . This is for ease of comparison to the provided curve from the manufacturer, which is presented in this form. In the model, the transformation between current and current density is obtained by equation 2.4.

The manufacturer polarization curve is not plotted for currents over 450 A, which corresponds to the concentration region. It is stated in Yang et al. (2018) that this region is often excluded because operation here is not allowed in practical conditions. This may be because the efficiency significantly decreases for this high current densities, which is depicted in figure 4.2 where the voltage efficiency is plotted. Moreover, it was mentioned in section 2.5 that electrolysers exhibit increased degradation rates during operation at high currents. Due to the similarities between fuel cells and electrolysers, fuel cells can possibly exhibit similar behaviors, which make operation in the concentration region even less advantageous.

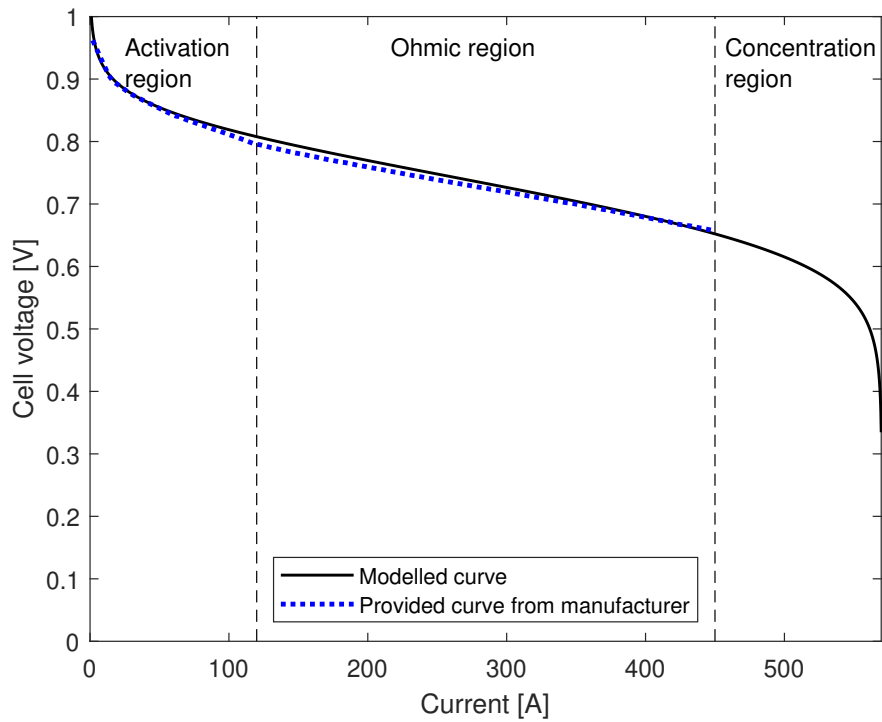


Figure 4.1: Modelled fuel cell polarization curve for PowerCell S3 compared to the provided curve by PowerCell Sweden AB (2020d)

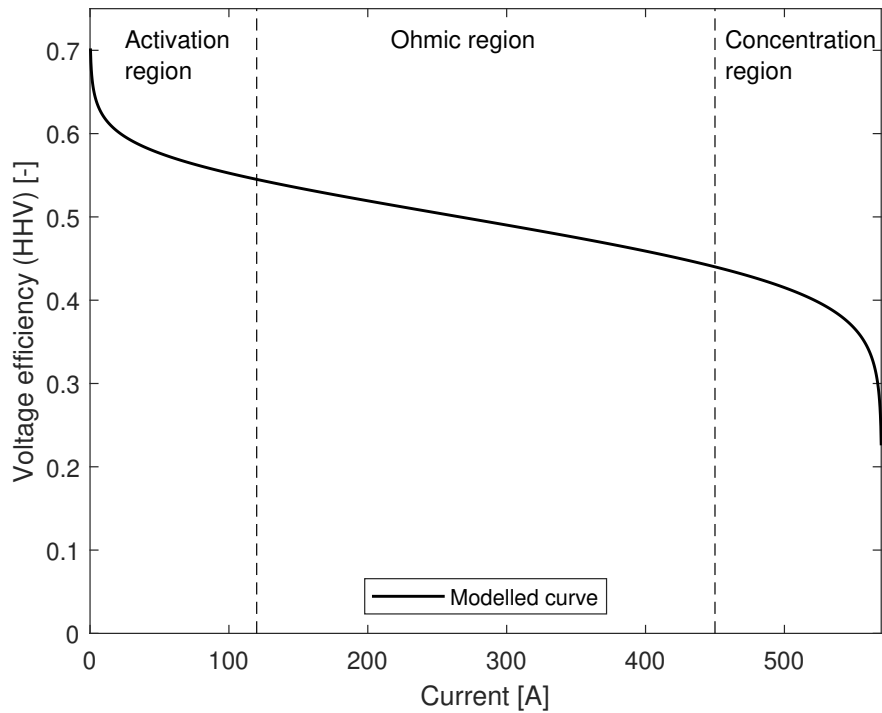


Figure 4.2: Modelled fuel cell voltage efficiency plotted towards current

It can be observed from figure 4.1 that the modelled polarization curve follows the provided curve reasonably in the activation region and the ohmic region. Because data are not provided for the last region, the model parameters are not tuned for this. The part of the modelled curve in the concentration region is therefore solely predicted by the theory behind model and the parameters fitted for the two other regions.

As mentioned, figure 4.2 plots the modelled voltage efficiency of the fuel cell stacks. Further are the Faradaic losses and other substance loss assumed to be negligible (section 3.2.3), from which it follows that the current efficiency (equation 2.49) is 100%. By means of equation 2.1.7, the voltage efficiency plotted in figure 4.2 therefore represents the overall fuel cell stack efficiency in the model from inlet gaseous hydrogen to output DC electricity from the stack. Furthermore, figure 4.2 outputs a fuel cell efficiency varying between approximately 30-70%. Moreover, the efficiency varies between roughly 45-55% in the ohmic region, which is likely to be the most frequently used operating region as it features a combination of relative high current and high efficiency. It has been claimed the PowerCell S3 will exhibit an efficiency of 52% when installed in the MS-100 system (Ekdunge, 2017), which is in the range of what figure 4.2 outputs. It must be emphasised that this efficiency might comprise additional losses than what is accounted for in the voltage efficiency, which consequently give lower efficiency values than the voltage efficiency. On the contrary, the efficiency was determined by means of the LHV which will output a slightly higher value than the HHV efficiency.

Figure 4.3 plots the cell power towards current, for which the modelled output curve and the provided curve from the manufacturer is plotted. Additionally, is a projected stack power displayed on the right axis, which is assumed to be the cell power scaled up according to the number of cells in one stack. It must therefore be emphasised that the provided power curve from the manufacturer only comprise the cell power and the stack power is modelled. Moreover are the characteristic regions identified in the polarization curve (figure 4.1) reprinted in the plot.

Similar as for the polarization curve, the provided power curve stops at 450 A. Yet, for lower currents, the modelled power curve appears to match the manufacturer data with relatively small deviations (order of few Ws). In the concentration region, the power drops radically according to voltage decrease observed in figure 4.1.

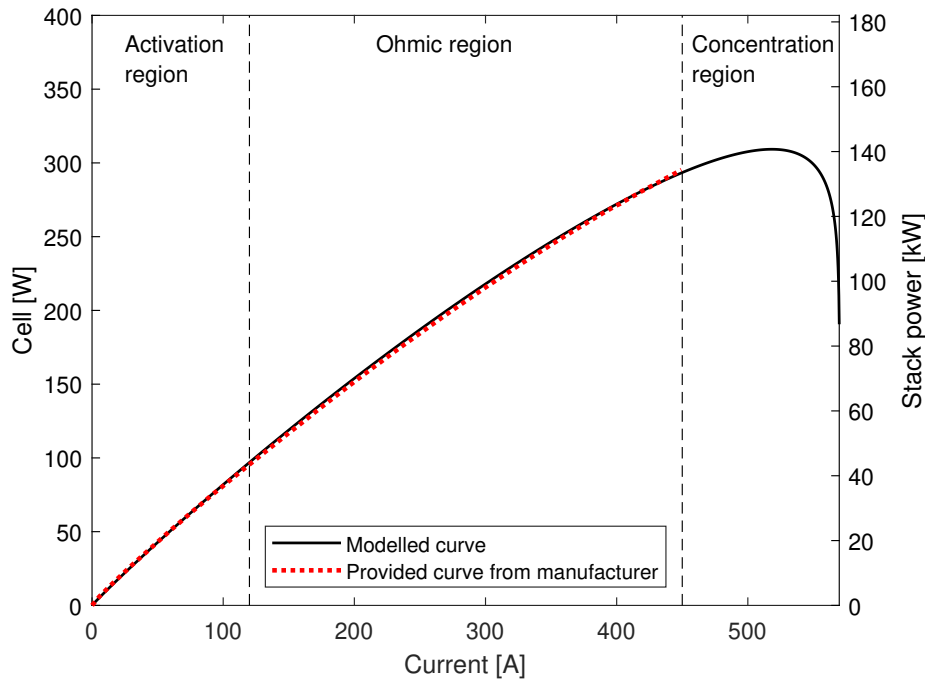


Figure 4.3: Modelled fuel cell power of PowerCell S3 compared to the provided curve in PowerCell Sweden AB (2020d). The stack power, which is cell power scaled by the number of cells is plotted on the right axis.

The modelled stack power peaks at approximately 140 kW, and the maximum stack power in the ohmic region is around 130 kW. Both of these values are beyond the claimed capacity from the manufacturer of PowerCell S3, which is 125 kW (PowerCell Sweden AB, 2020d). The modelled stack power obtained by scaling the cell power with the number of cells may therefore yield insufficiently high values. However, as it has been explained, fuel cells are rarely operated in the concentration region. Assuming that the power at the upper boundary of the ohmic region is what the manufacturers consider as the maximum power, the modelled power therefore corresponds reasonably with the rated power of the stack (125 kW).

A calculated performance parameter describing the electric energy production per mass of fuel consumed by the fuel cell stacks is plotted in figure 4.4. This parameter can be convenient for the understanding of the energy conversion in the hydrogen energy storage system. The voltage efficiency is plotted in the same graph, and it can be observed that the performance parameter curve follows the shape of the efficiency curve.

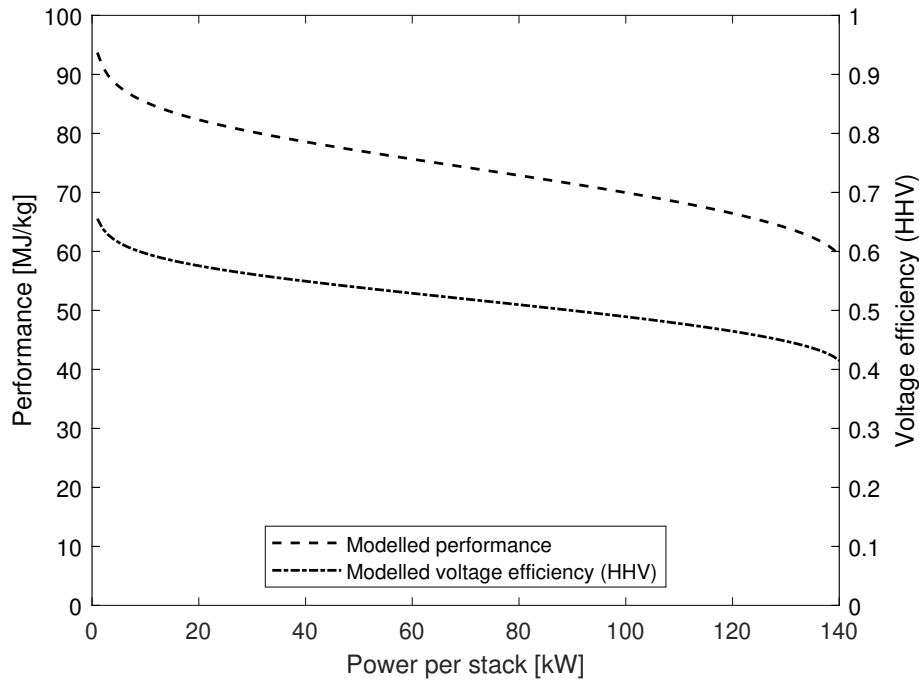


Figure 4.4: Modelled performance parameter [MJ/kg] and voltage efficiency plotted towards stack power

4.1.2 Dynamic Behaviour

Figure 4.5 plots the modelled dynamic fuel cell stack voltage, when the fuel cells are exposed to a step increase in current (at $t=15$ s). The current is increased from 250 A to 300 A, which spans within the ohmic region (Figure 4.1). Before the current increase ($t < 15$ s), the stack voltage is stable around 340 V, while after the current increase, the voltage stabilizes to approximately 330 V. Both of these voltages correspond to the steady state polarization curve in figure 4.1 (if the cell voltage is scaled by the number of cells). However, immediately after the current step is applied, the voltage undershoots significantly compared to the later obtained steady state voltage.

The undershoot effect can be ascribed to the mass transport delay inside the fuel cells caused by the inertia of reactant gas flows (equation 2.32). The voltage undershoot vanishes after approximately 1 second, which corresponds to 4 times the time constant τ_e in equation 2.32. According to the same equation, the voltage undershoot should have a maximum amplitude of $\lambda_e \cdot I$, obtained immediately after the current step. However, it can be observed from figure 4.5, that the bottom of the undershoot does not follow this abrupt behaviour predicted by equation 2.32, but is rather smoothed. This is explained by the double layer charge effect outlined in section 2.1.6. In this modelling activity, the effect is modelled by equation 3.1 which can further be reorganized to show that the charge double layer causes a damping effect to voltage changes:

$$V_C = V_{act} + V_{conc} - \underbrace{C \frac{dV_C}{dt}}_{\text{Damping effect}} (R_{act} + R_{conc}) \quad (4.1)$$

The first two parts of equation 4.1 are the activation and concentration losses (equation 2.18 and 2.23). These increase as the current increases (and opposite), which further change V_C similarly. Because C , R_{act} and R_{conc} are always positive, the last part of equation 4.1 will therefore always work against any change in V_C . In other words, the charge double layer will damp voltage fluctuation caused by current changes, since the charge double layer effect, V_C , is included in the overall fuel cell voltage (equation 3.2).

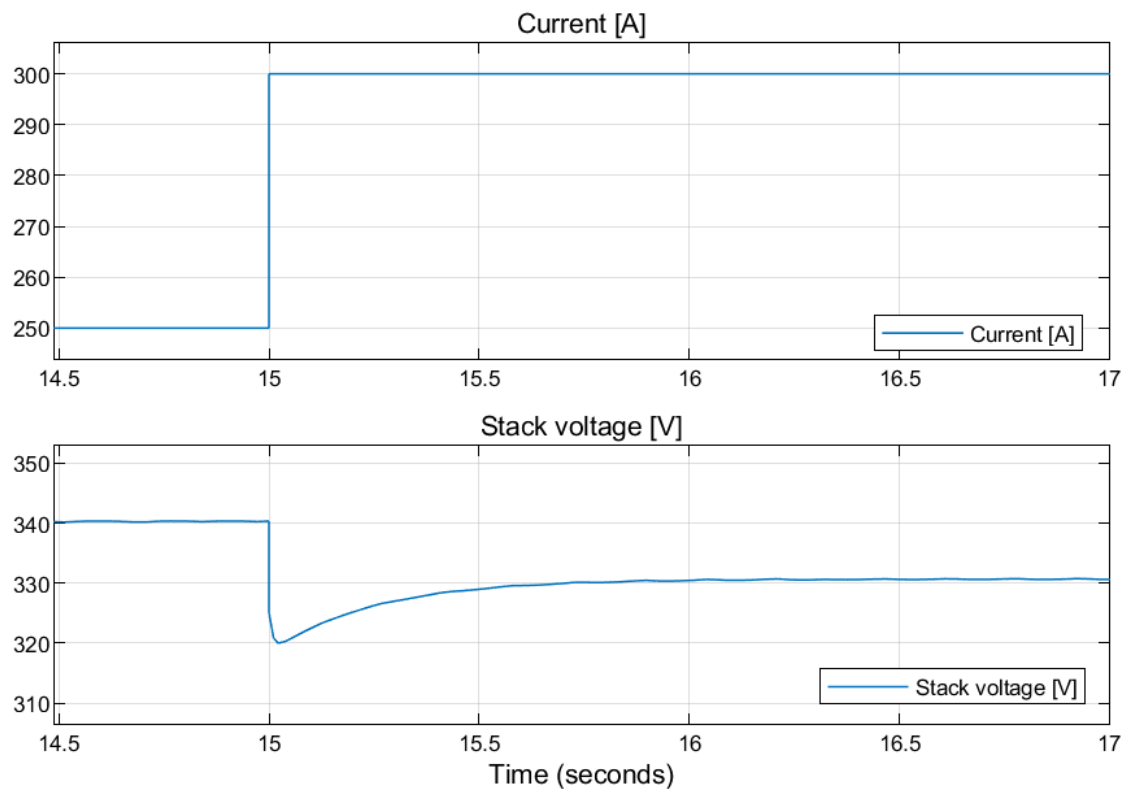


Figure 4.5: Response of modelled fuel cell stack voltage to a step increase in current.

Figure 4.6 plots the fuel cell stack voltage response when the current is step decreased. Opposite to the case where the current was increased (figure 4.5), the mass transport delay here contributes to a voltage overshoot. The peak of the overshoot is further smoothed because of the double layer charge effect which is present due to the current change.

In both figure 4.5 and 4.6, it can be observed small voltage oscillations at steady state stack voltage. These fluctuations can be ascribed to the charge double layer which appears to be somewhat unstable for the given parameters. Further tuning of the capacitance parameter C can perhaps prevent these oscillations from occurring.

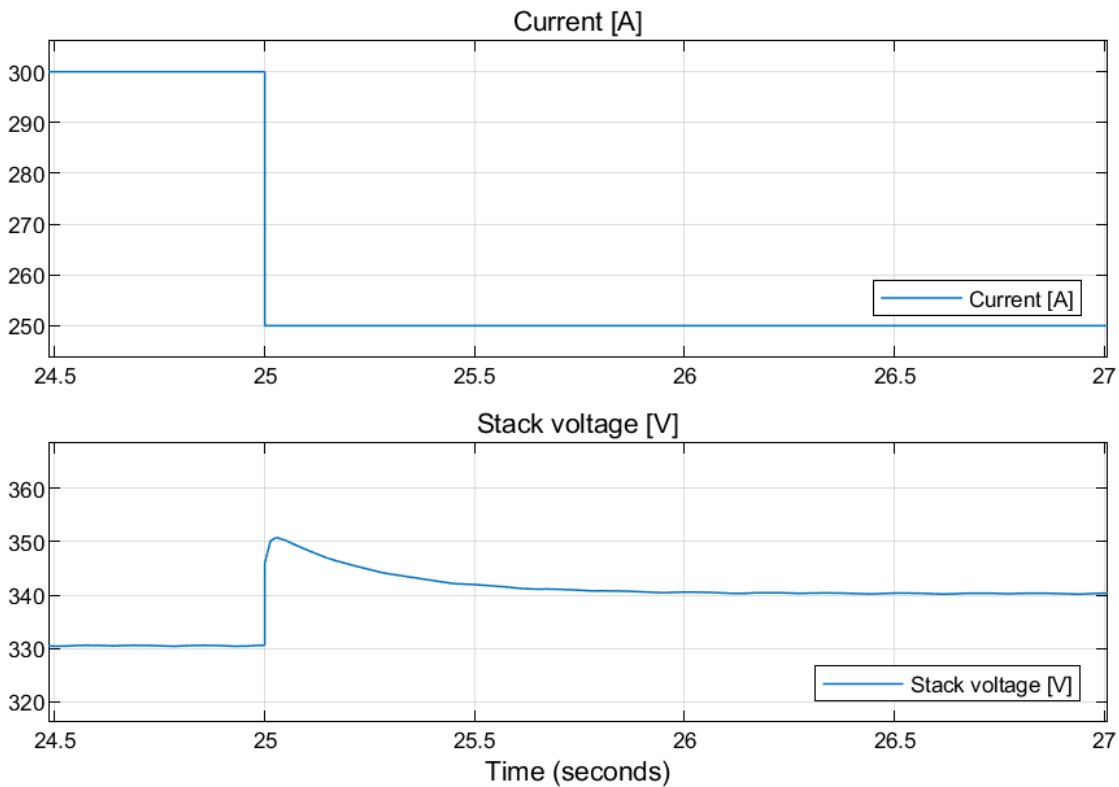


Figure 4.6: Response of modelled fuel cell stack voltage to a step decrease in current

4.2 Demonstration of Electrolyser Stack Submodel

As mentioned in section 2.2.4 there have not been found any sufficient dynamic models for electrolyser stacks. Electrolyser dynamics are generally less analysed in published research compared to fuel cell dynamics. Therefore, to developed a model for electrolyser stacks similar to what has been developed for fuel cells in this work, it therefore requires experimental activities or extensive access to experimental data for state-of-the-art electrolysers. This has been considered far beyond the scope of this work, and the dynamic behaviours of electrolysers are therefore not modelled. By means of current step variations which were performed for fuel cells in figure 4.5 and 4.6, the electrolyser voltage will therefore always be exactly the same as the steady state voltage (i.e. no charge double layer effect or voltage drops due to mass transport delays like in fuel cells). The dynamic behaviours are not illustrated for electrolysers in the similar way as what was performed for fuel cells in section 4.1.2, but the steady state diagrams are presented in the following.

4.2.1 Steady State Diagrams

The modelled polarization curve for the Proton OnSite M-series electrolyser stack is plotted in figure 4.7. Further are the three characteristic regions (activation, ohmic and concentration region) identified by visual inspection. The provided polarization curve from the manufacturer of the stack is plotted in the same figure for comparison. Similar as for

the fuel cell stacks, the electrolyser manufacturer polarization curve is not provided for the concentration region. Again, this might be explained by the unfavourable conditions in this region due to low efficiency (demonstrated in figure 4.8) and aggravated degradation (section 2.5). The modelled polarization curve appears to follow the provided polarization curve with deviations in the order of 0.01 V. The deviations are smaller in the ohmic region than in the activation region, which is favourable due to the expectation that the stacks will be mostly operated in this region as it features high currents yet relatively high efficiency.

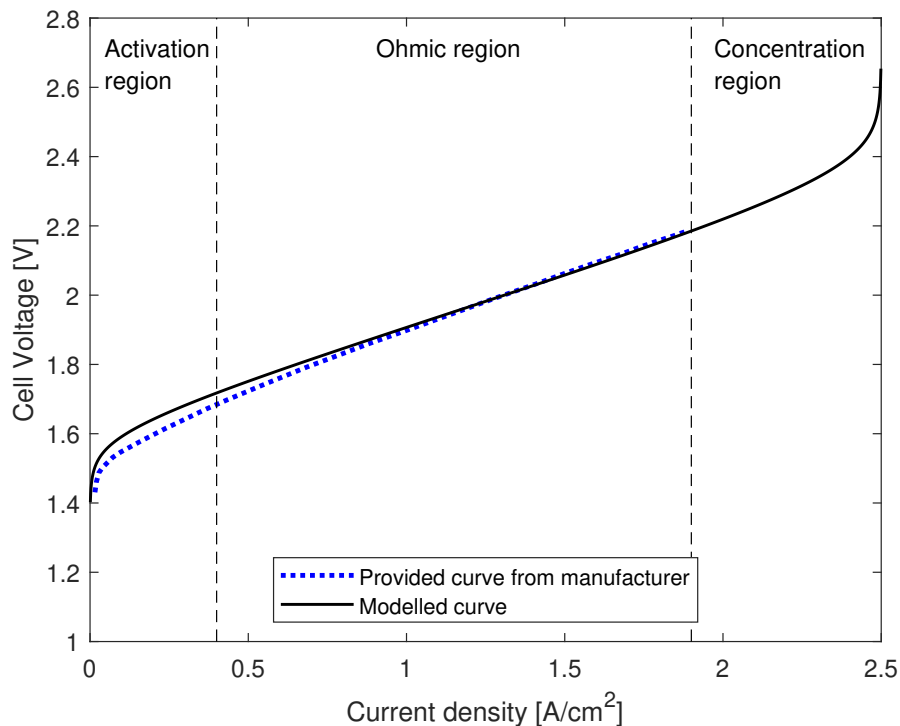


Figure 4.7: Modelled electrolyser polarization curve of Proton OnSite M-series 250 kW compared to the curve provided by Anderson (2016)

Figure 4.8 illustrates the modelled voltage efficiency of the electrolyser stacks, where the three characteristic regions are replotted from the visual inspection in figure 4.7. Again, the Faradaic losses are assumed to be negligible and voltage efficiency therefore also represents the overall stack efficiency. It can be observed that the voltage efficiency tends to be more than 100% for the instant of extremely low current density. This is because the electrolyser losses (activation, ohmic and concentration losses) which normally account for the waste heat release are very low, such that the electrolyser will rather consume heat due to the reversible heat in the chemical reaction of splitting water (equation 2.1). The electric power input to the electrolyser is therefore less than the energy stored in the product hydrogen and oxygen, and the efficiency exceeds 100%. However, for real electrolyzers where the Faradaic losses cannot be neglected, the voltage efficiency would most likely not be representative for the overall stack efficiency at this low currents. The

Faradaic losses, which were described in section 2.2.5 to be most present at low currents, would contribute to a lower overall stack efficiency in region of extremely low currents.

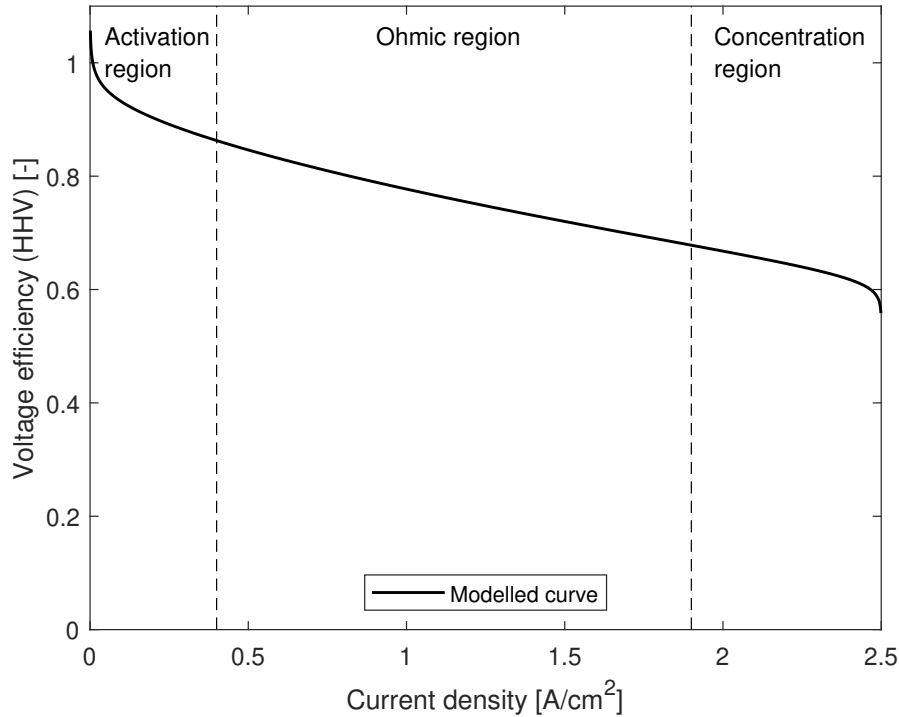


Figure 4.8: Modelled voltage efficiency of Proton OnSite M-series 250 kW electrolyser stack

The modelled electrolyser input power is plotted in figure 4.9. In section 3.1.3, it was mentioned that the Proton Onsite M-series stack has a rated power of 250 kW. The modelled stack power exceeds this value significantly, particularly in the concentration region. However, by reasons which have been mentioned, operation in the concentration region is unfavourable for electrolysers. Indeed, the provided polarization curve (figure 4.7) excludes this region, and the curve is provided up to a current density of approximately 1.8 A/cm^2 . At this current density, the modelled stack power is slightly above 250 kW. Hence, the rated power of 250 kW might therefore correspond to the maximum power which the electrolyser is practically operated under, and not the maximum achievable power.

A calculated performance parameter describing the amount of hydrogen produced per unit electric energy in the electrolyser stacks is plotted in figure 4.10. The curve of this parameter follows the shape of the efficiency curve which is plotted on the right axis in the figure.

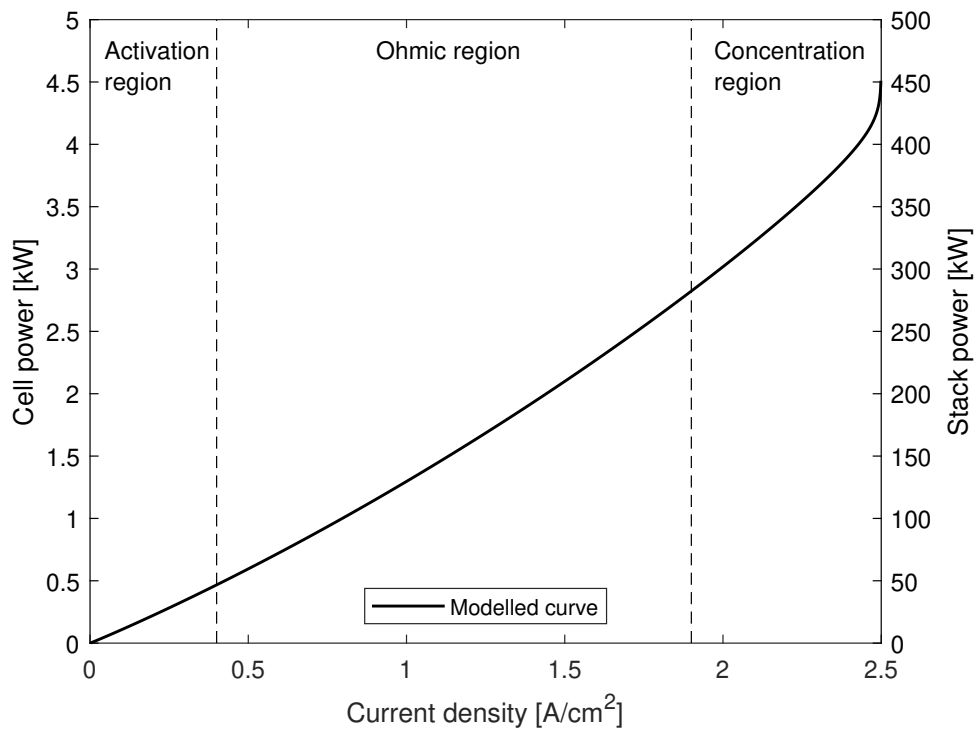


Figure 4.9: Modelled power of Proton OnSite M-series 250 kW electrolyser stack

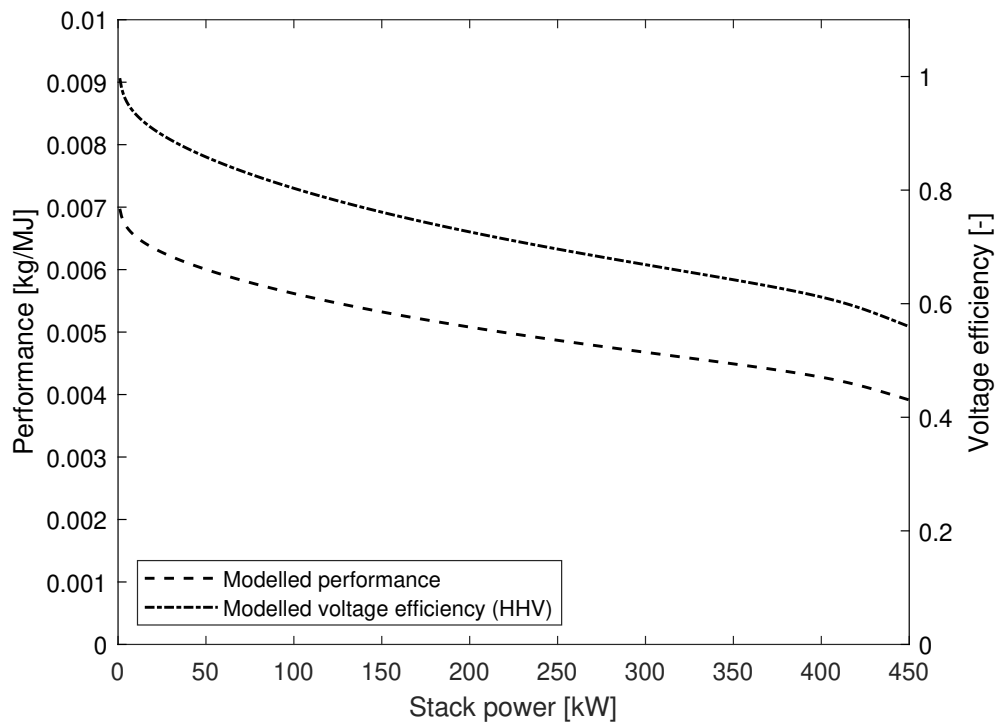


Figure 4.10: Modelled performance parameter [kg/MJ] and voltage efficiency of Proton OnSite M-series 250 kW electrolyser stack. Plotted towards stack power

4.3 Demonstration of Fuel Cell and Electrolyser Modules

4.3.1 Total Power and Demonstration of Modular Loading Opportunities

Figure 4.11 and 4.12 display the total power output from the hydrogen energy storage system when the fuel cell modules are loaded by means of two different strategies. The two cases have the same output power, but as it has been described in chapter 3, the modular design allows for non-simultaneous loading of the modules to obtain a specific power output.

Figure 4.11 displays the total system power output when all the modules are loaded equally. The lower plot shows that the stacks are first loaded at 300 A at $T = 30$ s which gives an approximate system output power of 1.5 MW (displayed in the uppermost plot). At $T = 100$ s, the fuel cells are gradually ramped up to a current of approximately 410 A which makes the system reach its capacity of 2 MW electric power output.

Figure 4.12 shows how the similar power output as obtained by the previous loading strategy can be obtained by a non-simultaneous loading of the modules. At $T = 30$ s, module 1, 2 and 3 are loaded with a current of 410 A, providing a system power output of 1.5 MW. Further ramping at $T = 100$ s to obtain the system capacity of 2 MW is obtained by ramping the last module from 0 – 410 A. With this loading strategy, the three first modules are operated at a constant load throughout the cycle, while it is only one module which undergoes the dynamic loading from $T = 100$ s. Less fuel cell stacks therefore undergo the potentially harmful load variations which was discussed in section 2.5. The example of the non-simultaneous loading is included in this work to showcase the opportunities provided by the modular design, which has been subject for discussions through the work with the HES-OFF project.

Similar as the fuel cells, the electrolyser modules can be loaded non-simultaneously. Figure 4.13 shows an example loading where all modules are loaded simultaneously giving a certain power input to the hydrogen energy storage system. Figure 4.14 shows how this same power input profile can be obtained by constant loading of three modules and ramping only one module.

4.3.2 Total Fuel Cell and Electrolyser Waste Heat

Figure 4.15 plots the waste heat produced by the fuel cells and electrolysers, when the fuel cell and electrolyser system are sequentially ramped up to their capacities of 2 MW. It can be observed that the waste heat is significantly larger during fuel cell operation, where the peak waste heat exceeds 2 MW.

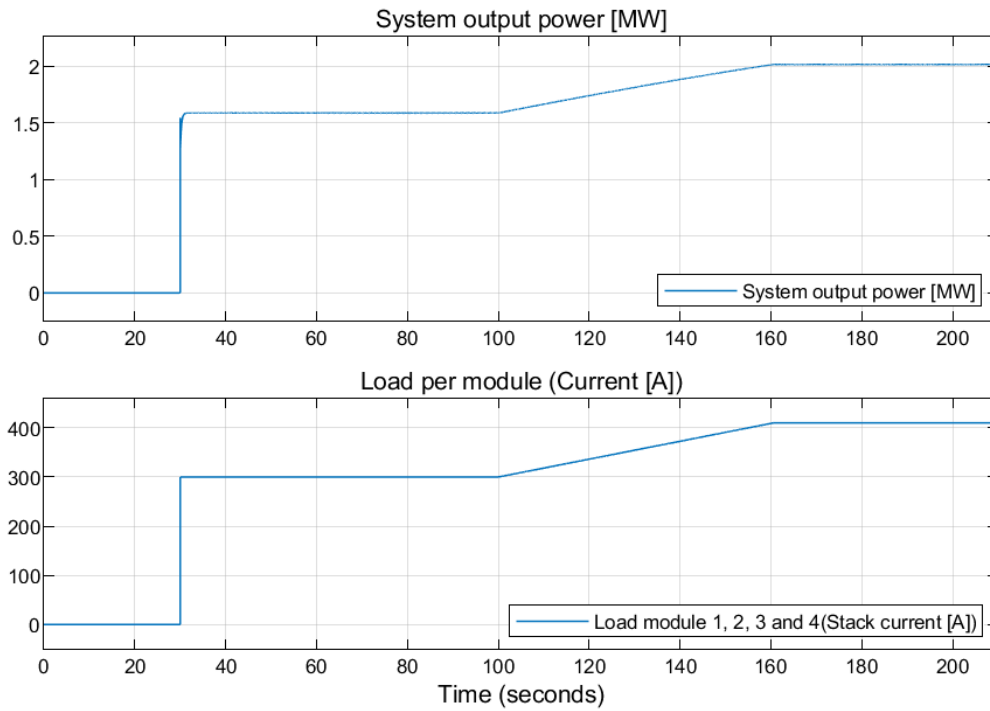


Figure 4.11: Total fuel cell power when all stacks are loaded simultaneously. The upper plot shows the total power and the lower plot shows the loading of each stack

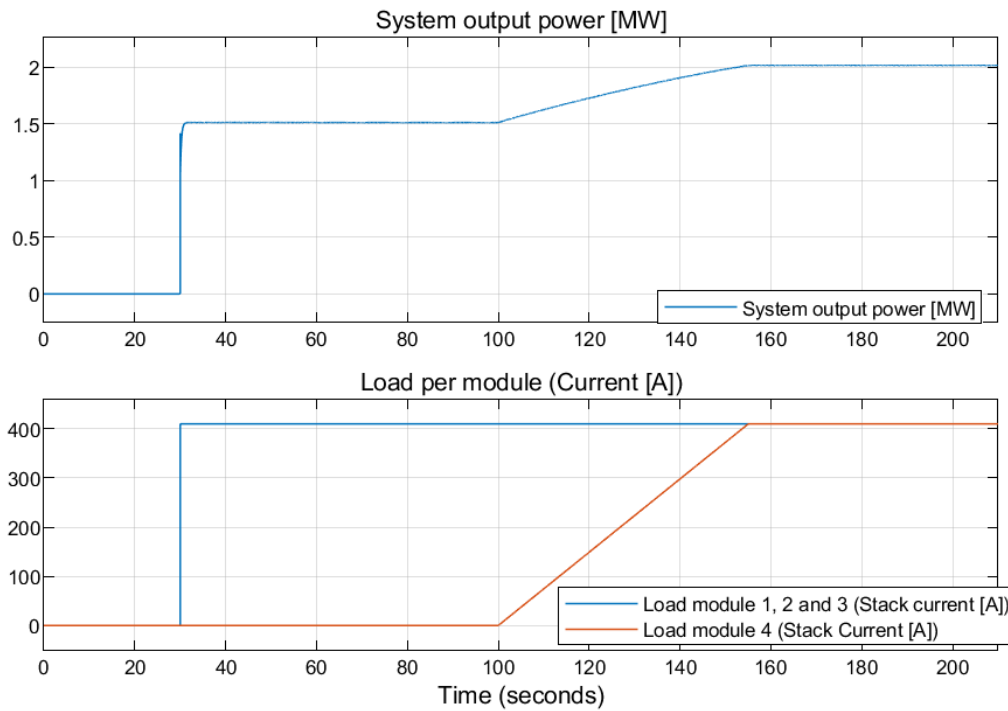


Figure 4.12: Total fuel cell power non-simultaneous loading of the modules. The upper plot shows the total power and the lower plot shows the loading of each stack in the given module

4.3 Demonstration of Fuel Cell and Electrolyser Modules

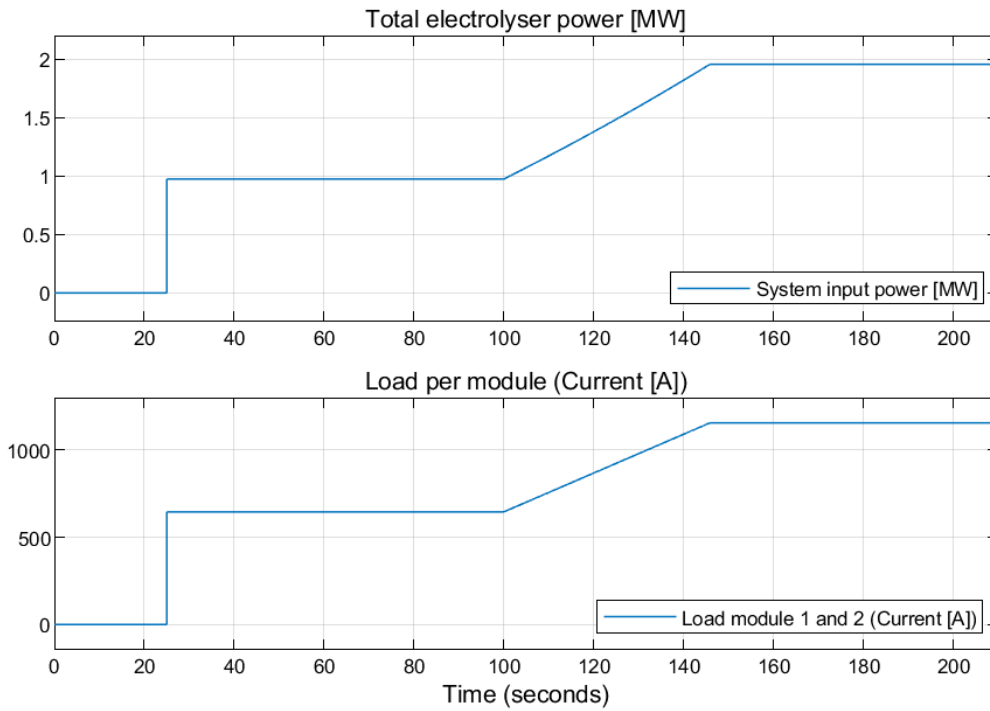


Figure 4.13: Total electrolyser power when all stacks are loaded simultaneously. The upper plot shows the total input power and the lower plot shows the loading of each stack

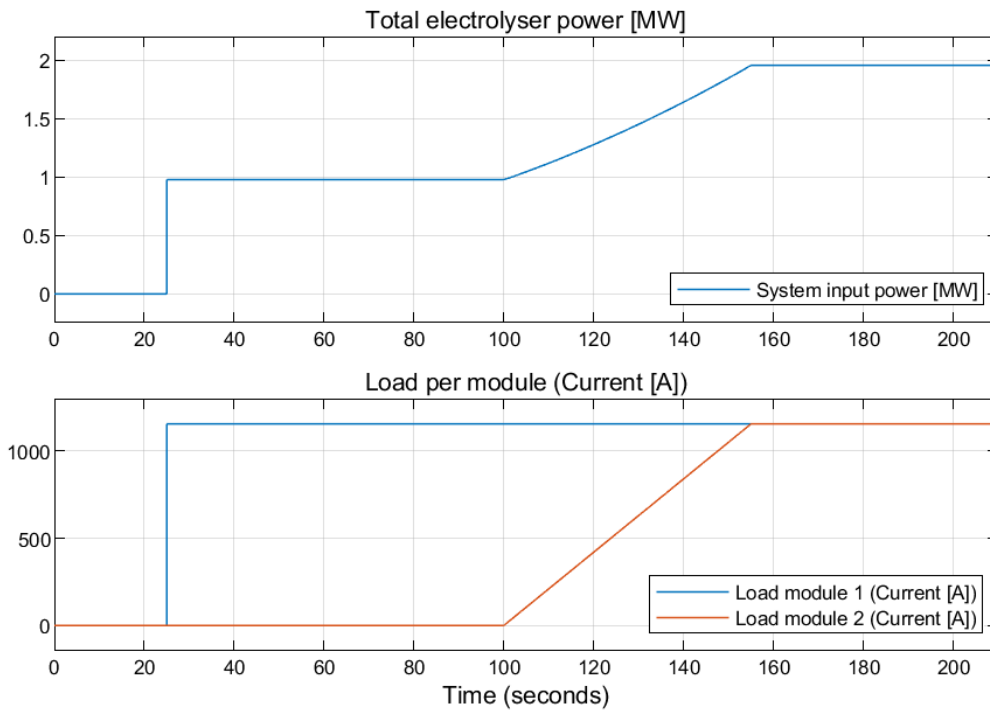


Figure 4.14: Total electrolyser power non-simultaneous loading of the modules. The upper plot shows the total power and the lower plot shows the loading of each module

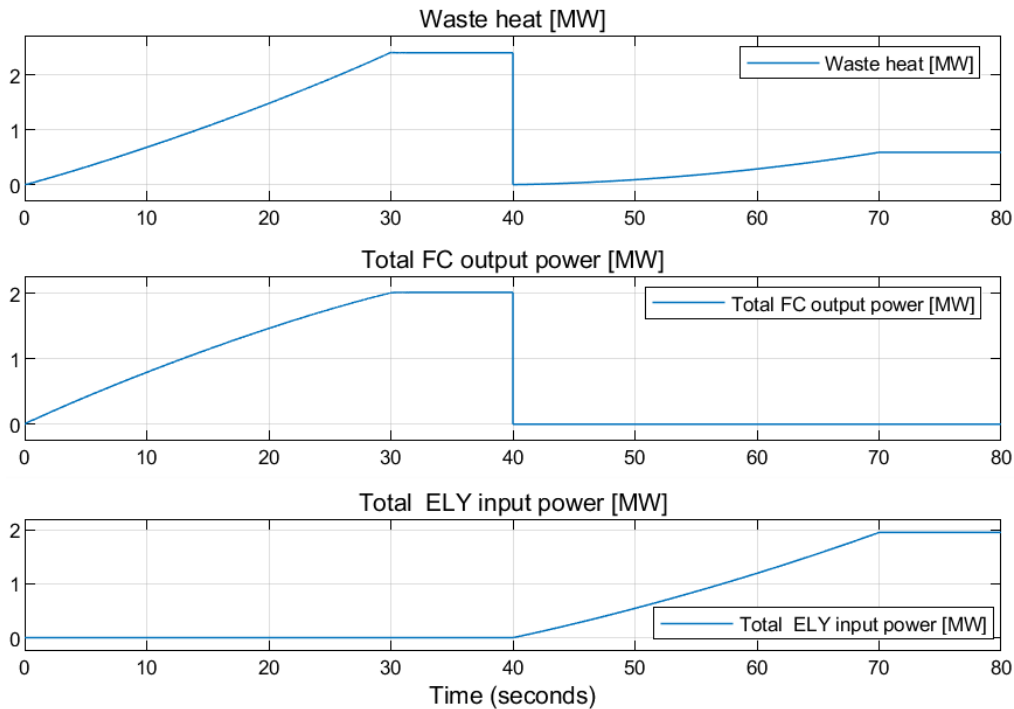


Figure 4.15: Waste heat when the system is ramped sequentially up to the maximum fuel cell and electrolyser capacity. Simultaneous loading of stacks is applied in this simulation

4.4 Demonstration of BoP Components

4.4.1 Air compressor

The air compressor behaviour is demonstrated by means of the compressor power in the lower plot of figure 4.16. The compressor power, given by equation 2.70, is dependent on the air mass flow into the fuel cells, which is further through Faraday's law dependent on the fuel cell current. As there has not been implemented any time delay on the compressor, the compressor power reacts instantly to the changes in fuel cell current (uppermost plot) and has no time lag as illustrated by the fuel cell power displayed in the middle plot of figure 4.16. The air compressor power at 2 MW fuel cell power is approximately 100 kW, which corresponds to roughly 5% of the fuel cell power. Time delays could possibly be implemented relatively simple in the compressor model by modelling first order time delays on different parameters. Yet, this is not performed in this work because it would also require information about how these time lags would affect the fuel cell operation.

4.4.2 Purifier

The behaviour of the hydrogen purifier is demonstrated in figure 4.17 by means of a step increase in electrolyser power. As it already has been discussed, there are no dynamics included in the modelling of the electrolyser stacks. The outlet mass flow of the electrolysers will therefore directly follow the electrolyser power plotted in the upper plot in figure

4.17. However, as discussed in section 2.4.7, the purification unit induce a time lag to this mass flow by means of a first order time lag. In figure 4.17, the electrolyzers are ramped from 0 to 2 MW input power (corresponding to min to max loading) at $T = 10$ s, and it can be observed in the lower plot that the mass flow after the purifier uses roughly 10 seconds to respond to this change. The time constant for the purifier was set to match the response time of the Nel 2 M-series 2 MW system (table 3.4), which is claimed to have a response time of less than 10 seconds for min to max load change (Nel ASA, 2020).

4.4.3 Hydrogen Compressor and Storage Tank

The hydrogen compressor power is showcased in figure 2.4.2 by loading the electrolyzers at 2 MW for a prolonged time. By means of equation 2.76, it follows that the compressor power increases logarithmically with the storage tank pressure. To see the effects of a changing tank pressure, the simulation is run for 10 hours. Figure 2.4.2 shows how the compressor power increases as the tank pressure increases. For the initial pressure of approximately 150 bar, the compressor power is roughly 45 kW, but as the tank pressure approaches 350 bar, the compressor is consuming about 62 kW electric power.

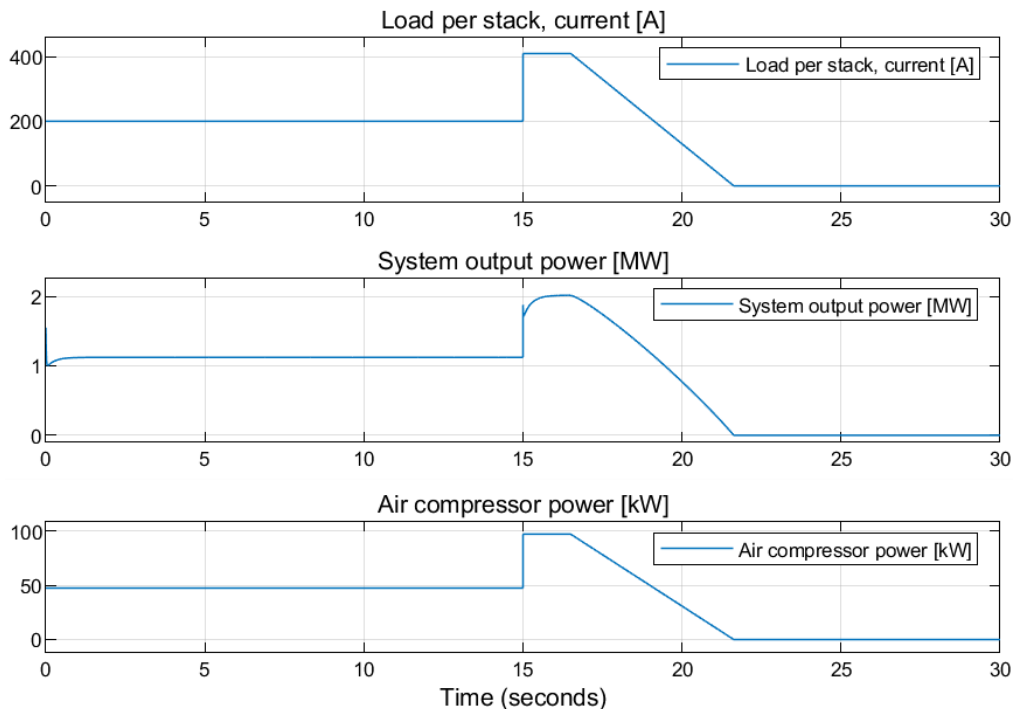


Figure 4.16: Demonstration of air compressor power (lower plot) when all the fuel cell stacks are loaded according to the upper plot

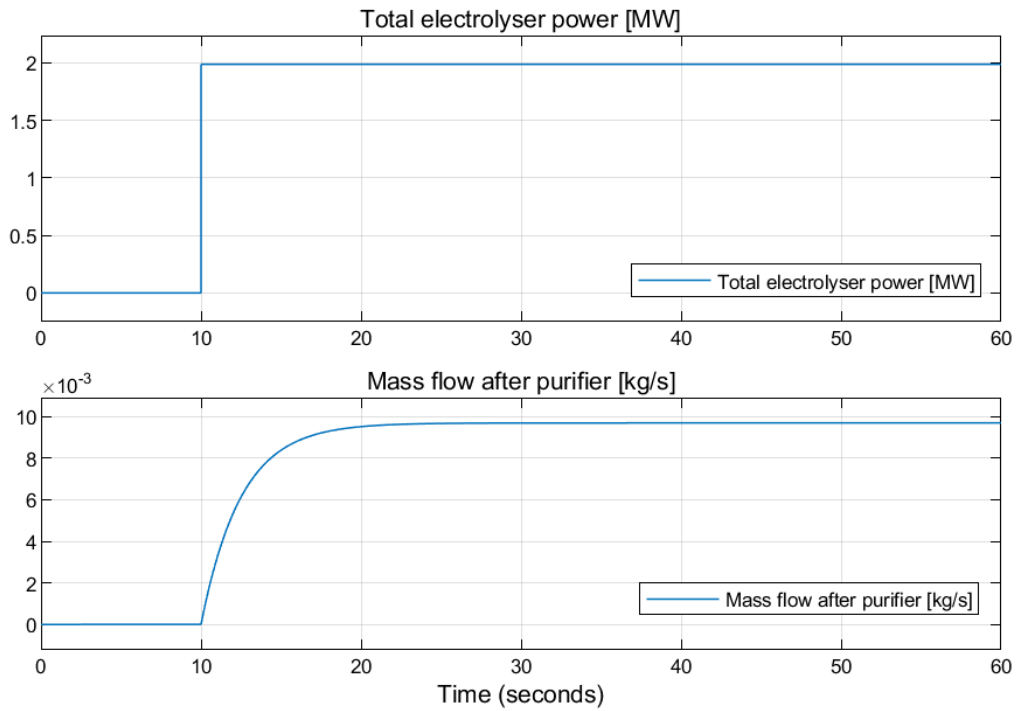


Figure 4.17: Demonstration of time lag induced on the hydrogen flow by the purifier after the electrolyzers.

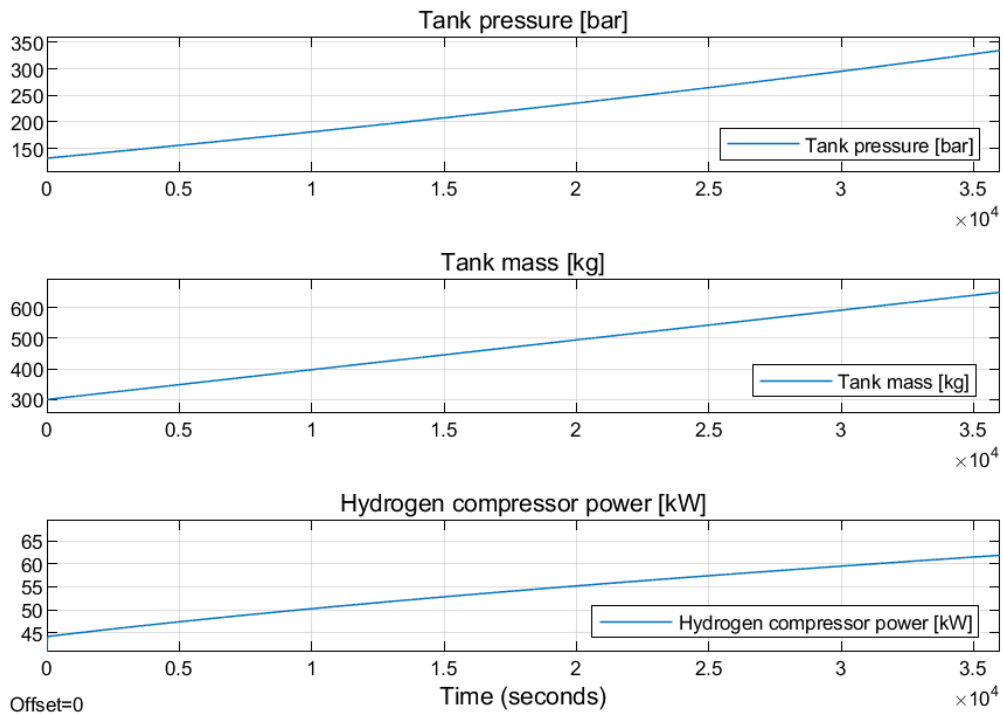


Figure 4.18: Demonstration of hydrogen compressor power (lower plot) for increasing tank pressure (upper plot)

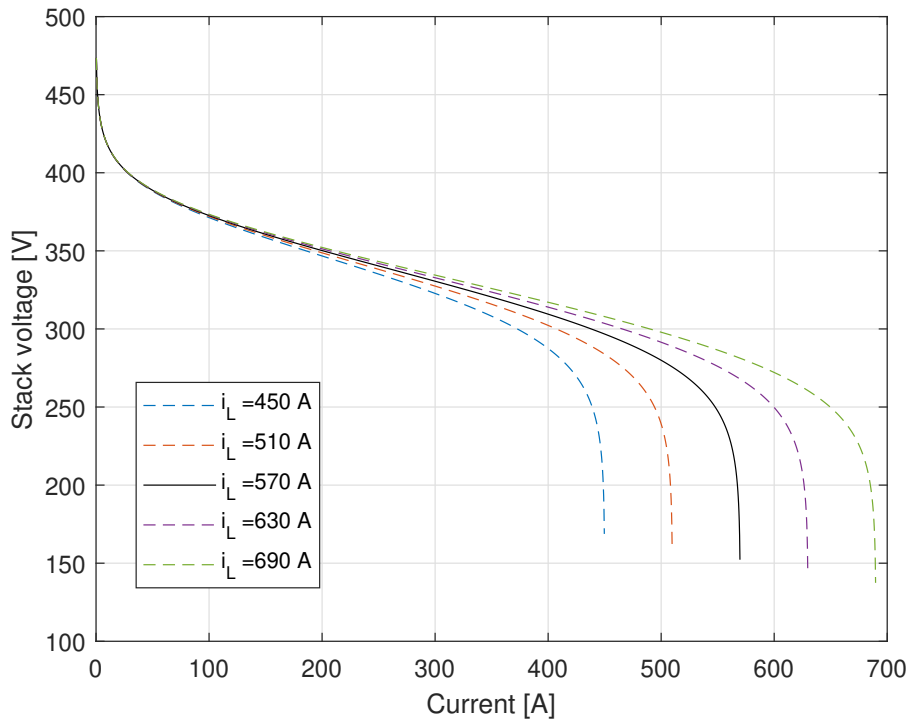
4.5 Sensitivity Analysis

To achieve a broader understanding of how the developed model depends on the input parameters, a sensitivity analysis of certain parameters has been conducted. The analysis was performed by simple means of sequentially varying each parameter within reasonable limits, while holding the remaining parameters fixed to what is listed in table 3.1 to 3.4. By plotting the model outputs, the sensitivity of the parameters is highlighted. The analysis was only performed for operational parameters or parameters which it is considered difficult to determine, which implies that the following parameters have been analysed:

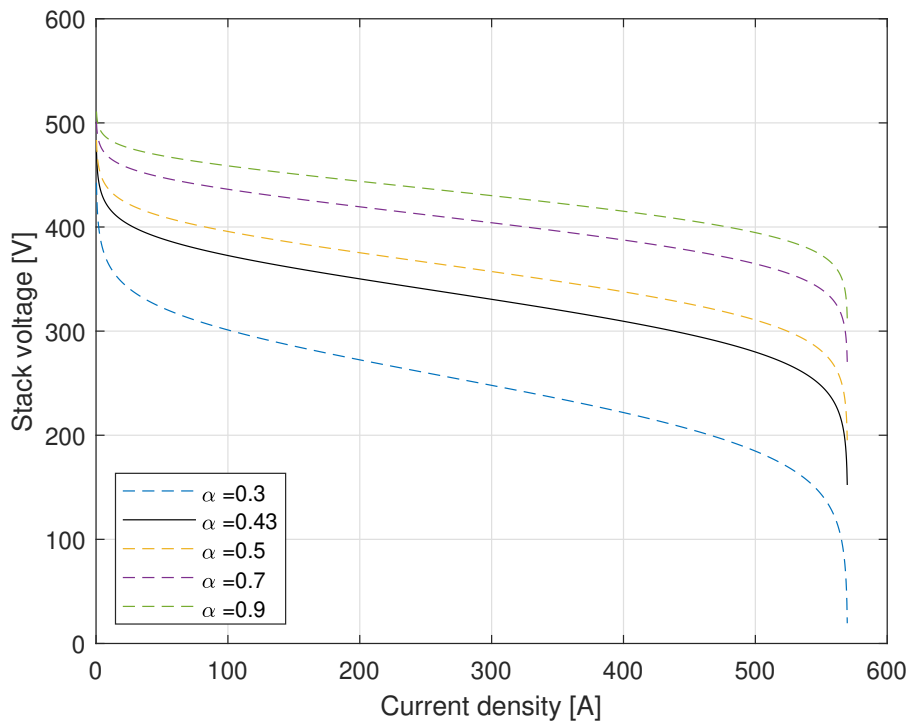
- For the fuel cell stack model: $I_L, \lambda_m, P_{H_2}, P_{air}, T, l_m, \alpha, i_0, C, \lambda_e, \tau_e$
- For the electrolyser stack model: $i_L, \lambda_m, P_{H_2}, P_{air}, T, l_m, \alpha, i_0$

The cell area and cell number for the fuel cell and electrolyser stacks are fixed and relatively easy to acquire for given stacks, and have therefore not been analysed. The sensitivity of the parameters regarding BoP components (table 3.4) are neither considered as it has been less focus on these components through the work.

For steady state simulations, both the fuel cell and electrolyser stack submodels have found to be particularly dependent on the limiting currents, i_L , and the charge transfer coefficient α . This is demonstrated with the fuel cell polarization curves plotted in figure 4.19. i_L determines the span of the polarization curve with respect to the current. Moreover, by virtue of equation 2.23, it determines for which current the concentration losses are becoming significant. By increasing the limiting current, the ohmic region is extended as the concentration losses will be significant for higher currents. The sensitivity of α can be explained by the fact that both the concentration and activation losses in the fuel cells and electrolyzers are inversely proportional to the parameter. Moreover, it was described in section 2.1.4 that α is typically around 0.5, yet it can possibly be in the range of 0 to 1. The results of the sensitivity analysis regarding the remaining parameters incorporated in steady state simulations is included in Appendix D. The significance of these parameters was less, which can either be explained by their presence in the equations outlined chapter 2, or as a combination with the fact that realistic variations in the value of the parameters will not contribute to a large percentage variation of the parameter. As an example, this is evident for the cell temperature which the Nernst voltage, activation losses and concentration losses have a proportional dependency on. However, as the cell temperature in the fuel cell model already is set to 341 K, the absolute change must be of a large magnitude to make a significant difference in the fuel cell voltage.



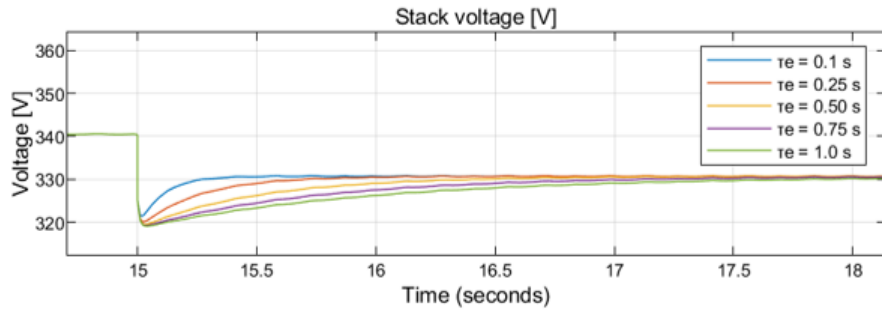
(a) Sensitivity of i_L on fuel cell submodel



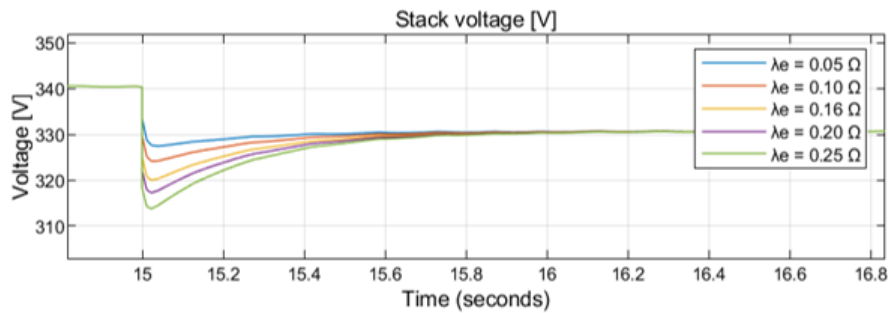
(b) Sensitivity of α on fuel cell submodel

Figure 4.19: Fuel cell polarization curves demonstrating the sensitivity the limiting current density, i_L , and the charge transfer coefficient α

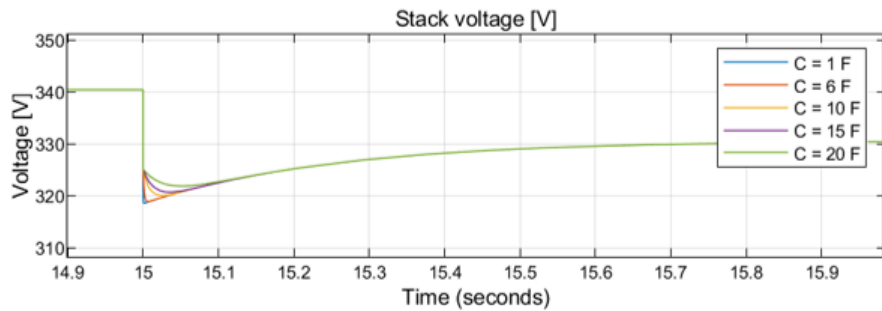
Regarding the fuel cell dynamics, the sensitivity of C , λ_e and τ_e is analysed in figure 4.20 by means of the voltage response of a current step increase from 250 to 300 A. It can be observed how the response time of the voltage is approximately 4-5 times the time constant τ_e . Further will an increase in λ_e proportionally increase the magnitude of the voltage undershoot, while an increase of C will give an increased smoothing effect on the undershoot.



(a) Sensitivity of τ_e . $\tau_{e, \text{used}} = 0.25 \text{ s}$ is used in the model



(b) Sensitivity of λ_e . $\lambda_{e, \text{used}} = 0.16 \Omega$ is used in the model



(c) Sensitivity of C . $C = 6 \text{ F}$ is used in the model

Figure 4.20: Sensitivity analysis for the fuel cell parameters τ_e , λ_e and C . Note that the time scales are different for the three plots.

4.6 Benchmarking of the Fuel Cell Model

As described in section 3.3, the developed fuel cell model has been benchmarked with the Simscape FC block. This comprehend tuning of both models to the 6 kW stack which is available as a preset in the Simscape FC block. The polarization and power curves obtained with both models are plotted in figure 4.21. It is stated in the documentation of the Simscape FC block, that the model does not include the concentration region. Also here, this is explained by the claim that most fuel cells do not operate in this region. However, the developed model in this work does comprise modelling of the concentration region, which is the reason why the curve for the developed model spans to higher currents.

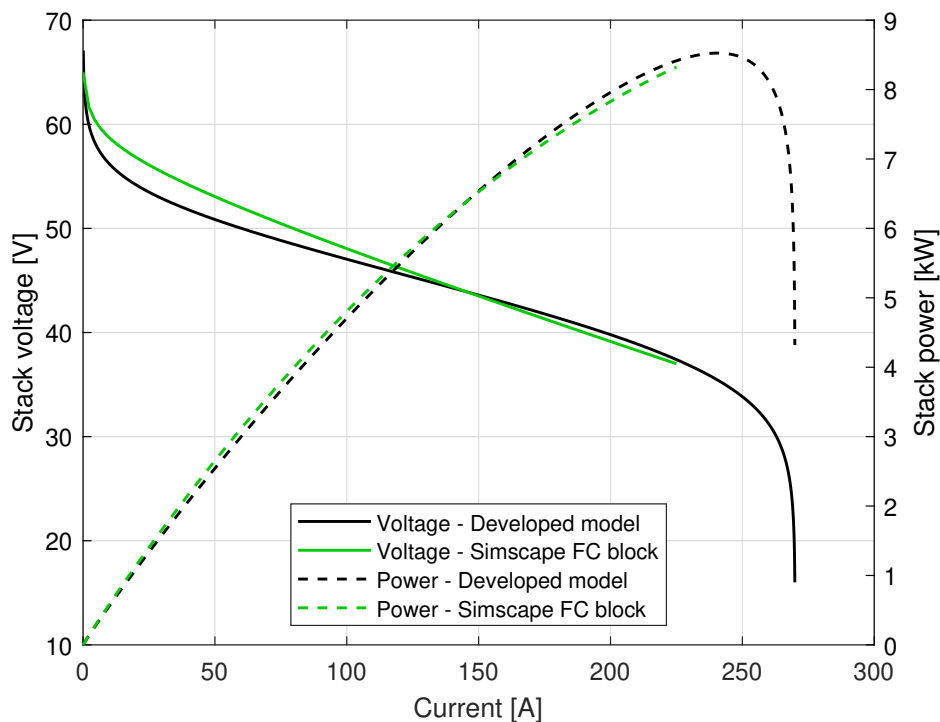


Figure 4.21: Polarization and power curve obtained from the developed model and the Simscape FC block, both tuned to the 6 kW stack available as a preset in the Simscape FC block

The dynamic response of the models are compared in figure 4.22. The upper plot shows the loading of the modelled stack, where the stack is exposed to a current step increase at $T = 10$ s from 133.3 A to 180 A, followed by an equivalent current decrease in $T = 20$ s. The lower plot of the figure shows the voltage response modelled by the two models. It can be observed that both models stabilize to the same steady state voltages and these voltages corresponds to the polarization curves. Moreover, both of the models use approximately 1 second to adjust to the steady state voltage after the currents steps are applied.

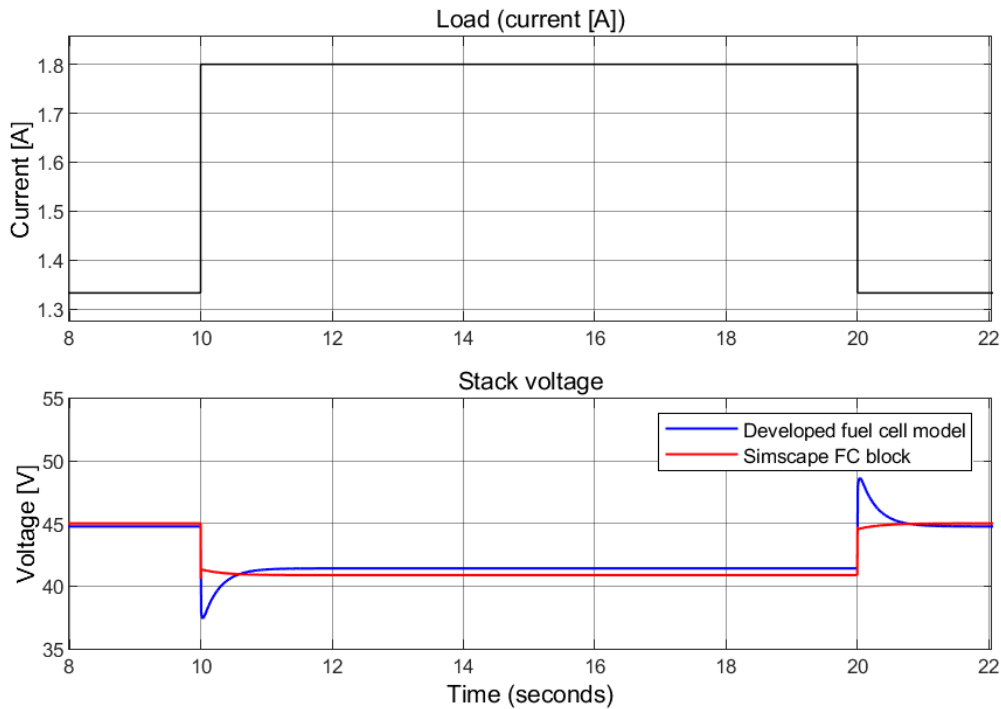


Figure 4.22: Comparison of the voltage response of the developed model and the Simscape FC block when both are tuned to the 6 kW stack available as a preset in the Simscape FC block

However, the behaviour of the models are different immediately after the current step changes are applied. After the current increase, the voltage of the developed model clearly undershoots compared to the steady state voltage. As it was described in section 4.1.2, this is explained by the mass transport delay and the slight tendency of smoothing of this abrupt change is ascribed to the double layer charge effect. The Simscape FC block voltage does not undershoot after the current step increase. The voltage appears to decrease abruptly immediately when the current increase is applied to a voltage slightly higher than the steady state voltage. Afterwards it decreases slowly to the steady state voltage. However, immediately after the current increase, the voltage seems to undershoot very slightly. The undershoot is very little (approximately 1 V), but is yet existing. Also for the current decrease, the two models behave immediately differently, where the voltage of the developed model clearly overshoots while the Simscape FC block has an abrupt voltage increase followed by a slower rise.

Even though the two models respond differently to current steps and decreases, this does not provide the basis for determining which model is best. The superior model should be designated based on the purpose it is aimed to fulfill. Therefore, the differences between the models can be important to be aware of when adapting the models in future modelling activities.

4.7 Consideration of Weight and Footprint

One of the objectives of this work listed in chapter 1 was to perform a brief weight and footprint analysis of the modelled HES-OFF system. This is because weight and footprint are crucial parameters on board offshore installations. In chapter 3, the HES-OFF system was assumed to have total fuel cell and electrolyser capacities each of 2 MW. Weight and footprint of state-of-the-art commercial fuel cell and electrolyser systems was screened in section 2.6 in chapter 2. However, again it was experienced that data acquisition for fuel cell and electrolyser system is very difficult to perform. Therefore, it has not been conducted an exact weight and footprint analysis of the HES-OFF system in this work. Instead, the following paragraph rather discuss briefly possible values for weight and volume of 2 MW fuel cell and electrolyser systems.

Regarding fuel cells, it was found in section 2.6 that the automotive industry provide the most compact stacks, both with regard to weight and volume. The fuel cell stack with the highest power/weight and power/volume ratio is the PowerCell S3. This has a power/weight ratio of 2.9 kW/kg and a power/volume ratio of 3359 kW/m^3 . By applying this stack in a system with total capacity of 2 MW, only the stacks would therefore weight about 690 kg and measure a volume of 0.6 m^3 . However, it was further found in the screening of fuel cell systems that BoP components contribute to a large fraction of the total mass and volume of. The system with the highest power/weight ratio was found to be the Swiss Hydrogen HY-REX installing the PowerCell S3 stack and is intended for automotive applications. This system has a power/weight ratio of 1.0 kW/kg and power/volume ratio of 371 kW/m^3 . If a 2 MW system can be made with the same density values, the system would weight 2000 kg and measure 5.4 m^3 . It must be emphasised that such scaling by means of the density values to obtain the weight and volume of a 2 MW system is not necessarily a valid assumption, because it does not account for the extra (or less) amount of supporting systems which are required. Further, it is important to emphasise that it was only found available systems with capacities in the MW range intended for stationary applications. These are containerised systems and possesses typically substantially lower power/weight and power/volume ratios than the systems intended for automotive applications.

For electrolyser stacks, the data acquisition was found to be even more difficult. However, it was found that the Proton Onsite M-series 250 kW stack weights 295 kg and has a volume of approximately $0,27 \text{ m}^3$. For an electrolyser system with total capacity of 2 MW, only the stacks would therefore contribute to a weight of 2360 kg and a volume of approximately 2.16 m^3 . For electrolyser systems, data was only found for stationary gas production. Further most of these were containerised. By average, per 40ft container, it can typically be stored electrolyser systems with capacities of 1 MW. Very few manufacturers provide weight of their electrolyser systems, which makes it difficult to give any comments on the weights of the 2 MW system.

4.8 Discussion of Work

4.8.1 Strengths and Weaknesses of the Developed Model

Strengths

For steady state modelling, the model includes only quite well-known parameters with somewhat physical understandings. Moreover, table 3.1 to 3.4 show that these parameters can be set within reasonable limits of what is suggested through acknowledged research to match the polarization curves provided from manufacturers (figure 4.1 and 4.7). Compared to the NW fuel cell model presented in section 2.7.1, the developed fuel cell model has fewer empirical parameters. If experimental data is not abundantly available, the developed model can therefore be easier to adapt and more generic than the NW model. Compared to the Simscape FC block, the developed fuel cell model requires less knowledge about power electronics and can therefore be easier to adapt. As mentioned in section 2.7.2, the Simscape FC block have a positive and negative pole which require a certain knowledge about power electronics, even if the power electronics are not intended to be modelled.

Weaknesses

The developed model also feature some weaknesses which are important to be aware of. First of all, the electrolyser stack model does not comprise any dynamics, as models for this was not found in the open literature. Further, the dynamics accounted for in the fuel cell stack and hydrogen purifier models suffer from lack of data. Ideally, the parameters in these models should have been tuned according to experimental data, eventually the parameters should have been well documented from other research. This is not the case for this work and applies especially to the empirical constant, λ_e , used to model voltage undershoots and overshoots due to mass transport delays in fuel cells. The value of this parameter is set equal to what was used in the NW model (section 2.7.1), because it was not found any other data from which this parameter could be determined. The steady state parameters in the model are as mentioned mostly conventional parameters having a physical understanding. Yet, polarization curves for the fuel cell and electrolyser stacks are required to tune the parameters accurately. Moreover, it can be a weakness of the model that certain of these parameters can still be difficult to obtain as the manufacturers are cautious with providing them. Through discussions with the industry partners of the HES-OFF project, it has been identified that the manufacturers often choose to remain certain parameters as trade secrets due to competition concerns.

4.8.2 Implications

Compared to other research within fuel cell and electrolyser modelling, this work is quite broad as it covers fuel cells, electrolysers and BoP components. Commonly, other research focuses on only one of the system components. For example, Nehrir and Wang (2009), O'Hayre et al. (2016) and Larminie and Dicks (2003) are books designated only for fuel cell modelling. It can be discussed whether this work also should have been

more specialised by means of limiting the scope further, in order to get more detailed models of certain components. However, the goal of the thesis was to pave the way in future modelling of hydrogen energy storage systems. By having the scope such broad, this gives a basis for further work within the field.

4.8.3 Reliability and Validity of the Work

Ideally the developed model in this work should have been validated by means of experimental data or other acknowledged models. However, as it has been repeated throughout the thesis, lack of data has been a persistent obstacle in the work, such that it has not been obtained any data sufficient to validate the work. Moreover, no already developed models have been found adequate to validate the work. The validity of the fuel cell part of the developed model was somewhat discussed by the benchmarking with the Simscape FC block. Yet, the comparison is not sufficient for either validation nor as a disproof as the Simscape FC block clearly does not model the voltage undershoots and overshoots occurring because of mass transfer delays when the fuel cell is controlled by the current, which is a well documented phenomenon in the literature.

Having the issue with validation discussed, the developed model is based mostly on acknowledged research and should by means of this basis give reasonable outputs. However, there are some approaches which are more unconventional and even self-developed. This applies especially for the modelling of the charge double layer where an own approach was developed as a combination of two previous researches (section 3.2.2). Moreover, the specific combination of different research to obtain the developed model is new. Therefore, further validation of the work should be performed, but this must be left for further work because sufficient methods has currently not been identified.

Conclusion and Further Work

5.1 Conclusion

To revisit the statements in the introduction, the purpose of this thesis was to to pave the way in modelling of big-size PEM fuel cell and electrolyser systems. The main goal was to develop a comprehensive model of the hydrogen energy storage system in the HES-OFF concept.

Chapter 2 outlined a technical background about hydrogen energy storage using PEM fuel cells and electrolysers. The following conclusions can be drawn from this chapter:

- It was outlined how the literature suggests PEM fuel cells stacks can be modelled in the steady and dynamic state.
- For PEM electrolysers, it was only outlined how the stacks can be modelled in the steady state. It was not found any acknowledged research sufficient for modelling in the dynamic state.
- Regarding BoP components, essential components in fuel cell and electrolyser systems running on gaseous hydrogen was discussed. Assumed that the hydrogen is stored in high pressure tanks, the fuel cell stacks typically requires support from an air compression unit, humidifiers, heat exchangers and a hydrogen re-circulation unit. The latter can be achieved by ejectors driven by the high pressure hydrogen from the storage tanks. In addition, certain fuel cell systems incorporate turbines harvesting energy from potential excess air fed to the fuel cells. The outlet hydrogen stream from electrolysers must typically be purified by a purification unit, before it is compressed in a hydrogen compressor to the tank storage pressure. Moreover, both fuel cells and electrolysers must in most applications be supported by power electronics, which is is a comprehensive subject. This has therefore not been discussed in detail.
- Degradation phenomena where analysed for fuel cell and electrolysers stacks, with regard to specific operating conditions which were considered typical for the HES-OFF system which would intensify the degradation. For fuel cells it was found that

load variations, start/stop/cycling, poor humidification, freeze/thaw cycles increase degradation, and it is expected that these conditions will occur in the HES-OFF system. Less research has been conducted on electrolyser degradation. However, studies indicate that high temperature, high current density and load cycling increases electrolyser degradation. The reported degradation rates for electrolysers are commonly lower than for fuel cells, and it is concluded that this is because electrolysers generally have less daunting operating profiles.

- Weight and footprint of state-of-the art fuel cell and electrolyser systems were screened. The most compact fuel cell stacks and systems are provided in the automotive industry. The most compact fuel cell stack exhibit a power/weight ratio of 2.9 kW/kg and a power/volume ratio of 3359 kW/kg . However, the BoP components in fuel cell systems typically contribute to a large fraction of the total weight and volume and the most compact fuel cell system has a power/weight ratio of 1 kW/kg and power/volume ratio of 371 kW/m^3 . For electrolysers, there is generally less focus on stack characteristics, but rather on full systems. Therefore, limited data was acquired for weight and footprint for individual electrolyser stacks. Regarding electrolyser systems, these are currently mostly available for steady state gas production. Commonly, the systems in the MW scale are available as containerised systems, where one 40 ft container can averagely store electrolyser equipment with a total capacity of roughly 1 MW.
- It was searched for developed models implemented in the Matlab Simulink® environment which could be adapted and used in the modelling of the HES-OFF system. Two fuel cell stack models were found, referred to as the NW model and the Simscape FC block in the text. The NW model was found insufficient, as it incorporates several empirical constants which require a wide use of experimental data for tuning. The Simscape FC block is more acknowledged, but requires understanding of power electronics to function.

Based on the the technical background outlined in chapter 2, a design of the HES-OFF system was assumed and modelled. The modelled system has both a total fuel cell and electrolyser capacity of 2 MW. This is achieved by sixteen fuel cell stacks modelled as the 125 kW PowerCell S3 stack and eight electrolyser stacks modelled as the 250 kW Proton OnSite M-series stack. The stacks are organised in modules containing four stacks each, where all stacks within a module are loaded simultaneously. This gives a compromise between flexibility and system cost. Additionally, the system incorporates compressors, humidifiers, heat exchangers, ejectors, a hydrogen purification unit, power electronics and a hydrogen storage tank.

The input load to the developed model is the fuel cell and electrolyser current. The fuel cells and electrolysers were further modelled mostly by the equations outlined in chapter 2. However, for the modelling of the charge double layer effect, a combination of two approaches was applied. Regarding the BoP components, the air compressor, hydrogen compressor, hydrogen purification unit and the hydrogen storage tank was modelled by means of simple equations. One of the largest obstacles in the modelling of fuel cell

and electrolyser systems, has been to obtain data for the fuel cell and electrolyser stacks. Therefore, it has been strived to develop a model applying mostly common correlations widely used in the research community, to avoid dependency on special empirical constants which require extensive access to experimental data for tuning. Yet, the develop model requires access to certain data for tuning of the parameters. In this work, a few input parameters were found for the particular stacks. Further, the remaining parameters included in steady state equations were tuned to fit provided polarization curves from the manufacturers. No experimental data was obtained for dynamic operation of the stacks, which imply that the parameters included in dynamic equations are tuned with a more narrow basis. The parametric tuning is simplified by provision of more data for the stack, as it will decrease the number of parameters which have to be tuned.

Through simulations performed with the model, the model showed to exhibit the following features and capabilities:

- The steady state polarization curves of the fuel cell and electrolyser stacks fit well with the provided curves from the manufacturers in the activation and ohmic region. In the upper boundary of the ohmic region, the modelled stack powers are approximately 125 kW and 250 kW, which are the respective rated powers of the Power-Cell S3 fuel cell stack and the Proton Onsite M-series electrolyser stack. However, it is concluded the the curves provided from the manufacturers do not comprise the concentration region, because the stacks are rarely operated in this region. Yet, the developed model includes these regions, and the modelled stack powers are here larger than the rated stack powers.
- By applying a current step increase to the fuel cell stack model, the stack voltage clearly undershoots before it stabilizes to the steady state voltage in accordance to the polarization curve. When exposing the stacks to a current step decrease, the similar response is observed, but the voltage instead overshoots. This phenomena are ascribed to the delay of gas flows in the fuel cell. For both cases, the peak of the undershoot/overshoot is smoothed, which is explained by the charge double layer effect.
- By applying current step increases and decreases to the electrolyser stack model, no dynamic behaviour is observed, and the voltage immediately adjusts to the steady state voltage given by the polarization curve.
- By non-simultaneous loading of the fuel cell and electrolyser modules, less stacks need to undergo dynamic operation to produce the given total power profile, compared loading all modules simultaneously.
- Regarding the BoP components, the air compressor consumes approximately 100 kW at full load. The hydrogen compressor power is dependent on the pressure in the storage tank. The hydrogen purifier induces a time delay on the mass flow from the electrolysers to the storage tank.

A sensitivity analysis of operational parameters and assumed parameters in the fuel cell and electrolyser models was performed. From this, it can be concluded that both models are strongly dependent on the limiting current (eventually the limiting current density) and the charge transfer coefficient, α . In addition, the fuel cell dynamics are sensitive for variations in the parameters: τ_e , λ_e and C .

The developed fuel cell stack model was benchmarked with the Simulink[®] block, here referred to as the Simscape FC block. The two models adjust to the same steady state voltage, but by applying current step increases and decreases, the immediate voltage responses are different. It is not concluded that neither of the models are wrong, but it is suggested that the models are developed with different purposes and are therefore not comparable when the current is used as the load to the models. Nevertheless, it is concluded that the comparison showed a satisfactory degree of agreement between the models.

By virtue of the screening of weight and footprint of state-of-the-art fuel cell and electrolyser systems, it was attempted to give an estimate for possible weight and footprint of the modelled HES-OFF system. However, due to lack of data, an exact value was not calculated. It is estimated that the fuel cell stacks will have a total weight of 690 kg and the electrolyser stacks will have a total weight of 2360 kg. However, in commercial systems, the stacks typically contribute to only a small fraction of the total weight and volume. Therefore, the total weight of the HES-OFF system is likely to be substantially higher than the total weight of the installed stacks, but a good estimate is difficult to provide due to lack of information.

Overall, obtaining data has been a major obstacle in the work. This is also evident in the difficulties around the validation of the developed model. Consequently, it has been attempted to develop a model relying on the least amount of empirical parameters which require data for tuning. However, for the HES-OFF project the developed model fulfills the current research needs. The model will be used in analyses of the HES-OFF concept, which will contribute to a deeper insight in the employed fuel cell and electrolyser technology. Moreover, the scope of this work has been quite broad compared to other research within the same field, and therefore provides a basis for future modelling of fuel cell and electrolyser systems.

5.2 Fulfillment of Objectives

Regarding the objectives of the work set in section 1.2.3, they are evaluated to have been accomplished to the following extent:

1. A literature review was performed on gaseous hydrogen energy storage systems in chapter 2, considering PEM fuel cells and electrolysers and necessary BoP components.
2. Two fuel cell models implemented in the Matlab Simulink[®] developed by others

were presented in chapter 2. None of these models were applied in the modelling of the HES-OFF system.

3. A simplified design of the HES-OFF system was suggested in chapter 3
4. A model of the suggested system was created and presented in chapter 3, and further implemented in the Matlab Simulink[®]. The model considers steady and dynamic phenomena of fuel cell stacks, while only steady state phenomena of electrolyser stacks. Certain BoP components are covered by means of simple equations.
5. Various simulations were performed showcasing the features and capabilities of the model.
6. A brief weight and footprint analysis of the suggested system was attempted to perform, but lack of data resulted in difficulties with providing tangible estimates.

5.3 Further Work

The following lines of further work is suggested for the modelling of the HES-OFF system:

- Extensive data for fuel cell and electrolyser stacks should be acquired. This for both validation of the current model and for further developing of the model
- For further developments of the model, the purpose of the model could be identified more specifically, in order to limit the scope further. The scope of the current model is quite broad to fulfill the purpose of paving the way for future modelling. However, developing a model can be time consuming, but by limiting the scope the development process can be more streamlined.
- For testing of how generic the developed fuel cell model is, it could be interesting to tune the model to several other fuel cell stacks.
- Further research should be conducted in order to model the dynamics of electrolyser stacks. If no sufficient research is found on this field, opportunities for adapting the fuel cell model could be investigated.
- As intended, the model can be implemented in an OPAL-RT platform for both testing and validation of the model, and further as a research tool in future projects.

Bibliography

- Anderson, E., 2016. Pem electrolyzer reliability based on 20 years of product experience in commercial markets. *2nd International Workshop on Durability and Degradation Issues in PEM Electrolysis Cells and its Components*.
- Anderson, E., Ayers, K., Capuano, C., 2013. R&d focus areas based on 60,000 hr life pem water electrolysis stack experience. *First International Workshop on Durability and Degradation Issues in PEM Electrolysis Cells and its Components*, Freiburg, Germany.
- Areva H2Gen, 2020. *AREVA H2Gen hydrogen generators* [datasheet]. URL: https://www.arevah2gen.com/wp-content/uploads/2019/10/AREVA_H2GEN_FICHE_ENERGY_v5-UK.pdf. [Accessed 8 May 2020].
- AUTO-STACK CORE, 2018. *Final Report Summary - AUTO-STACK CORE*. URL: <https://cordis.europa.eu/project/id/325335/reporting>. [Accessed 1 April 2020].
- Awasthi, A., Scott, K., Basu, S., 2011. Dynamic modeling and simulation of a proton exchange membrane electrolyzer for hydrogen production. *International Journal of Hydrogen Energy* 36(22), 14779 – 14786. doi:<https://doi.org/10.1016/j.ijhydene.2011.03.045>.
- Ballard Power Systems Inc., 2020a. *Product Data Sheet FCgen 1020 ACS* [datasheet]. URL: https://www.ballard.com/docs/default-source/spec-sheets/fcgen-1020-acs-v2.pdf?sfvrsn=c3ebc380_2. [Accessed: 6 May 2020].
- Ballard Power Systems Inc., 2020b. *Product Data Sheet FCgen LCS* [datasheet]. URL: https://www.ballard.com/docs/default-source/motive-modules-documents/fcgen-lcs.pdf?sfvrsn=c86dc080_2. [Accessed: 6 May 2020].
- Ballard Power Systems Inc., 2020c. *Product Data Sheet FCvelocity 9SSL* [datasheet]. URL: https://www.ballard.com/docs/default-source/spec-sheets/fcvelocity9ssl.pdf?sfvrsn=4aebc380_2. [Accessed: 6 May 2020].

-
- Ballard Power Systems Inc., 2020d. *Product Data Sheet FCvelocity HD* [datasheet]. URL: https://www.ballard.com/docs/default-source/spec-sheets/fcvelocity-hd.pdf?sfvrsn=2debc380_2. [Accessed 7 May 2020].
- Barbir, F., 2005. Pem electrolysis for production of hydrogen from renewable energy sources. *Solar Energy* 78(5), 661 – 669. doi:<https://doi.org/10.1016/j.solener.2004.09.003>.
- Barbir, F., 2013. *PEM Fuel Cells*. 2nd ed., Academic Press.
- Bessarabov, D., Millet, P., 2018. *PEM Water Electrolysis*. Academic Press.
- Borup, R., Meyers, J., Pivovar, B., Kim, Y.S., Mukundan, R., Garland, N., Myers, D., Wilson, M., Garzon, F., Wood, D., Zelenay, P., More, K., Stroh, K., Zawodzinski, T., Boncella, J., McGrath, J.E., Inaba, M., Miyatake, K., Hori, K., Ota, K., Ogumi, Z., Miyata, S., Nishikata, A., Siroma, Z., Uchimoto, Y., Yasuda, K., Kimijima, K., Iwashita, N., 2007. Scientific aspects of polymer electrolyte fuel cell durability and degradation. *Chem. Rev.* 107(10), 3904–3951.
- Boudellal, M., 2018. *Power-to-Gas : Renewable Hydrogen Economy for the Energy Transition*. De Gruyter.
- de Bruijn, F.A., Dam, V.A.T., Janssen, G.J.M., 2007. Review: Durability and degradation issues of pem fuel cell components. *Fuel Cells* 8(1), 3–22.
- Burheim, O.S., 2017. *Engineering Energy Storage*. Academic Press.
- Buttler, A., Spliethoff, H., 2018. Current status of water electrolysis for energy storage, grid balancing and sector coupling via power-to-gas and power-to-liquids: A review. *Renewable and Sustainable Energy Reviews* 82, 2440 – 2454. doi:<https://doi.org/10.1016/j.rser.2017.09.003>.
- Campanari, S., Guandalini, G., Coolegem, J., Have, J., Hayes, P., Pichel, A., 2019. Modeling, development and testing of a 2 mw pem fuel cell plant fueled with hydrogen from a chlor-alkali industry. *Journal of Electrochemical Energy Conversion and Storage* 16. doi:10.1115/1.4042923.
- Carmo, M., Fritz, D.L., Mergel, J., Stolten, D., 2013. A comprehensive review on pem water electrolysis. *International Journal of Hydrogen Energy* 38(12), 4901 – 4934. doi:<https://doi.org/10.1016/j.ijhydene.2013.01.151>.
- Climate Change Act, 2018. Act relating to norway’s climate targets. URL: <https://lovdata.no/dokument/NLE/lov/2017-06-16-60>. [Accessed 11 May 2020].
- Coker, A.K., 2007. *Ludwig’s Applied Process Design for Chemical and Petrochemical Plants*. Gulf Professional Publishing.

-
- Coolegem, J., Yildirim, H., de Bruijn, F., 2013. 30,000 hours of pemfc system operation at a chlor-alkali plant. *Oslo, 2-3 April 2013*.
- Coutanceau, C., Baranton, S., Audichon, T., 2018. *Hydrogen Electrochemical Production*. Academic Press. doi:<https://doi.org/10.1016/B978-0-12-811250-2.00003-0>.
- Dedigama, I., Ayers, K., Shearing, P., Brett, D., 2014. An experimentally validated steady state polymer electrolyte membrane water electrolyser model. *International journal of electrochemical science* 9, 2662–2681.
- Dicks, A., Rand, D.A.J., 2018. *Fuel Cell Systems Explained*. 3rd ed., Wiley.
- Dincer, I., Acar, C., 2014. Review and evaluation of hydrogen production methods for better sustainability. *International Journal of Hydrogen Energy* 49(34), 11094–11111.
- Ekdunge, P., 2017. H2 and fuel cells in maritime application, 15-15 June 2017, Valencia. URL: <https://www.fch.europa.eu/sites/default/files/Per%20Erkunge-PowerCell.pdf>. [Accessed = 26 May 2020].
- Feng, Q., Yuan, X., Liu, G., Wei, B., Zhang, Z., Li, H., Wang, H., 2017. A review of proton exchange membrane water electrolysis on degradation mechanisms and mitigation strategies. *Journal of Power Sources* 366, 33 – 55. doi:<https://doi.org/10.1016/j.jpowsour.2017.09.006>.
- Frensch, S.H., Fouda-Onana, F., Serre, G., Thoby, D., Araya, S.S., Kær, S.K., 2019. Influence of the operation mode on pem water electrolysis degradation. *International Journal of Hydrogen Energy* 44(57), 29889 – 29898. doi:<https://doi.org/10.1016/j.ijhydene.2019.09.169>.
- Gao, F., Blunier, B., Miraoui, A., 2012. *Proton Exchange Membrane Fuel Cells Modeling*. John Wiley & Sons Inc.
- García-Valverde, R., Espinosa, N., Urbina, A., 2012. Simple pem water electrolyser model and experimental validation. *International Journal of Hydrogen Energy* 37(2), 1927 – 1938. doi:<https://doi.org/10.1016/j.ijhydene.2011.09.027>.
- Giner ELX, 2020. *PEM Electrolyzer Systems*[online]. URL: <https://www.ginerelx.com/electrolyzer-systems>. [Accessed: 9 June 2020].
- Gou, B., Na, W., Diong, B., 2016. *Fuel Cells: Dynamic Modeling and Control with Power Electronics Applications*. 2nd ed., CRC Press.
- Grigoriev, S., Porembsky, V., Fateev, V., 2006. Pure hydrogen production by pem electrolysis for hydrogen energy. *International Journal of Hydrogen Energy* 31(2), 171 – 175. doi:<https://doi.org/10.1016/j.ijhydene.2005.04.038>.
- Görgün, H., 2006. Dynamic modelling of a proton exchange membrane (pem) electrolyzer. *International Journal of Hydrogen Energy* 31(1), 29 – 38. doi:<https://doi.org/10.1016/j.ijhydene.2005.04.001>.
-

-
- H-TEC SYSTEMS GmbH, 2020. *H-TEC Series-ME: ME 450/1400* [datasheet]. URL: https://www.h-tec.com/fileadmin/Content/PDFs/19022019/H-TEC_SYSTEMS_Datenblatt_Elektrolyseur_ME450_1400_EN.pdf. [8 May 2020].
- Haberl, F., 2017. Deliverable 1.4 of project inn-balance v. 1.3: Public results of the architecture and system level optimization. URL: https://www.innbalance-fch-project.eu/fileadmin/user_upload/downloads/D1.4_submitted.pdf. accessed 8 April 2020.
- Hamdan, M., Harrison, K., 2019. Mw-scale pem-based electrolyzers for res applications. *2019 Annual Merit Review and Peer Evaluation Meeting*.
- HES Energy Systems, 2020a. *Aerostak 1500* [datasheet]. URL: https://5f2a1a41-f4b9-47ec-b17d-b8538e0e0660.filesusr.com/ugd/3029f7_d5a8d243f2b94fb1ae52da14f171662c.pdf. [Accessed 6 May 2020].
- HES Energy Systems, 2020b. *Aerostak 250* [datasheet]. URL: https://5f2a1a41-f4b9-47ec-b17d-b8538e0e0660.filesusr.com/ugd/3029f7_845facc09dff414d9bc3ff3a4e8acf4a.pdf. [Accessed: 6 May 2020].
- Hydrogenics Corporation, 2020a. *FUEL CELL MEGAWATT POWER GENERATION PLATFORM* [datasheet]. URL: <http://www.hydrogenics.com/wp-content/uploads/Fuel-Cell-MW-Power-Plant-Platform.pdf>. [Accessed: 7 May 2020].
- Hydrogenics Corporation, 2020b. *HYPM-HD 180 POWER MODULE* [datasheet]. URL: <http://www.hydrogenics.com/wp-content/uploads/HyPM-180-SpecSheet.pdf>. [Accessed: 7 May 2020].
- ITM Power, 2020a. *HGas2SP* [datasheet]. URL: <https://www.itm-power.com/images/Products/HGas2SP.pdf>. [Accessed: 8 May 2020].
- ITM Power, 2020b. *HGas3SP* [datasheet]. URL: <https://www.itm-power.com/images/Products/HGas3SP.pdf>. [Accessed: 8 May 2020].
- Jaouen, F., Lindbergh, G., Wiezell, K., 2003. Transient techniques for investigating mass-transport limitations in gas diffusion electrodes : Ii. experimental characterization of the pefc cathode. *Journal of The Electrochemical Society* 150(12). doi:<https://doi.org/10.1149/1.1624295>.
- Kienitz, B., 2020. Optimizing polymer electrolyte membrane thickness to maximize fuel cell vehicle range. *International Journal of Hydrogen Energy* doi:<https://doi.org/10.1016/j.ijhydene.2020.03.126>.
- Klell, M., 2010. *Handbook of Hydrogen Storage*. John Wiley Sons, Ltd. doi:10.1002/9783527629800.ch1.

Knights, S.D., Colbow, K.M., St-Pierre, J., Wilkinson, D.P., 2004. Aging mechanisms and lifetime of pefc and dmfc. *Journal of Power Sources* 127(1), 127 – 134. doi:<https://doi.org/10.1016/j.jpowsour.2003.09.033>.

Larminie, J., Dicks, A., 2003. *Fuel Cell Systems Explained*. 2nd ed., Wiley.

Lebbal, M., Lecœuche, S., 2009. Identification and monitoring of a pem electrolyser based on dynamical modelling. *International Journal of Hydrogen Energy* 34(14), 5992 – 5999. doi:<https://doi.org/10.1016/j.ijhydene.2009.02.003>.

Lettenmeier, P., Wang, R., Abouatallah, R., Helmly, S., Morawietz, T., Hiesgen, R., Kolb, S., Burggraf, F., Kallo, J., Gago, A., Friedrich, K., 2016. Durable membrane electrode assemblies for proton exchange membrane electrolyzer systems operating at high current densities. *Electrochimica Acta* 210, 502 – 511. doi:<https://doi.org/10.1016/j.electacta.2016.04.164>.

Li, X., 2005. *Principles of Fuel Cells*. CRC Press.

Moran, M.J., Shapiro, H.N., Boettner, D.D., Bailey, M.B., 2015. *Principles of Engineering Thermodynamics*. 8 ed., Wiley.

Nedstack fuel cell technology B.V., 2020a. *CHP-FCP-1000* [datasheet]. URL: <https://nedstack.com/sites/default/files/2019-07/nedstack-chp-fcp-1000-pemgen-web-1.pdf>. [Accessed: 7 May 2020].

Nedstack fuel cell technology B.V., 2020b. *FCS 7-XXL* [online]. URL: <https://nedstack.com/en/pem-fcs-stack-technology/fcs-7-xxl>. [Accessed: 6 May 2020].

Nedstack fuel cell technology B.V., 2020c. *NEDSTACK FCS 10-XXL PEM FUEL CELL STACK* [datasheet]. URL: https://nedstack.com/sites/default/files/2019-11/20191105_nedstack_fcs_10-xxl.pdf. [Accessed: 6 May 2020].

Nedstack fuel cell technology B.V., 2020d. *NEDSTACK FCS 13-XXL PEM FUEL CELL STACK* [datasheet]. URL: https://nedstack.com/sites/default/files/2019-11/20191105_nedstack_fcs_13-xxl.pdf. [Accessed: 6 May 2020].

Nedstack fuel cell technology B.V., 2020e. *NEDSTACK FCS 7-XXL PEM FUEL CELL STACK* [datasheet]. URL: https://nedstack.com/sites/default/files/2019-11/20191105_nedstack_fcs_7-xxl.pdf. [Accessed: 6 May 2020].

Nedstack fuel cell technology B.V., 2020f. *PemGen MT-FCPP-100* [datasheet]. URL: <https://nedstack.com/sites/default/files/2019-07/nedstack-mt-fcpp-100-pemgen-web.pdf>. [Accessed: 6 May 2020].

-
- Nedstack fuel cell technology B.V., 2020g. *PemGen MT-FCPP-40* [datasheet]. URL: https://nedstack.com/sites/default/files/2019-07/nedstack-mt-fcpp-40-pemgen-web_0.pdf. [Accessed: 6 May 2020].
- Nehrir, M., Wang, C., 2009. *Modeling and control of fuel cells: Distributed generation applications*. Wiley.
- Nel ASA, 2020. *Nel M Series Containerized* [datasheet]. URL: <https://nelhydrogen.com/wp-content/uploads/2020/03/M-Series-Containerized-Spec-Sheet-Rev-A.pdf>. [Accessed: 8 May 2020].
- Norwegian Environment Agency, 2020. *Klimagassutslipp fra olje- og gassutvinning* [online]. URL: <https://miljostatus.miljodirektoratet.no/tema/klima/norske-utslipp-av-klimagasser/klimagassutslipp-fra-olje--og-gassutvinning/>. [Accessed: 11 May 2020].
- NTNU, 2020. *Innovative Hybrid Energy System for Stable Power and Heat Supply in Off-shore Oil & Gas Installation (HES-OFF)* [online]. URL: <https://www.ntnu.edu/ept/hes-off#/view/about>. [Accessed: 10 June 2020].
- O'Hayre, R., Cha, S., Colella, W.G., Prinz, F., 2016. *Fuel Cell Fundamentals*. 3rd ed., Wiley.
- Perry, M.L., Patterson, T., Reiser, C., 2006. Systems strategies to mitigate carbon corrosion in fuel cells, in: ECS Transactions, ECS. doi:10.1149/1.2356198.
- PowerCell Sweden AB, 2018. D1.3 – everywh2ere gensets enabling technologies (fc and h2 storage) assessment report. URL: <https://ec.europa.eu/research/participants/documents/downloadPublic?documentIds=080166e5bb1a07a9&appId=PPGMS>.
- PowerCell Sweden AB, 2020a. *Coop in Switzerland launches lorries with fuel cells* [online]. URL: <https://www.powercell.se/en/cases/swiss-coop/>. [Accessed: 7 May 2020].
- PowerCell Sweden AB, 2020b. *PowerCell MS-100: The game changer for electrification* [online]. URL: <https://www.powercell.se/en/products/powercell-ms-100/>. [Accessed: 7 May 2020].
- PowerCell Sweden AB, 2020c. *PowerCell S2 datasheet* [datasheet]. URL: <https://www.powercell.se/wordpress/wp-content/uploads/2018/12/S2-datasheet-190513.pdf>. [Accessed: 6 May 2020].
- PowerCell Sweden AB, 2020d. *PowerCell S3 datasheet* [datasheet]. URL: <https://www.powercell.se/en/products/powercell-s3/>. [Accessed: 6 May 2020].

-
- Rakousky, C., Reimer, U., Wippermann, K., Kuhri, S., Carmo, M., Lueke, W., Stolten, D., 2017. Polymer electrolyte membrane water electrolysis: Restraining degradation in the presence of fluctuating power. *Journal of Power Sources* 342, 38 – 47. doi:<https://doi.org/10.1016/j.jpowsour.2016.11.118>.
- del Real, A.J., Arce, A., Bordons, C., 2007. Development and experimental validation of a pem fuel cell dynamic model. *Journal of Power Sources* 173(1), 310 – 324. doi:<https://doi.org/10.1016/j.jpowsour.2007.04.066>.
- Reiser, C., Bregoli, L., Patterson, T., Yi, J., Yang, J., Perry, M., Jarvi, T., 2005. A reverse-current decay mechanism for fuel cells. *Electrochemical and Solid State Letters* 8(6). doi:10.1149/1.1896466.
- Sdanghi, G., Maranzana, G., Celzard, A., Fierro, V., 2019. Review of the current technologies and performances of hydrogen compression for stationary and automotive applications. *Renewable and Sustainable Energy Reviews* 102, 150 – 170. doi:<https://doi.org/10.1016/j.rser.2018.11.028>.
- Selamet, F., Becerikli, F., Mat, M.D., Kaplan, Y., 2011. Development and testing of a highly efficient proton exchangemembrane (pem) electrolyzer stack. *International Journal of Hydrogen Energy* 36(17), 11483–11484.
- Sherif, S., Goswami, D., Stefanakos, E., Steinfeld, A., 2016. *Handbook of Hydrogen Energy*. 1st ed., CRC Press.
- Spiegel, C., 2008. *Modeling and Simulation Using MATLAB®*. Elsevier. p. 71.
- Swiss Hydrogen SA, 2020. *HY-REX100 RANGE EXTENDER FOR HEAVY DUTY VEHICLES* [datasheet]. URL: <https://www.swisshydrogen.ch/wp-content/uploads/2017/10/HY-REX100.pdf>. [Accessed 7 May 2020].
- The MathWorks Inc, . *Documentation of the Fuel Cell Stack block in the Simulink® Simscape™ library* [online]. URL: <https://it.mathworks.com/help/physmod/sps/powersys/ref/fuelcellstack.html>. [Accessed: 2 June 2020].
- Toyota Motor Corporation, 2019. *2019 Mirai* [brochure]. URL: https://www.toyota.com/mirai/assets/modules/carpagellfeatures/docs/MY19_Mirai_Lifestyle.pdf. [Accessed: 6 May 2020].
- Toyota Motor Corporation, 2020. *Mirai* [online]. URL: <https://www.toyota-europe.com/world-of-toyota/feel/environment/better-air/fuel-cell-vehicle>. [Accessed: 6 May 2020].
- Tribioli, L., Cozzolino, R., Evangelisti, L., Bella, G., 2016. Energy management of and off-grid hybrid power plant with multiple energy storage systems. *Energies* 9(661).
- Yang, Q., Yang, T., Li, W., 2018. *Smart Power Distribution Systems: Control, Communication, and Optimization*. 1st ed., Academic Press.

Zohuri, B., 2019. *Hydrogen Energy - Challenges and Solutions for a Cleaner Future*. 1st ed., Springer International Publishing AG.

Appendix **A**

Matlab Code for Steady State Diagrams

For ease of programming the steady state diagrams, the Matlab code was structured in an object oriented fashion. The following five pages show a print of the class declaration of the developed class modelling the fuel cell stack. The class also handles electrolyser modelling by tuning of the input parameters.

```

% Class declaration of the FuelCellStack class
% See use manual below

classdef FuelCellStack
    properties
        % Input parameters
        conc_loss_valid = 1;% 1 if conc. losses are included, 0 if not
        R = 8.314;          % Ideal gas constant [J/molK]
        F = 96485;         % Faraday's constant [C]
        Tc = 68;           % Temperature [C]
        P_H2 = 1.54;       % Hydrogen pressure [atm]
        P_air = 2;         % Air pressure [atm]
        A_cell = 300;      % Area of cell [cm^2]
        N_cells = 455;     % Number of cells
        Alpha = 0.43;      % Transfer coefficient
        io = 1*10^-5;      % Exchange current density [A/cm^2]
        il = 1.9;          % Limiting current density [A/cm^2]
        Gf_liq = -228170;  % Gibbs function in liquid form [J/mol]
        lm = 5*10^-3;      % Membrane thickness [cm]
        lambdam = 14;      % Membrane hydration parameter

        % Calculated values
        Tk;                % Temperature in Kelvin
        V_out_FC;          % Cell output voltage for fuel cell mode
        V_out_EL;          % Cell INPUT voltage for electrolyser mode
        i;                 % Vector of currents evenly distributed between
                        % 0 and il, used for plotting
        P_out_FC;          % Stack output power for fuel cell mode
        P_out_EL;          % Stack INPUT power for electrolyser mode
        E_nernst;          % Nernst voltage
        E_thermoneutral;
        Efficiency_FC;     % Efficiency, based on O'Hayre Fuel Cell
                        % Fundamentals definition, modified with Frano
                        % Barbir PEM Fuel Cells Chapter 2
        Efficiency_EL;     % "
        V_act;             % Activation losses
        V_ohmic;           % Ohmic losses
        V_conc;            % Concentration/mass transfer losses
        r;                 % Area specific ohmic resistance [Ohm*cm^2]
        perf_FC;           % [J/kgH2]
        perf_EL;           % [kgH2/J]
        mass_flow;         % [kg/s]
    end

    methods
        %%%%%%%%%%%%%%%%%%%%%%%%%%%%%%%%%%%%%%%%%%%%%%%%%%%%%%%%%%%
        % Constructor (Sets all the member values called "calculated values"
        % according to the default parameters at declaration of the object)
        function obj = FuelCellStack()
            obj = updateCalculatedValues(obj);
            % Calls the member function under, which calculates all the
            % member values called "calculated values"
        end
    end
end

```

```

%%%%%%%%%%%%%%%%%%%%%%%%%%%%%%%%%%%%%%%%%%%%%%%%%%%%%%%%%%%%%%%%%%%%%%%%
% Function for calculating all the member variables (properties)
% To be used every time an input parameter is changed to
% calculate/update the calculated values
function obj = updateCalculatedValues(obj)
    % Convert degrees C to K
    obj.Tk = obj.Tc + 273.15;

    % Creating vector for current density
    obj.i=0:0.001:(obj.i1-0.001);

    % Saturation pressure of water
    x = -2.1794 + 0.02953.*obj.Tc-9.1837.*(10.^-5).*(obj.Tc.^2)...
        + 1.4454.*(10.^-7).*(obj.Tc.^3);
    P_H2O = 10^x;

    % Partial pressures of hydrogen and oxygen
    pp_H2 = 0.5.*((obj.P_H2)./(exp(1.653.* obj.i./...
        (obj.Tk.^1.334))))-P_H2O);
    pp_O2 = (obj.P_air./exp(4.192.*obj.i/(obj.Tk.^1.334)))-P_H2O;

    % Activation losses
    b = obj.R .* obj.Tk./(2 .* obj.Alpha .* obj.F);
    obj.V_act = -b .* log(obj.i./obj.io);

    % Ohmic losses
    obj.r = obj.lm * 1 / (( 0.005139 * obj.lambdam + 0.00326 )...
        * exp(1267*(1/303-1/obj.Tk))); % Triboli
    obj.V_ohmic = -(obj.i.*obj.r);

    % Mass transport losses
    obj.V_conc = - obj.R.*obj.Tk./(2*obj.F).*(1+1/obj.Alpha).*...
        log(1./(1-obj.i./obj.i1));

    % Calculation of Nernst voltage
    obj.E_nernst = - obj.Gf_liq./(2.*obj.F) - ((obj.R.*obj.Tk).*...
        log(P_H2O./(pp_H2.*(pp_O2.^0.5))))/(2.*obj.F); % =1.1964
    obj.E_thermoneutral = 285800/(2.*obj.F)*ones(1,length(obj.i));

    % Calculation of output voltage
    obj.V_out_FC = obj.E_nernst +...
        (obj.V_ohmic + obj.V_act + obj.conc_loss_valid*obj.V_conc);
    obj.V_out_EL = obj.E_nernst...
        - (obj.V_ohmic + obj.V_act +...
        obj.conc_loss_valid*obj.V_conc);

    % Eliminating wrong numbers
    for j=1:length(obj.V_out_FC)
        if obj.V_out_FC(j) < 0
            obj.V_out_FC(j) = 0;
        elseif obj.V_out_EL(j) <=0
            obj.V_out_EL(j) = NaN;
        end
    end

    % Calculations of stack power
    obj.P_out_FC = obj.V_out_FC.*obj.i .*obj.A_cell*obj.N_cells;

```

```

obj.P_out_EL = obj.V_out_EL.*obj.i .*obj.A_cell*obj.N_cells;

% Calculations of efficiencies
obj.Efficiency_FC = obj.V_out_FC./1.482;% 1.482 is HHV/nF [V]
obj.Efficiency_EL = 1.482./obj.V_out_EL;

% Calculations of performance
obj.mass_flow = obj.A_cell * obj.N_cells .* obj.i ./...
    (2*obj.F) * 0.002; % 0.002 as 1 mol H2 weights 0.002 kg
obj.perf_FC = obj.P_out_FC ./ obj.mass_flow;
obj.perf_EL = obj.mass_flow ./ obj.P_out_EL;
end

%%%%%%%%%%%%%%%%%%%%%%%%%%%%%%%%%%%%%%%%%%%%%%%%%%%%%%%%%%%%%%%%%%%%%%%%
% Get functions for finding values at given powers:

% A set of get functions has been developed to access variables for
% given operating powers.

% For finding the current density for a given power output from FC.
% The code only handles the region where the power-currenty curve is
% even.
function i_return = find_i_at_given_P_out_FC(obj,P_in)
    P = round(P_in);% Round as comparing float var is inconvenient
    max_P = max(obj.P_out_FC);
    if P > max_P
        fprintf('ERROR: Inserted power is larger than max power!');
        i_return = NaN;
    end
    for j=1:(length(obj.i)-1)
        if j == 1 && obj.P_out_FC(j+1) > P || j == 1 &&...
            isnan(obj.P_out_FC(j))
            i_return = obj.i(j);
        elseif obj.P_out_FC(j+1)>P&&obj.P_out_FC(j)<P||...
            obj.P_out_FC(j+1)<P&&obj.P_out_FC(j)>P
            % Linear interpolation
            i_return = obj.i(j) + (P - obj.P_out_FC(j))/...
                (obj.P_out_FC(j+1)-obj.P_out_FC(j)) *...
                (obj.i(j+1)-obj.i(j));
            break;
        end
    end
end

% For finding the current density for a given power input to EL
function i_return = find_i_at_given_P_out_EL(obj,P_in)
    P = round(P_in);% Round as comparing float var is incovenient
    P_max = max(obj.P_out_EL);

    if P > P_max
        fprintf('ERROR: Inserted power is larger than max power!');
        i_return = NaN;
    end

    for j=1:(length(obj.i)-1)
        if j == 1 && obj.P_out_EL(j+1) > P || j == 1 &&...
            isnan(obj.P_out_EL(j))

```

```

        i_return = obj.i(j);
    elseif obj.P_out_EL(j+1)>P&&obj.P_out_EL(j)<P||...
        obj.P_out_EL(j+1)<P&&obj.P_out_EL(j)>P
        % Linear interpolation
        i_return = obj.i(j) + (P - obj.P_out_EL(j))/...
            (obj.P_out_EL(j+1)-obj.P_out_EL(j)) *...
            (obj.i(j+1)-obj.i(j));
        break;
    end
end
end

% Finding mass flow for a given fuel cell power
function m = mass_flow_for_given_P_FC(obj,P_in)
    i_FC = find_i_at_given_P_out_FC(obj,P_in);
    m = obj.A_cell * obj.N_cells * i_FC / (2*obj.F) * 0.002;
end

% Finding mass flow for a given electrolyser power
function m = mass_flow_for_given_P_EL(obj,P_in)
    i_EL = find_i_at_given_P_out_EL(obj,P_in);
    m = obj.A_cell * obj.N_cells * i_EL / (2*obj.F) * 0.002;
end

% For finding the efficiency for a given power output from FC
function eff_return = find_eff_at_given_P_out_FC(obj,P_in)
    P = round(P_in);
    max_P = max(obj.P_out_FC);
    if P > max_P
        fprintf('ERROR: Inserted power is larger than max power!');
        eff_return = NaN;
    end
    for j=1:(length(obj.i)-1)
        if j == 1 && obj.P_out_FC(j+1) > P || j == 1 &&...
            isnan(obj.P_out_FC(j))
            eff_return = obj.Efficiency_FC(j);
        elseif obj.P_out_FC(j+1)>P&&obj.P_out_FC(j)<P||...
            obj.P_out_FC(j+1)<P&&obj.P_out_FC(j)>P
            % Linear interpolation
            eff_return = obj.Efficiency_FC(j) +...
                (P - obj.P_out_FC(j))/...
                (obj.P_out_FC(j+1)-obj.P_out_FC(j)) *...
                (obj.Efficiency_FC(j+1)-obj.Efficiency_FC(j));
            break;
        end
    end
end

% For finding the efficiency for a given power input to EL
function eff_return = find_eff_at_given_P_out_EL(obj,P_in)
    P = round(P_in);
    max_P = max(obj.P_out_EL);
    if P > max_P
        fprintf('ERROR: Inserted power is larger than max power!');
        eff_return = NaN;
    end
    for j=1:(length(obj.i)-1)

```

```

        if j == 1 && obj.P_out_EL(j+1) > P || j == 1 &&...
            isnan(obj.P_out_EL(j))
            eff_return = obj.Efficiency_EL(j);
        elseif obj.P_out_EL(j+1)>P&&obj.P_out_EL(j)<P||...
            obj.P_out_EL(j+1)<P&&obj.P_out_EL(j)>P
            % Linear interpolation
            eff_return = obj.Efficiency_EL(j) +...
                (P - obj.P_out_EL(j))/...
                (obj.P_out_EL(j+1)-obj.P_out_EL(j))...
                * (obj.Efficiency_EL(j+1)-obj.Efficiency_EL(j));
            break;
        end
    end
end

% For finding the fuel cell performance [J/kgH2] at given power
function perf_fc = calculate_perf_fc(obj,P)
    current_density = find_i_at_given_P_out_FC(obj,P);
    mass_flow_at_given_P = obj.A_cell * obj.N_cells *...
        current_density / (2*obj.F) * 0.002;
    perf_fc = P / mass_flow_at_given_P;
end

% For finding the electrolyser performance [kgH2/J] at given power
function perf_el = calculate_perf_el(obj,P)
    current_density = find_i_at_given_P_out_EL(obj,P);
    mass_flow_at_given_P = obj.A_cell * obj.N_cells *...
        current_density / (2*obj.F) * 0.002;
    perf_el = mass_flow_at_given_P / P;
end
end
end

%%%%%%%%%%%%%%%%%%%%%%%%%%%%%%%%%%%%%%%%%%%%%%%%%%%%%%%%%%%%%%%%%%%%%%%%
% USER MANUAL:

% To declare (make) a variable of type FuelCellStack:
%     example_stack = FuelCellStack;

% Every time input parameters of a FuelCellStack is changed, the code:
%     example_stack = updateCalculatedValues(example_stack);
% must be run to update member variables
%%%%%%%%%%%%%%%%%%%%%%%%%%%%%%%%%%%%%%%%%%%%%%%%%%%%%%%%%%%%%%%%%%%%%%%%

```

Appendix **B**

Screenshots from the Simulink[®] Implementation

With reference to chapter 3, this appendix has the purpose of showcasing important parts of the Simulink[®] implementation of the developed model. Because of the complexity of the implementation, only the fuel cell model is showed. This has the most complex implementation. Since the electrolyser model is very similar, yet simpler, than the fuel cell model, the implementation of this is very similar to the fuel cell implementation showcased here. As outlined in the thesis, the BoP components are covered by simple means, and their Simulink implementation is therefore also relatively simple.

In order to set the constant input parameters in the Simulink[®] implementation, the script on the following page has to be run.

```

% Parameters for the Simulink implementation
clear all
clc

% Fuel cell parameters
R = 8.314;           % Ideal gas constant [J/molK]
Gf_liq = 228170;    % Gibbs function in liquid form [J/mol]
F = 96485;          % Faraday's constant [C]
Tc = 68;            % Temperature [C]
Tk = Tc + 273;     % Temperature [K]
P_H2 = 1.54;        % Hydrogen pressure [atm]
P_air = 2.0;        % Air pressure [atm]
A_cell = 300;       % Area of cell [cm^2]
N_cells = 455;      % Number of cells
Alpha = 0.43;       % Transfer coefficient [-]
io = 1*10^-5;       % Exchange current density [A/cm^2]
il = 1.9;           % Limiting current density [A/cm^2]
lm = 5*10^-3;       % Membrane thickness [cm]
lambdam = 14;       % Membrane hydration parameter
C = 6;              % Capacitance of charge double layer
tau_e = 0.25;       % Time constant for gas flows [s]
lambda_e = 0.16;    % Empirical constant dependent on mass flow delay

% Additional electrolyser parameters
TC_EL = 58;         % Temperature [C]
TK_EL = TC_EL + 273; % Temperature [K]
P_H2_EL = 13;       % Hydrogen pressure [atm]
P_air_EL = 1;        % Air pressure [atm]
A_cell_EL = 680;    % Area of cell [cm^2]
N_cells_EL = 100;   % Number of cells
Alpha_EL = 0.4;     % Transfer coefficient [-]
io_EL = 1*10^-5;    % Exchange current density [A/cm^2]
il_EL = 2.5;        % Limiting current density [A/cm^2]
lm_EL = 250 * 10^-4; % Membrane thickness [cm]

% Balance of Plant Components Paramters
V_tank = 30;         % Volume of storage tank [m^3]
T_tank_c = 15;       % Storage tank temperature [Celsius]
T_tank_k = T_tank_c + 273; % Storage tank temperature [Kelvin]
m_init = 300;        % Initial hydrogen level in tank[kg]
cp_air = 1;          % Heat capacity of air [kJ/kgK]
kappa_air = 1.4;     % Specific heat ratiokappakapp
comp_eff = 0.7;      % Compressor efficiency
a = 0.025;           % Coeff. in van der waals' equation [m^6Pa/mol^2]
b = 2.66 * 10^-5;    % Coeff. in van der waals' equation [m^3/mol]
T_amb_c = 15;        % Ambient temperature [Celsius]
T_amb_k = T_amb_c + 273; % Ambient temperature [Kelvin]
tau_p = 2.5;         % Purifier time constant [s]

```

B.1 Fuel Cells

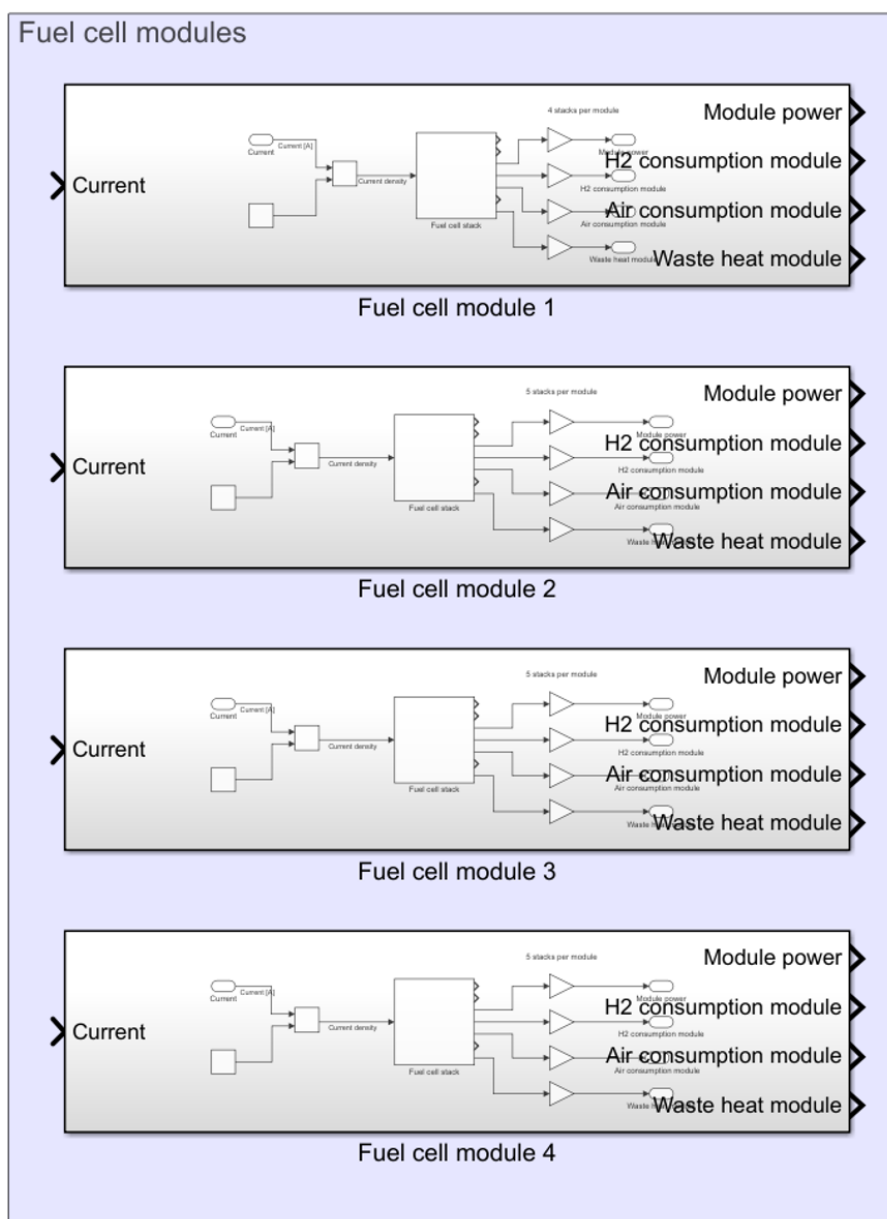


Figure B.1: Overview of the fuel cell modules in the Simulink® implementation

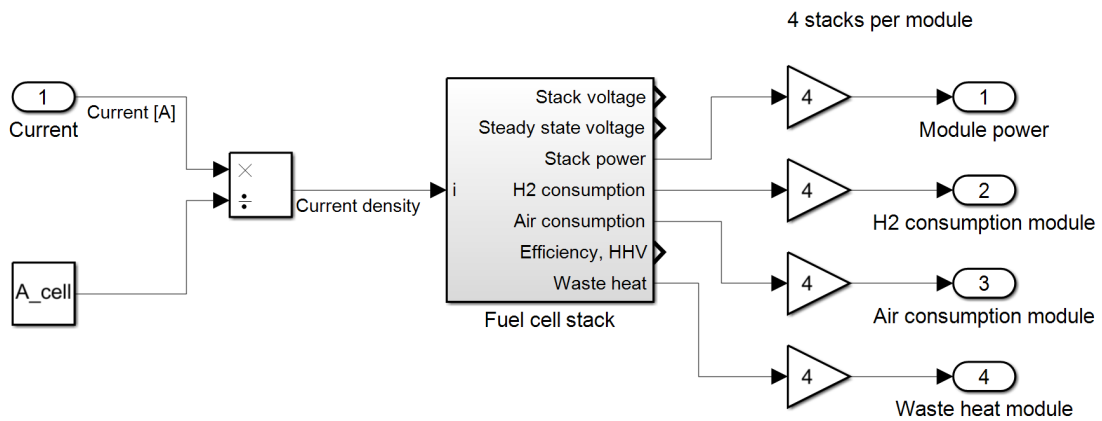


Figure B.2: The subsystem accessed under "Fuel cell module 1-4" in figure B.1. 4 stacks are here implemented in one module

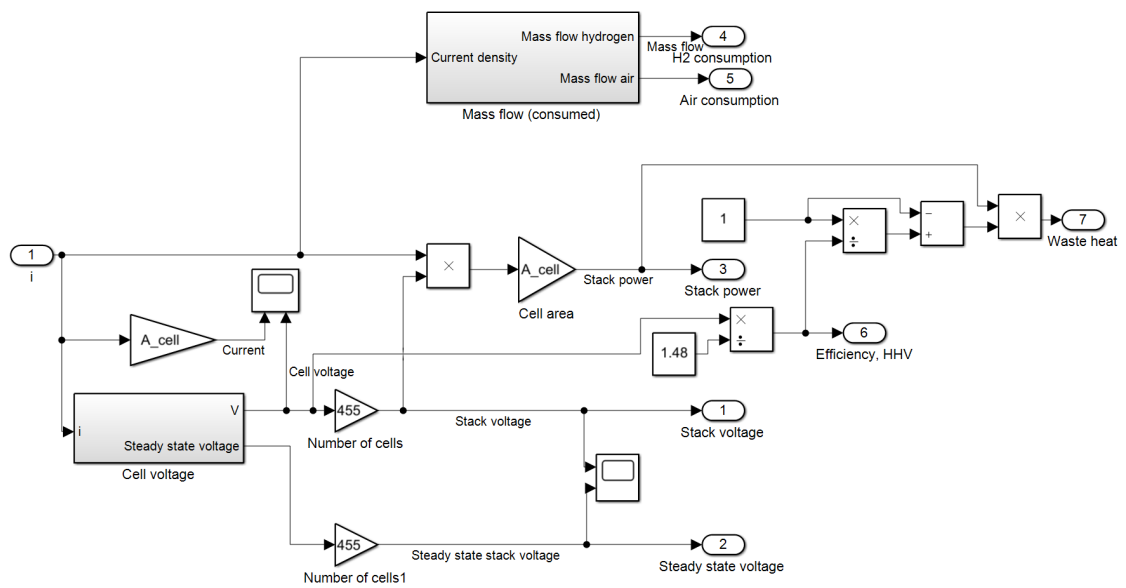


Figure B.3: The subsystem accessed under "Fuel Cell Stack" in figure B.2.

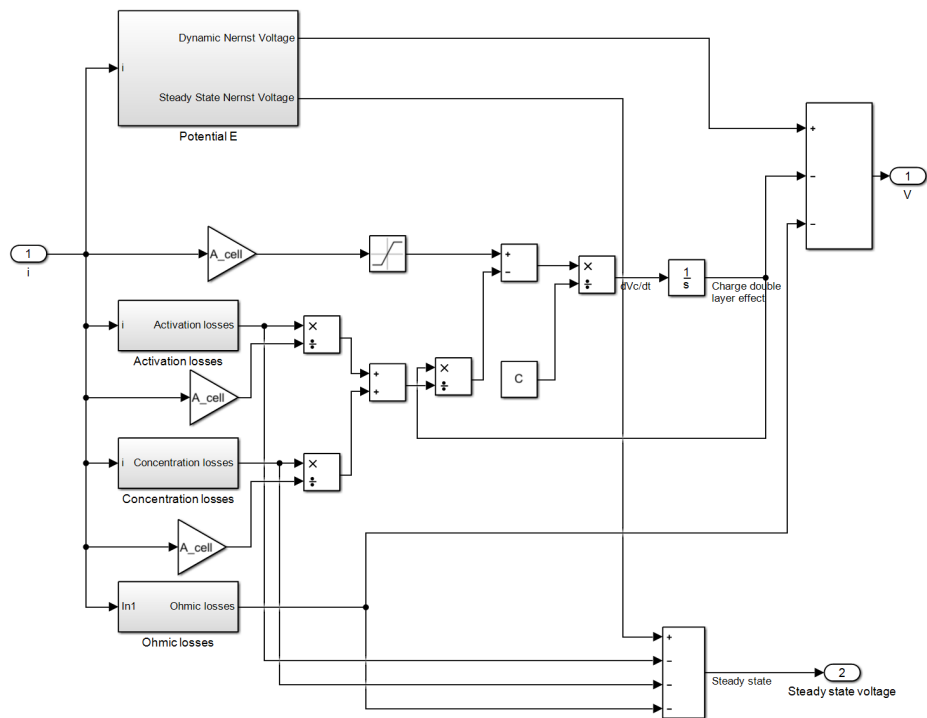


Figure B.4: The subsystem accessed under "Cell voltage" in figure B.3.

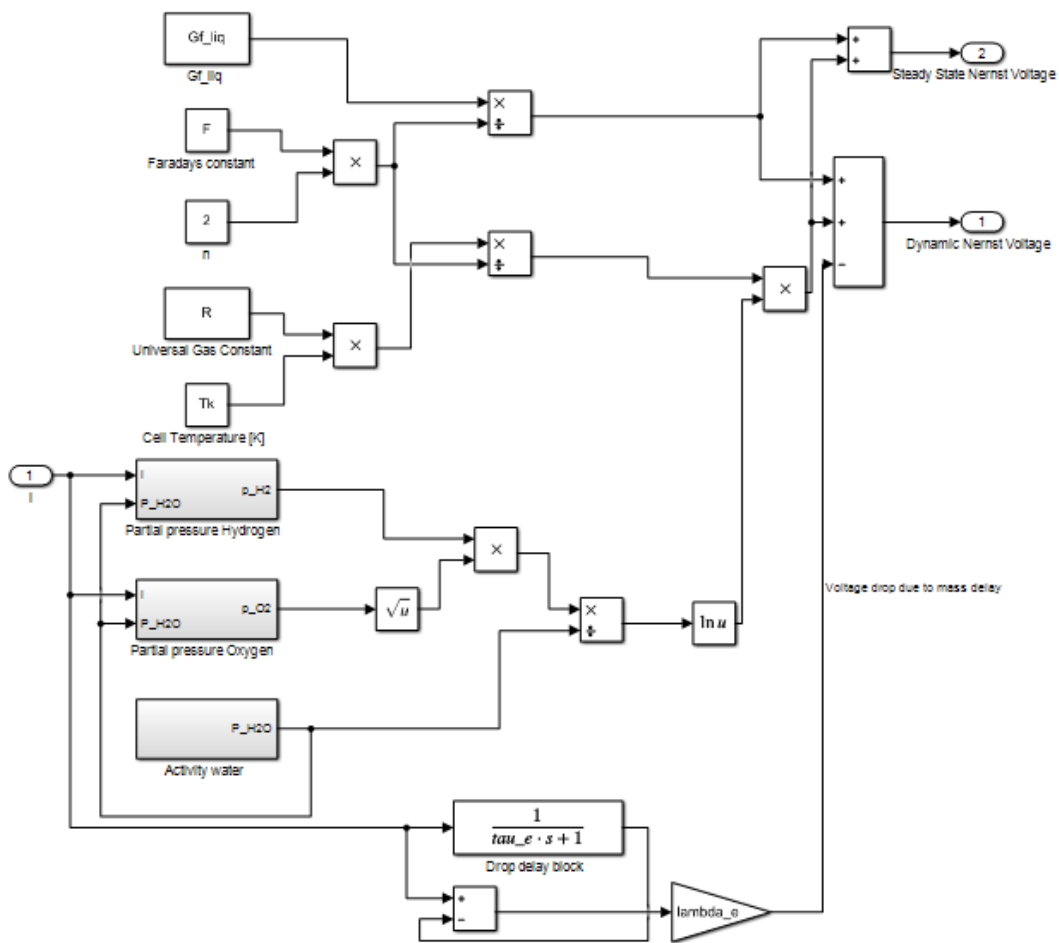


Figure B.5: The subsystem accessed under "Potential E" in figure B.4

Benchmarking with the Simscape FC Block

This appendix shows the Simulink® implementation used when the developed fuel cell stack model was benchmarked with the Simscape FC block (section 3.3).

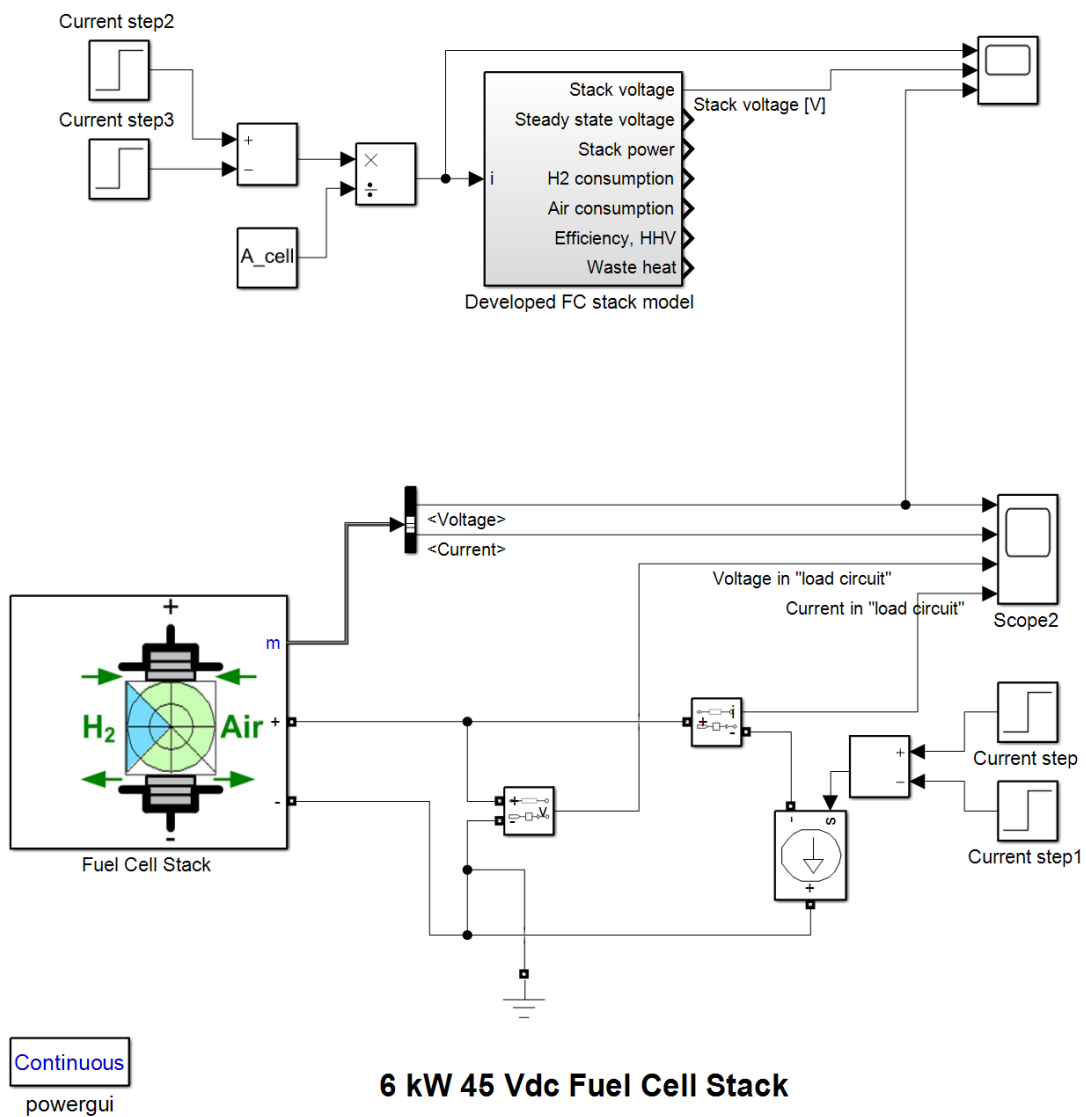


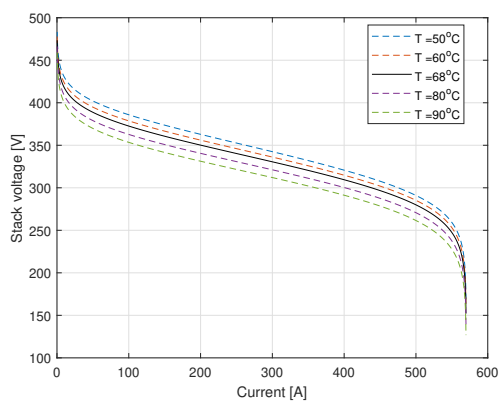
Figure C.1: Screenshot of the Simulink[®] implementation used when benchmarking the developed fuel cell stack model with the Simscape FC block

Appendix D

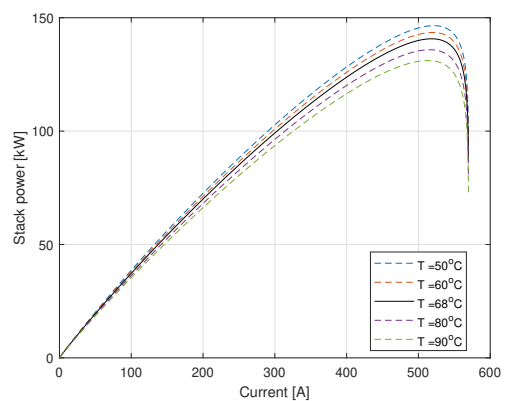
Sensitivity Analysis

This appendix shows all the graphs plotted in the sensitivity analysis (section 4.5).

D.1 Fuel Cell Stack Model

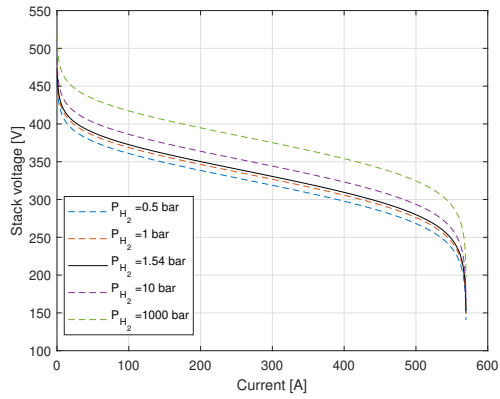


(a) Fuel cell stack voltage

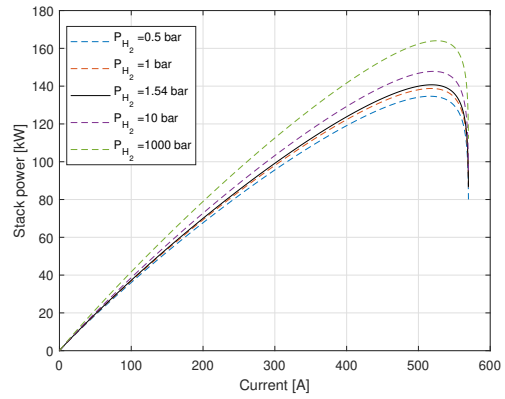


(b) Fuel cell stack power

Figure D.1: Sensitivity analysis for operating temperature T [$^{\circ}C$]. $T = 68^{\circ}C$ is used in the model

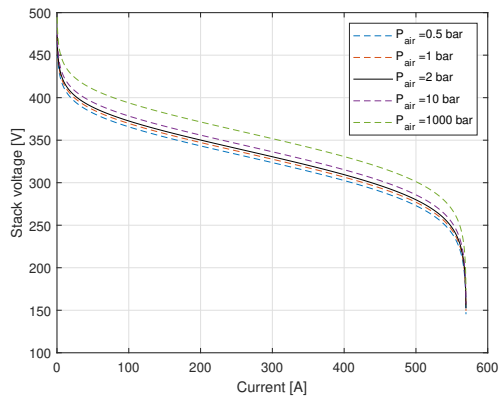


(a) Fuel cell stack voltage

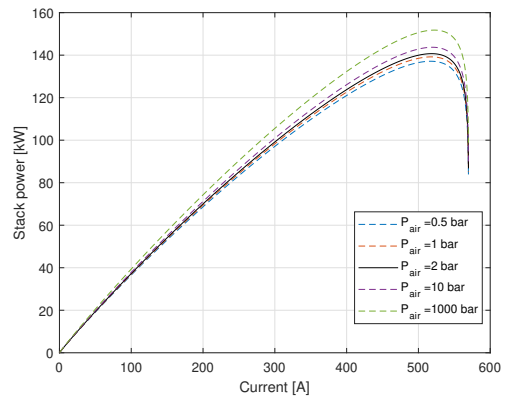


(b) Fuel cell stack power

Figure D.2: Sensitivity analysis for inlet H_2 pressure P_{H_2} [bar]. $P_{H_2} = 1.54$ bar is used

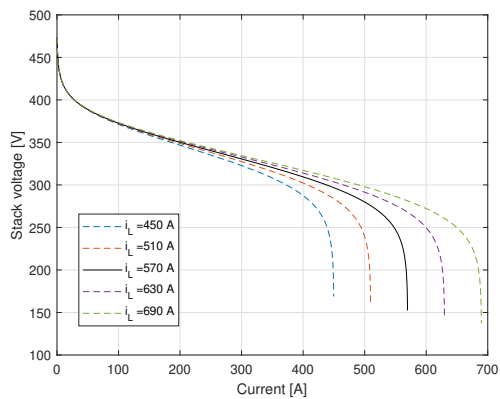


(a) Fuel cell stack voltage

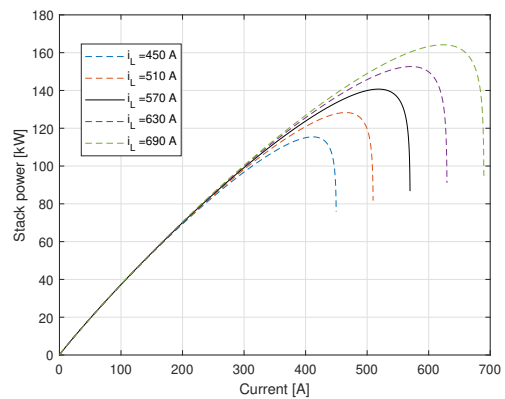


(b) Fuel cell stack power

Figure D.3: Sensitivity analysis for inlet air pressure P_{air} [bar]. $P_{air} = 2$ bar is used in the model

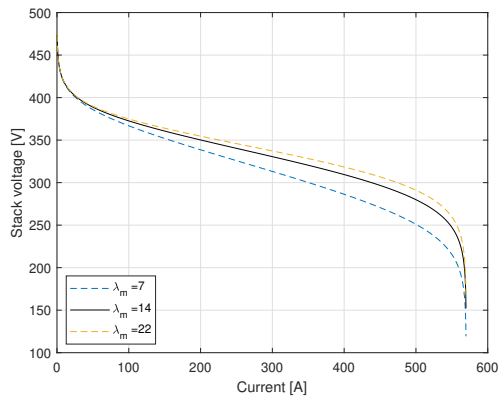


(a) Fuel cell stack voltage

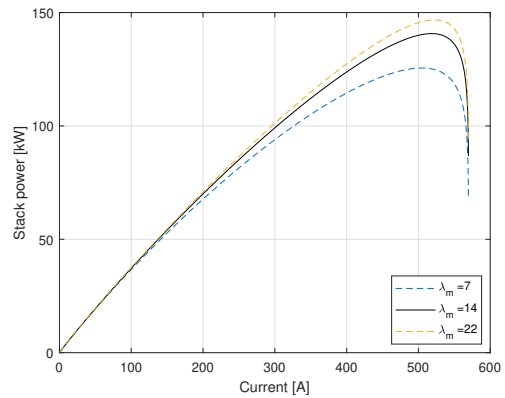


(b) Fuel cell stack power

Figure D.4: Sensitivity analysis for limiting current I_L [A]. $I_L = 570$ A is used in the model

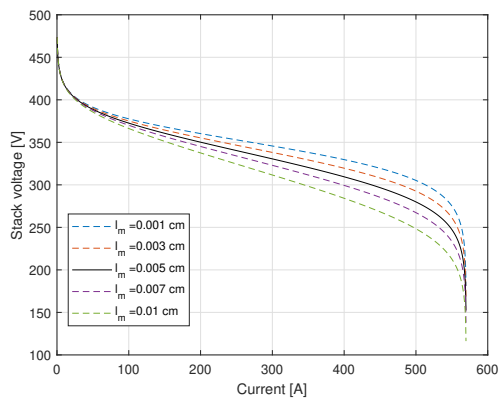


(a) Fuel cell stack voltage

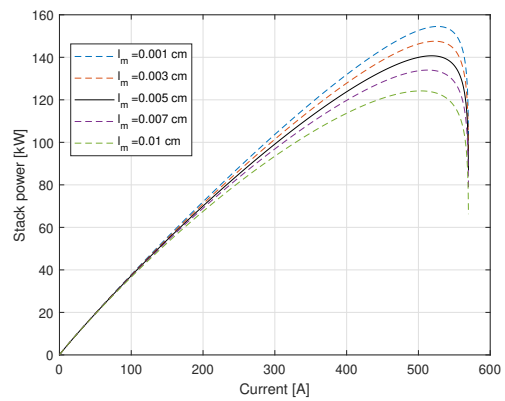


(b) Fuel cell stack power

Figure D.5: Sensitivity analysis for the hydration parameter λ_m [-]. $\lambda_m = 14$ is used in the model

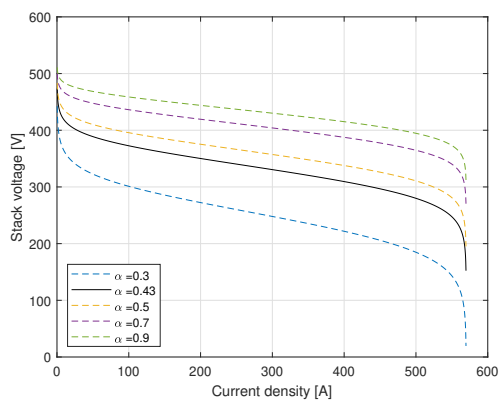


(a) Fuel cell stack voltage

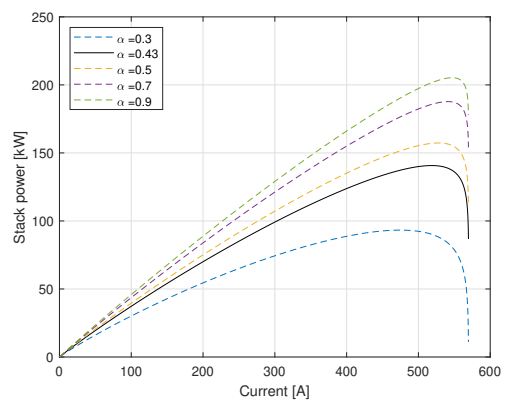


(b) Fuel cell stack power

Figure D.6: Sensitivity analysis for membrane thickness l_m [cm]. $l_m = 5 \cdot 10^{-3}$ cm is used

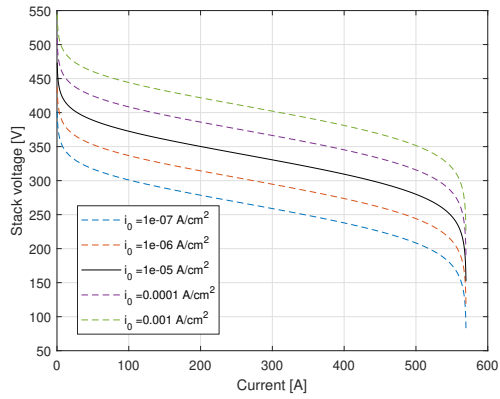


(a) Fuel cell stack voltage

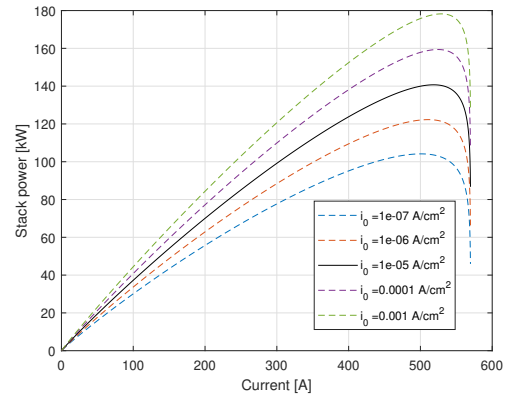


(b) Fuel cell stack power

Figure D.7: Sensitivity analysis for the charge transfer coefficient α [-]. $\alpha = 0.43$ is used

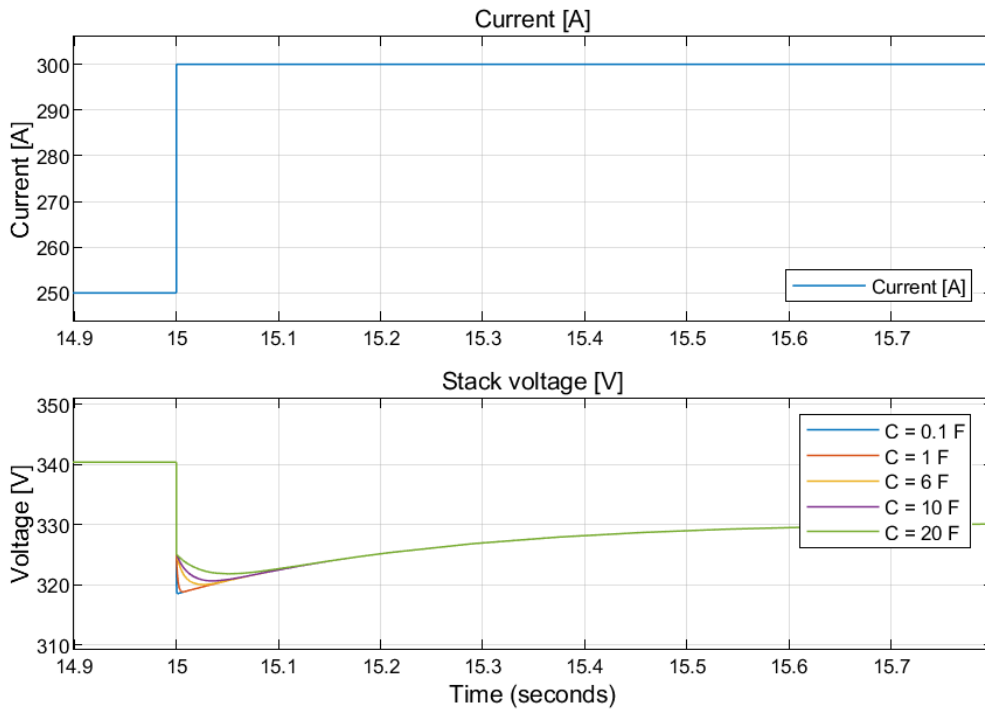


(a) Fuel cell stack voltage

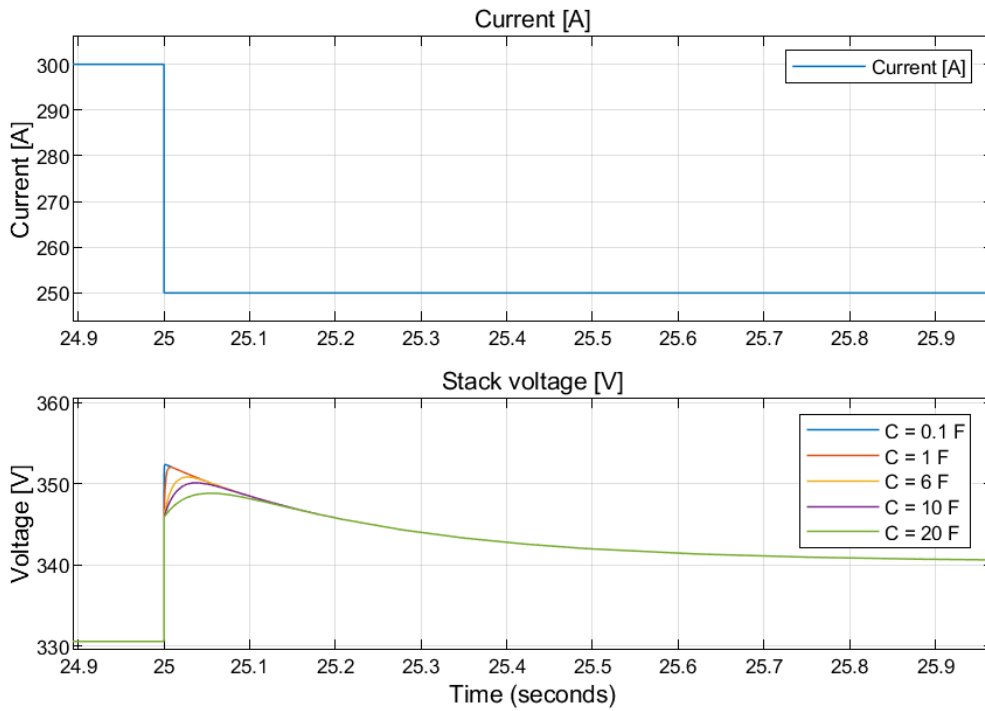


(b) Fuel cell stack power

Figure D.8: Sensitivity analysis for the exchange current density i_0 [A/cm^2]. $i_0 = 1 \cdot 10^{-5} A/cm^2$ is used in the model

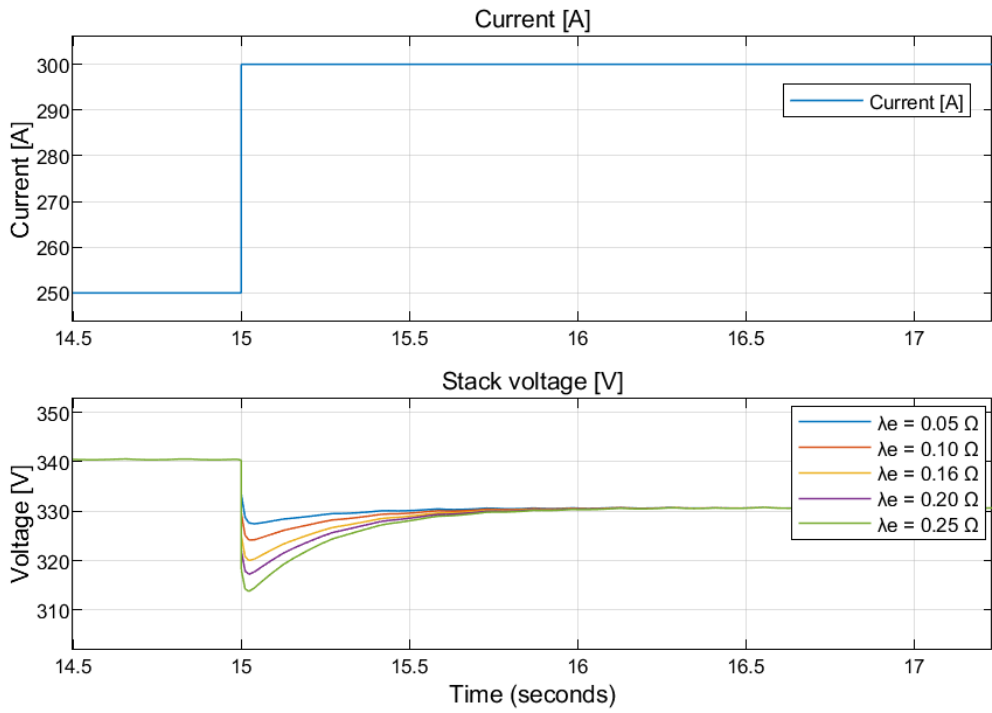


(a) Current step increase

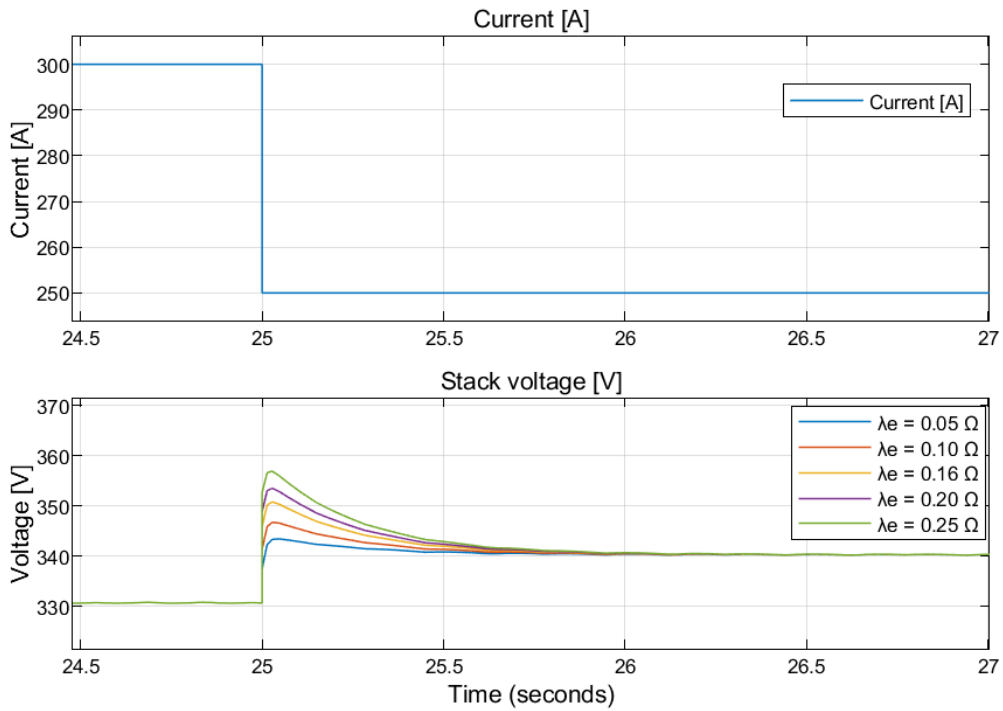


(b) Current step decrease

Figure D.9: Sensitivity analysis for the capacitance of charge double layer, C . $C = 6\text{ F}$ is used in the model

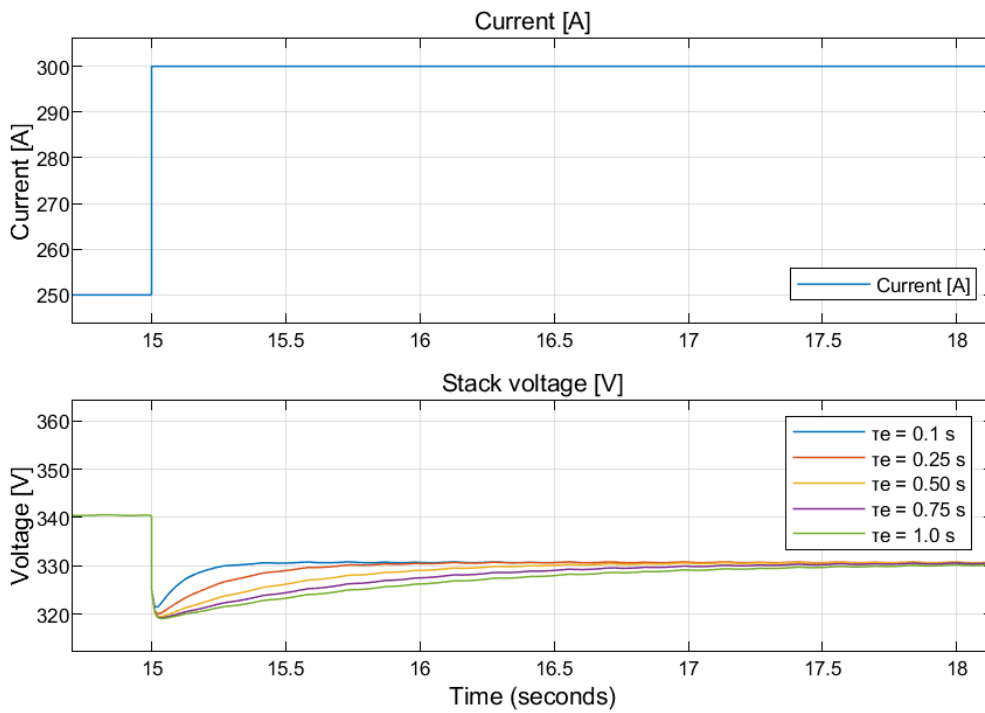


(a) Current step increase

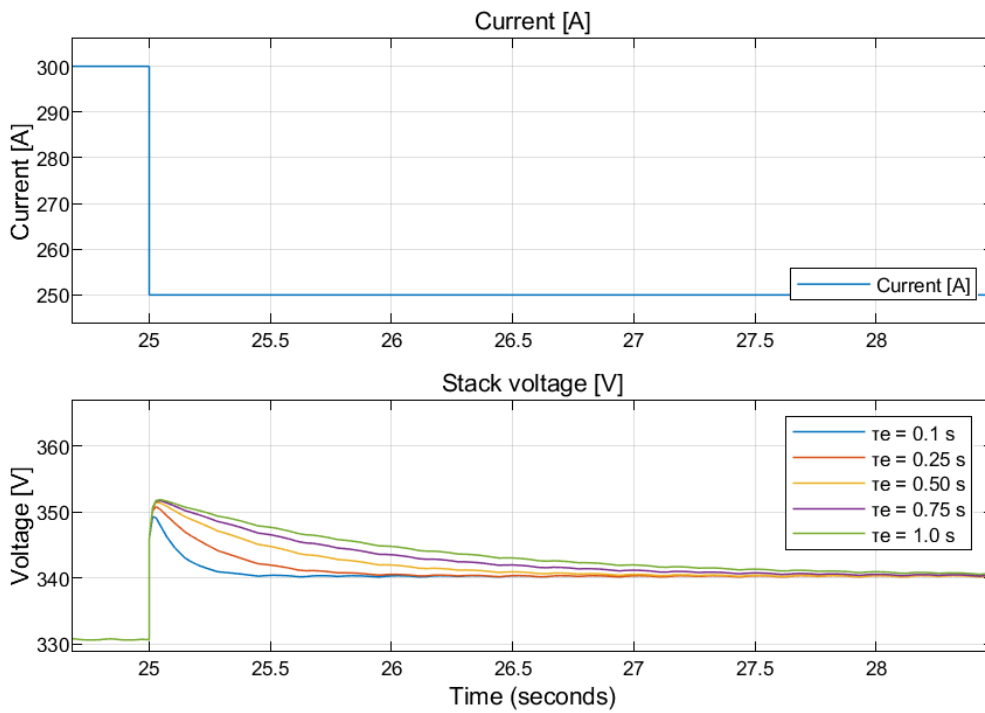


(b) Current step decrease

Figure D.10: Sensitivity analysis for the λ_e constant. $\lambda_e = 0.16 \Omega$ is used in the model



(a) Current step increase



(b) Current step decrease

Figure D.11: Sensitivity analysis for the time constant, τ_e . $\tau_e = 0.25$ s is used in the model

D.2 Electrolyser Stack Model

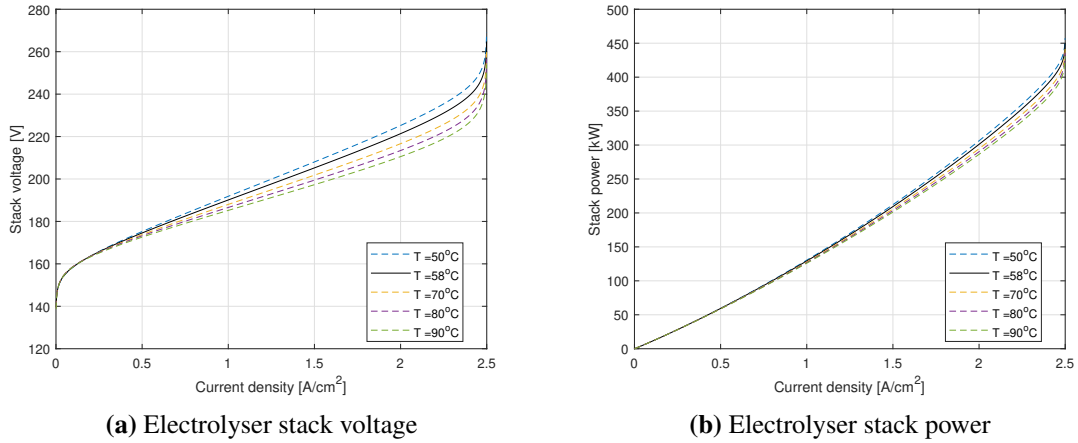


Figure D.12: Sensitivity analysis for operating temperature T [°C]. $T = 58^\circ\text{C}$ is used in the model

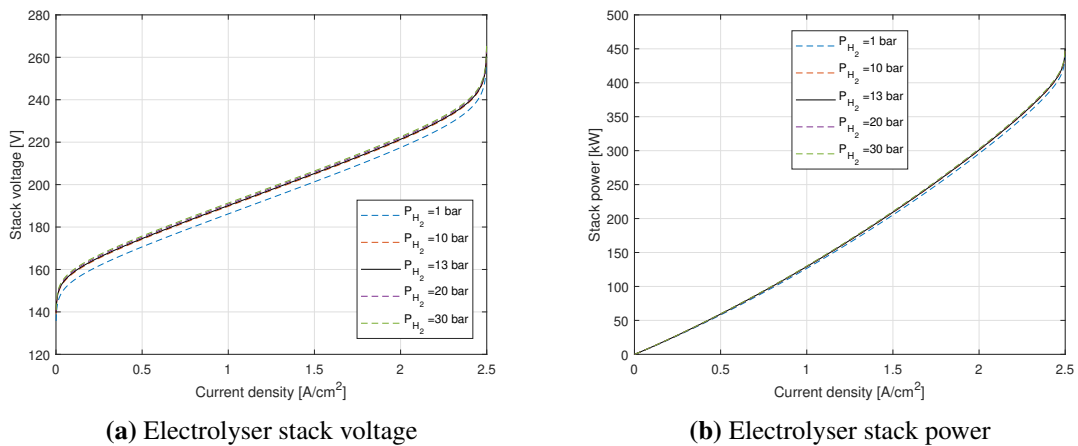
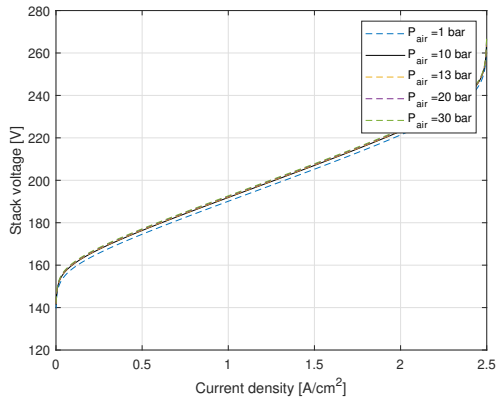
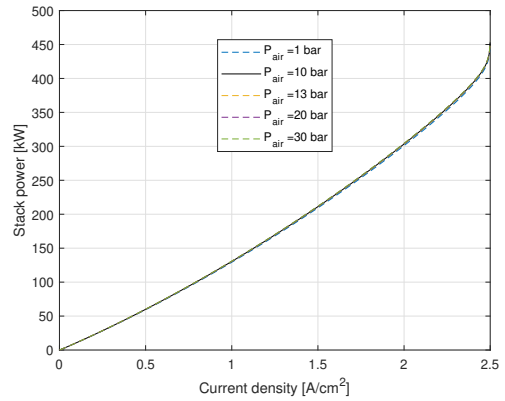


Figure D.13: Sensitivity analysis for inlet H_2 pressure P_{H_2} [bar]. $P_{H_2} = 13$ bar is used

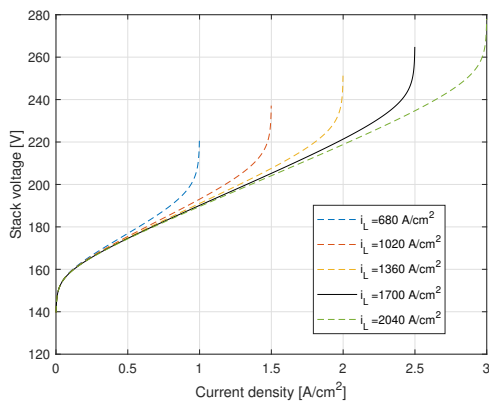


(a) Electrolyser stack voltage

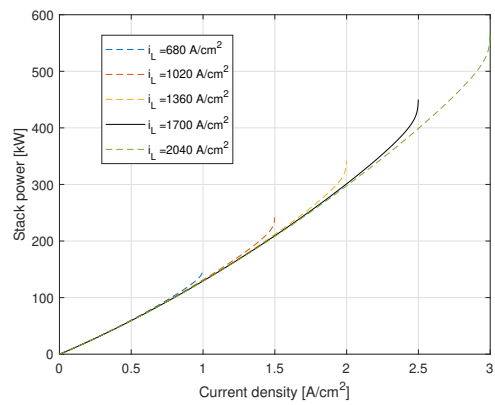


(b) Electrolyser stack power

Figure D.14: Sensitivity analysis for inlet air pressure P_{air} [bar]. $P_{air} = 1$ bar is used

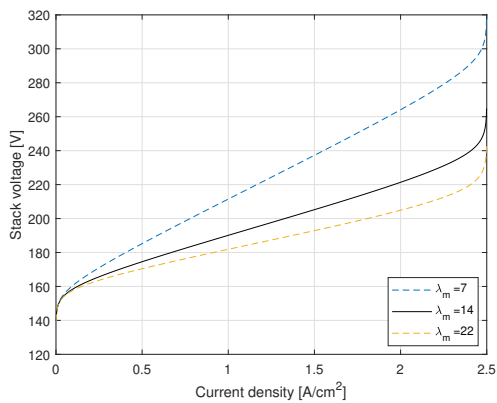


(a) Electrolyser stack voltage

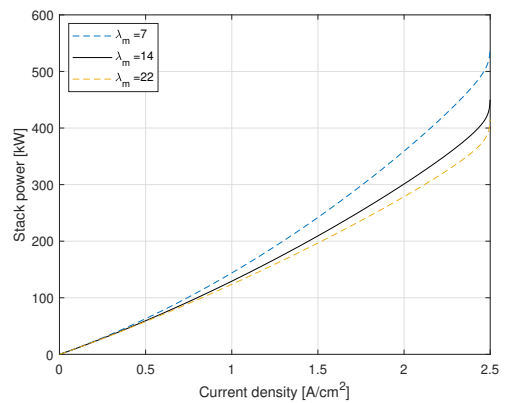


(b) Electrolyser stack power

Figure D.15: Sensitivity analysis for limiting current density i_L [A]. $i_L = 2.9$ A/cm² is used

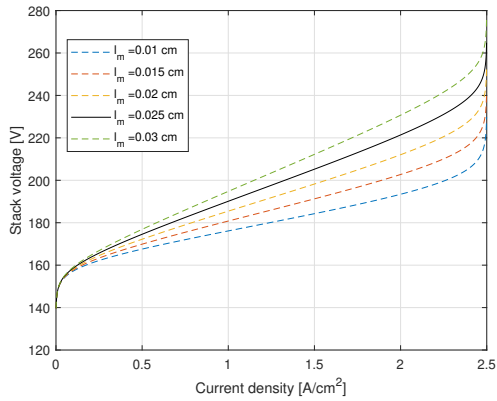


(a) Electrolyser stack voltage

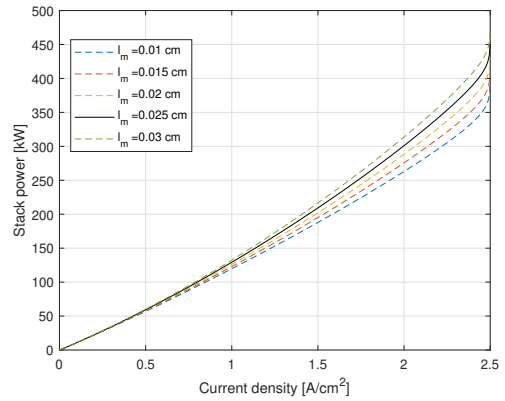


(b) Electrolyser stack power

Figure D.16: Sensitivity analysis for the hydration parameter λ_m . $\lambda_m = 14$ is used in the model

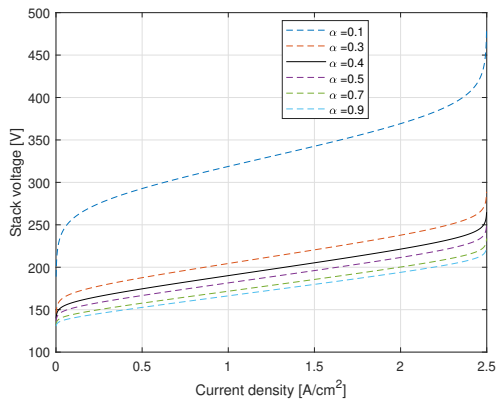


(a) Electrolyser stack voltage

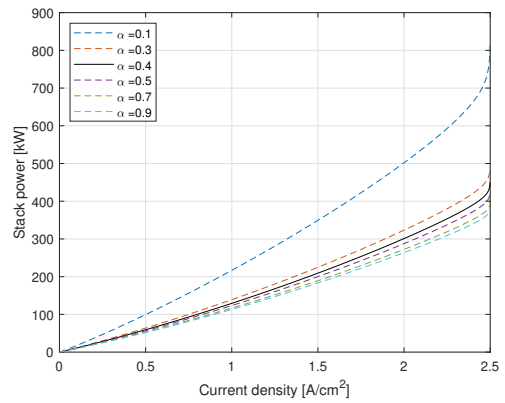


(b) Electrolyser stack power

Figure D.17: Sensitivity analysis for membrane thickness l_m [cm]. $l_m = 0.025$ cm is used

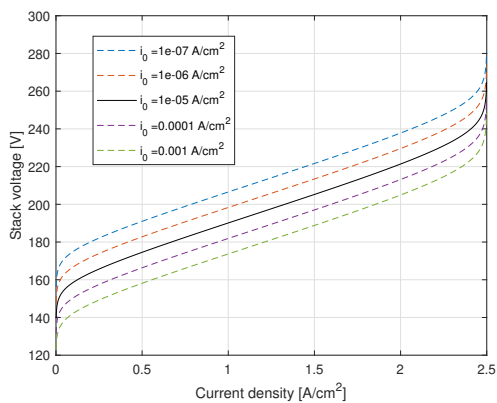


(a) Electrolyser stack voltage

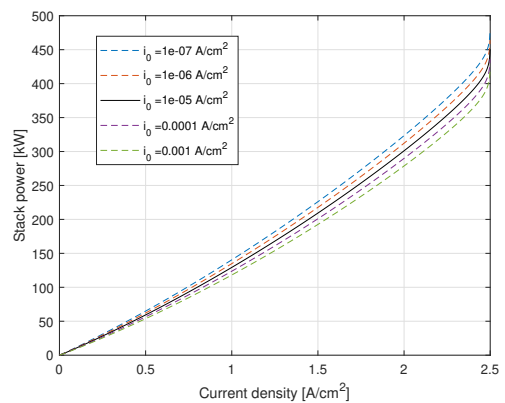


(b) Electrolyser stack power

Figure D.18: Sensitivity analysis for the charge transfer coefficient α [-]. $\alpha = 0.4$ is used



(a) Electrolyser stack voltage



(b) Electrolyser stack power

Figure D.19: Sensitivity analysis for the exchange current density i_0 [A/cm^2]. $i_0 = 1 \cdot 10^{-5}$ A/cm^2 is used in the model

